

Université du Québec  
Institut National de la Recherche Scientifique  
Énergie Matériaux Télécommunications

**HYDROTHERMAL EPITAXY  
OF FUNCTIONAL PEROVSKITE THIN FILMS**

par

**Ivan Alejandro Velasco-Davalos**

Thèse présentée pour l'obtention du grade de  
Philosophae Doctor (Ph.D.)  
en Sciences de l'énergie et des matériaux

Jury d'évaluation

Président du jury et  
examineur interne

Professeur Fiorenzo Vetrone,  
INRS - EMT, Canada

Examinatrice externe

Professeure Clara Santato,  
École Polytechnique de Montréal

Examineur externe

Professeur Fabio Variola,  
University of Ottawa

Directeur de recherche

Professeur Andreas Ruediger,  
INRS - EMT

10 février 2016

## Abstract

Functional oxides and their thin film epitaxy have become increasingly requested and further improvement in the existing technologies of information storage and energy harvesting heavily depends on the performance of such heterostructures at the nanoscale. Ferroelectric materials show a spontaneous electric polarization, which can be switched repeatedly by applying an external electric field. Since the discovery of ferroelectric  $\text{BaTiO}_3$  as the first oxide ferroelectric, the period prior to 1988 was mainly restricted to modelling ferroelectric phase transitions and discovering new ones. However, the focus has been significantly changed in the nineties, when thin films were developed and integrated into semiconductors at the nanoscale. This down scaling and bi-stable polarization of ferroelectrics were attractive in memory devices through ferroelectric random access memory, smart cards etc., and in tunable microwave devices through phase shifters, delay lines, resonators etc., apart from the conventional capacitor applications. Similarly, work on multiferroic can be traced back to pioneering research in the 1950s and 1960s, but there has been a recent resurgence of interest driven by long-term technological aspirations. For more than a decade,  $\text{BiFeO}_3$ , being a magnetic and a strong ferroelectric material at room temperature, has been renowned as a multiferroic materials that addresses a range of possible applications that no other material class exhibits so far. Out of many possible options, photovoltaic applications are being extensively considered due to the relatively low band-gap ( $\sim 2.5$  eV). These two material systems,  $\text{BaTiO}_3$  and  $\text{BiFeO}_3$  are widely considered as the model systems for ferroelectric and multiferroic properties and hence epitaxial thin film growth on lattice matched  $\text{SrTiO}_3$  substrates by an inexpensive hydrothermal method are considered in this thesis.

One of the main requirements of producing high quality epitaxial thin films on  $\text{SrTiO}_3$  substrates is the single termination of its surface. To this effect, a novel microwave-assisted hydrothermal etching was successfully applied to the surface preparation of pure and Nb-doped  $\text{SrTiO}_3$  single crystals with (100), (110) and (111) orientations. Without the possibility of fluorine contaminations from the Teflon liner and by avoiding the etching chemistry involved with HF widely used, the surface structure appears perfect within the limitations of the in-plane and out-of-plane miscut angles. These results indicate that the utilization of this method, without any

corrosive chemicals during the preparation steps, to achieve atomically flat surface with single chemical termination of SrTiO<sub>3</sub> substrates is feasible and compatible with batch processing. This technique is inexpensive, fast, safe, environmentally benign, compatible with batch processes, and showed remarkable reproducibility. Further, this method does not need an ultra-high vacuum environment and long annealing time at high temperatures. The possibility to reduce the etching time significantly avoids the formation of etch pits and holes on the substrate surface.

The hydrothermal technique is shown to be a feasible way to obtain good crystalline quality thin films of BaTiO<sub>3</sub> and BiFeO<sub>3</sub>. This method is an inexpensive alternative technique, which is defined as any chemical reaction in presence of aqueous solvents conducted at autogenous pressure, which corresponds to the vapor pressure above room temperature and below the critical point, generally lower than 370 °C for water, in a closed system. As for the synthesis of the thin films, two hydrothermal technique modes were employed; conventional hydrothermal for BaTiO<sub>3</sub> and microwave assisted hydrothermal for BiFeO<sub>3</sub>. The conventional hydrothermal mode, where the heating process happens by convection at heating rates of 10 °C/min using a stainless steel reactor in a conventional oven; and, the microwave assisted hydrothermal mode, which consists in utilizing a relatively low budget high strength polymer reactor in a microwave oven for which the heating process happens by absorption through water molecules of the 2.45 GHz radiation which allows a more efficient heating process to synthesize films in less time compared to the conventional process.

In the case of BaTiO<sub>3</sub> films, TiO<sub>2</sub> nanoparticles dispersed in the Ba(OH)<sub>2</sub> alkaline solution are used as precursors. The incorporation of H<sub>2</sub>O<sub>2</sub> into precursor solution served as a strong oxidant and catalyst for the uniform nucleation of BaTiO<sub>3</sub> on the substrate surface. Polarization reversal in single phase epitaxial and polycrystalline BaTiO<sub>3</sub> thin films were demonstrated on Nb:SrTiO<sub>3</sub> and Pt/Al<sub>2</sub>O<sub>3</sub>/SiO<sub>2</sub>/Si substrates, respectively. Raman scattering studies revealed the necessity of cumulative depositions with 10 min of microwave radiation at a power of 120W for the single phase formation of BaTiO<sub>3</sub> films. No traces of impurity phases were present according to the x-ray diffraction and Raman scattering results which is primarily due to the absence of mineralizers. Local phase hysteresis of BaTiO<sub>3</sub> thin film on Nb:SrTiO<sub>3</sub> substrate confirms ferroelectricity and 180° switching.

Highly ordered BiFeO<sub>3</sub> thin films were successfully produced by hydrothermal synthesis on SrTiO<sub>3</sub>:Nb (100) substrates. Surfactants were avoided and significantly reduced the concentration of potassium hydroxide (KOH) by a factor of 10 compared to reports in literature to reduce the leakage current. Due to this reduction of mineralizer, leading to less solubility of the precursors and decreasing the reaction rate, deposition time of ~18 h were required to grow a 40 nm thin film. As-grown BiFeO<sub>3</sub> films were also annealed at 500 °C under nitrogen flow for better crystallization and to remove hydrogen. For the first time, polarization reversal is demonstrated by successful reduction of electronic leakage. A first demonstration of the bulk photovoltaic effect in hydrothermally grown BiFeO<sub>3</sub> shows that this technique can be used to produce multiferroics for photovoltaic applications. Our experimental results confirm realization of single termination of SrTiO<sub>3</sub> and epitaxial deposition of BaTiO<sub>3</sub> and BiFeO<sub>3</sub> by an inexpensive hydrothermal method with or without microwave radiation.

*Keywords: Functional oxides, Perovskites, BaTiO<sub>3</sub>, BiFeO<sub>3</sub>, Thin films, Epitaxial growth, SrTiO<sub>3</sub>, Single crystal, Substrate surface preparation, Etching, Step-terrace structure, Single termination. Hydrothermal synthesis, Atomic Force Microscopy, Ferroelectric polarization switching, Microwave-assisted hydrothermal method, Conventional hydrothermal process, Topography, Bulk photovoltaic effect, Photocurrent.*

## Acknowledgments

If I had known that coming to Canada to pursue my PhD would be a complete, sometimes painful, life changing, I would have done it anyways...

First of all, I would like to express my gratitude to my research director Andreas Ruediger for his invaluable pieces of advice, patience, encouragement and criticism in science and in personal life as a great human being that he is. I feel very fortunate to have counted on his mentorship and guidance. I will always have present the first contact email that I had with him. My complete admiration for him.

Thanks to the Institut national de la recherche scientifique, INRS, which provided me the facilities to perform my research. I would also like to thank the jury members, Professors Clara Santato, Fiorenzo Vetrone and Fabio Variola for accepting the invitation and for their helpful contribution.

Special mention goes to Dr. Reji Thomas and Fabian Vargas for their feedback and precious support expressly in the phase of developing and revising my thesis. Nothing would have been the same without them. The astounding good vibe was very inspirational in the research group of Andreas. I feel really pleased to have got along with inspiring colleagues in his research group, and to have had fruitful discussions with them ever since I started this journey. Christian, Mischa, Mathieu, Zabar, Chawki, Julien, Nordine, David, Gitanjali, Mert, Chahinez, Binod, Fernando, Andreas Buescher, Fabian Gersmeier, Thierry, Niklas, Brenda, Angelica, Josefina, Lucia, Manuel, Caroline, Cedric, Azza, and Clarick. There were many people from other groups and institutions who I will always be thankful for their support, friendship, great vibe and love during working hours and at party times: Shun, Maria, Bruno G, Gaston, Maribel, Marta, Eva, Antonio, Shadi, Oscar, Manoj, Belete, Joy, Teresa, Juliana, Mauricio, Bruno M, Denis, Marc, Mernusc, Esen, Maye, Hamid, Stefano, Catalin, Francesca, Romain, Spyros, Jussara, Hassan, Simon, Ania, Pao, Caro, Isabel, and Tim.

I also thank les messieurs Sylvain Gingras, George Lamoureux, and Christophe Chabanier for their technical support, as well to all members of the administration and last but not the least, to professor Federico Rosei whom I appreciate for his great labor to keep the INRS to be one of

## Acknowledgments

---

the most recognized institutions in Canada and in the world. I also thank him for allowing me to give me the chance to share great moments with him.

As always, to my parents, Laura and Salvador, who were the first in teaching me pro-feminist/anti-patriarchal values, (specially my mom), for their encouragement, support and endless love; to my sister Lilianita and brothers Josuesin and Vadimcho, my Tita and all my family and friends in Mexico who have been mindful and given moral support and love at every moment. To all my friends in Montreal who also were with me in the good and in the challenging moments and who have had a big spiritual influence. Some of them still in Montreal, others elsewhere, all of them pursuing new and encouraging projects: Lilia, Christelle, Horst, Helga, Andree, Yvan, Isabelle, Didier, Matilida, Samy, Fabien, Emma, Ximena, Mois, Juli, Miguel, Elodie, Oscar, Mcfly, Fercita, Marie, Ghita, Vanesa, Paulita, Berecita, Isaac, Nori, Carol-Anne, Laurie, Matias, Jorge, Hannita, Louison, Celia, Jairo, Margarita, Eve, Ariane, Maribel, Oussama, Emiluna, Salima, Cindy, Jessi, Angelica, Lucia, Luis, Olivita, Julieta, Romina, Etien, Caroline, Sylvie Frida, Pamelita, Renato, Daniela, Chantal Leblanc, Abraham, Lindita, Fernando, Oscar, Gilda, Chantal Latendresse, Florent, Nathalie, Susan, Mape, Candy, Angelika Voor, Helene, Juan Pablo, Marion, Lupita, Mateusz, Caro, Mario, Erandi and Jonathan. Thank you all. You all have a big special place in my heart.

Similar profound thanks goes to professor Carlos Gomez-Yanez who actually was my supervisor in Mexico for my engineer and master's degree, and with who we kept developing collaboration projects thanks to the financial support from Fonds de recherche du Québec nature et technologies, FRQNT; The Natural sciences and engineering research council of Canada, NSERC; the Canadian institute for photonics innovations, CIPI, support through a PBEEE-MELS fellowship and from Consejo nacional de ciencia y tecnología, CONACyT-Mexico.

Contents

Abstract.....	1
Acknowledgments.....	4
Contents .....	6
1. Introduction.....	9
1.1. Multifunctional perovskites .....	10
1.1.1. Barium titanate (BaTiO <sub>3</sub> ).....	13
1.1.2. Bismuth ferrite (BiFeO <sub>3</sub> ).....	14
1.2. Thin film epitaxy.....	16
1.2.1 Substrate selection .....	19
1.2.2 Substrate surface preparation.....	21
1.2.3 Deposition technique .....	25
1.3 Research objectives.....	27
2. Characterization tools .....	28
2.1. Atomic Force Microscopy .....	28
2.1.1. Piezoresponse Force Microscopy .....	31
2.1.2. Photoconductive Atomic Force Microscopy .....	31
2.2. X-Ray Diffraction .....	32
2.3. X-Ray Photoelectron Spectroscopy .....	32
3. Strontium titanate surface preparation.....	33
3.1. Experimental details.....	36
3.2. SrTiO <sub>3</sub> (100).....	38

---

## Contents

---

3.3.	SrTiO <sub>3</sub> (110).....	42
3.4.	SrTiO <sub>3</sub> (111).....	53
3.5.	Conclusion .....	57
4.	Multifunctional barium titanate and bismuth ferrite thin films .....	60
4.1.	BaTiO <sub>3</sub> thin films.....	60
4.1.1	Experimental details.....	61
4.1.2.	Surface coverage.....	64
4.1.3.	Reaction time and cycles .....	66
4.1.4.	Epitaxial BaTiO <sub>3</sub> on Nb:SrTiO <sub>3</sub> substrates.....	68
4.1.5.	Ferroelectric properties .....	73
4.2.	BiFeO <sub>3</sub> thin film.....	74
4.2.1	Experimental details.....	75
4.2.2	Morphology and microstructure .....	76
4.2.3	Ferroelectric properties .....	78
4.2.4	Photocurrent.....	79
4.3	Conclusion .....	82

## Contents

---

5. Summary and Outlook .....	84
6. References .....	88
7. Abbreviations .....	96
8. Publications, conference presentations and awards .....	98
Résumé en Français .....	102

### 1. Introduction

Multifunctional oxide materials are under continuous investigation and development to sustain the growth of integrated circuit and to improve the energy conversion/storage. Among them, perovskite oxides with ferroelectric and multiferroics properties, play an important role in the current state-of-the-art information storage and processing by realizing new functionalities and advanced electronic devices.<sup>1,2</sup> Ferroelectric materials show bi-stable electric polarization which can be switched by applying an external electric field. This ferroelectric effect was first observed by Valasek in 1921 in the Rochelle salt and it was not considered that time for any practical applications due to the water solubility. However, the ferroelectric switching in BaTiO<sub>3</sub> ceramic<sup>3</sup> and single crystals<sup>4</sup> was discovered later, through systematic dielectric anomaly studies and since then water insoluble ferroelectric oxide are widely used for many practical applications. However, recent interest in ferroelectric BaTiO<sub>3</sub> is in the growth of ultra-thin epitaxial film and strain engineering with enhanced ferroelectric properties for high density ferroelectric memories and electro-optic devices.<sup>5-9</sup> ‘Multiferroic’ is a relatively new term, originally introduced by Schmid,<sup>10</sup> which defines a class of materials which exhibit any type of long-range magnetic ordering and ferroelasticity (hysteretic strain), antiferroelectricity and/or ferroelectricity at the same time. However, according to the current usage, ‘multiferroics’ generally excludes the elastic part (most ferroelectrics are also ferroelastic, so that combination is not unusual) and refers only to magnetic and electric properties.<sup>11</sup> Since the discovery of enhancement of polarization in heteroepitaxially constrained thin films of ferromagnetic BiFeO<sub>3</sub> at room temperature, multiferroic BiFeO<sub>3</sub> recently ignited interest among materials scientists worldwide and is also attractive for photovoltaic applications.<sup>10,12</sup> So oxide materials are an attractive alternative to silicon technology because they possess multifunctional properties that can be utilized in various novel electronic and energy conversion/storage devices. The ability to realize atomically flat oxide substrates and production of epitaxial heterostructures with multifunctional oxides of atomic layer precision made “oxide electronics” a field of its own and is rival to semiconductors multilayers now. The preparation of conducting and insulating oxide single crystal substrates (SrTiO<sub>3</sub>) surface with single termination, the realization of ferroelectric (BaTiO<sub>3</sub>) and multiferroic (BiFeO<sub>3</sub>) heterostructures on such substrate by hydrothermal technique is the topic of this dissertation.

## 1.1. Multifunctional perovskites

All crystals can be divided into 32 different classes depending on their symmetry; 20 of them exhibit piezoelectricity and among those, 10 are pyroelectric. If the spontaneous polarization of the pyroelectric crystal has two stable states, and this polarization can be switched from one state to the other by the application of an electric field, then the crystal is ferroelectric.<sup>13</sup> A graphical overview of the crystal classification is given in Figure 1.1

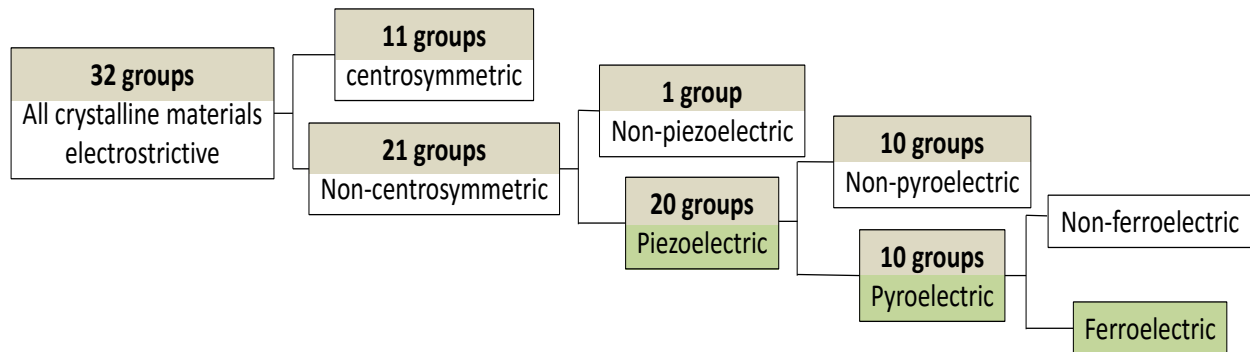


Figure 1.1: Classification of the 32 crystal groups; adapted from reference 14.

The dielectric behavior of a non-centrosymmetric crystal which possesses piezoelectric, pyroelectric and ferroelectric properties at the same time is described by:

$$D_i = \varepsilon_0(\varepsilon_{ij}E_j + d_{ijk}T_{jk} + p_i\Delta T + P_{Si}) \quad \text{Equation 1.1}$$

where  $D_i$  denotes the electrical displacement in direction  $i$ ;  $\varepsilon_{ij}$  is the relative permittivity,  $E_j$  the electric field in direction  $j$ ;  $d_{ijk}$  is the piezoelectric tensor element permitting a crystal to exhibit electric polarity when subject to a mechanical stress  $T$  and vice versa;  $p_i$  is the pyroelectric coefficient for small temperature changes  $\Delta T$ ; and,  $P_{Si}$  is the inherent spontaneous polarization<sup>20,21</sup>. The Figure 1.2a shows a typical ferroelectric  $P$ - $E$  hysteresis loop which represents the polarization reversal by the application of an external electric field. It has been noticed that several authors confuse ferroelectric behavior by reporting unrelated coercive field and remnant polarization from cigar-shaped loops (Figure 1.2b) that are typical of lossy dielectrics<sup>2,15</sup>.

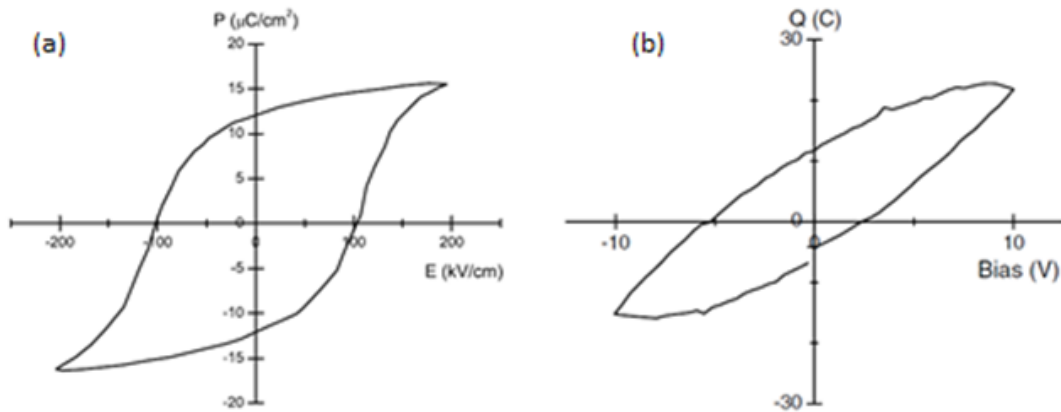


Figure 1.2: a) Ferroelectric hysteresis loop for a truly ferroelectric material; (b) charge versus voltage giving a cigar-shape loop typical for a lossy dielectric, in this case the peel of a banana; adapted from reference 15.

Some materials that exhibit ferroelectric properties belong to the group of so called perovskite structure. The perovskite structure has the general stoichiometry  $\text{ABO}_3$ , where A cations are located at the corner of the structure, B in the center of the body and O on the face centers as seen in *Figure 1.3*. The A and B cations can have a variety of charges and in the original perovskite mineral ( $\text{CaTiO}_3$ ) the A cation is divalent and the B cation is tetravalent. The ferroelectric effect is attributed to the dipole interaction between the B body centered cation and the oxygen anion located on the face centers resulting in the B- ionic displacement from the center in non-centrosymmetric structure. This spontaneous ionic displacements or as well named spontaneous polarization can be possible where the force to displace the ion is strong enough to overwhelm the repulsive force between the ions.<sup>16</sup>

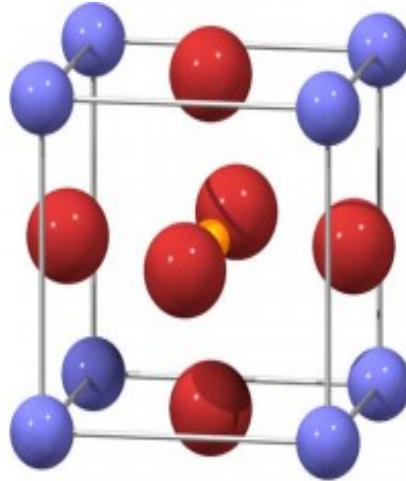


Figure 1.3: The perovskite structure has the general stoichiometry  $ABO_3$ , where  $A$  atoms are located at the corner of the structure,  $B$  in the center of the body and  $O$  in the face centers.

On the other hand, multiferroics are formally defined as materials that exhibit more than one primary ferroic order parameter simultaneously in one phase<sup>10</sup> as shown in Figure 1.4. In a ferroic material, polarization  $P$ , magnetization  $M$ , or strain  $\epsilon$  are spontaneously formed to produce ferroelectricity, ferromagnetism or ferroelasticity, respectively.

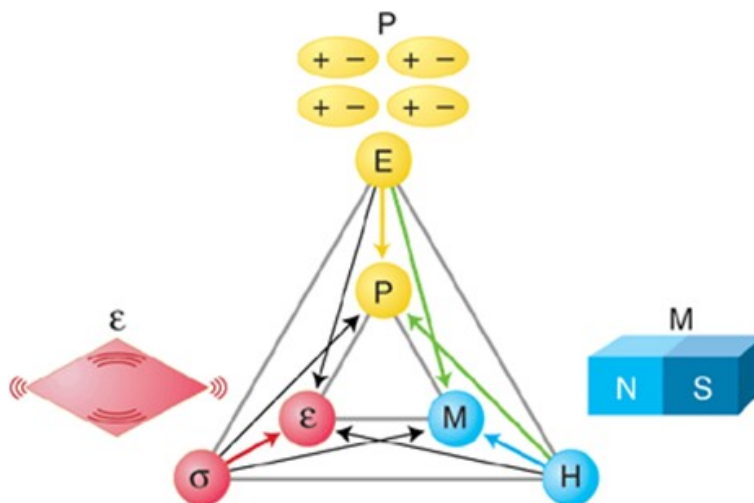


Figure 1.4: The electric field  $E$ , magnetic field  $H$  and stress  $\sigma$  control the electric polarization  $P$ , magnetization  $M$  and strain  $\epsilon$  respectively; adapted from reference 17.

### 1.1.1. Barium titanate ( $\text{BaTiO}_3$ )

Barium titanate has been considered as a paradigmatic ferroelectric material which possesses a perovskite tetragonal structure at temperatures between  $5^\circ\text{C}$  and  $120^\circ\text{C}$  of the type  $\text{ABO}_3$  as shown in the previous *Figure 1.3*. The unit cell parameters for the tetragonal phase are:  $a = 0.3992$  nm and  $c = 0.4036$  nm. The transition from the ferroelectric tetragonal phase to the paraelectric cubic one occurs around  $120^\circ\text{C}$  which corresponds to the Curie temperature. At room temperature,  $\text{BaTiO}_3$  exhibits a polarization along the  $c$  axis which is reversible when applying an electric field.<sup>18-21</sup> The applications of particular interest with this material are positive temperature coefficient of resistivity (PTCR) thermistors, multilayer ceramic capacitors (MLCCs) and electro-optic devices.<sup>2</sup> More recently, ferroelectric properties of  $\text{BaTiO}_3$  have been coupled with the electron tunneling phenomena to develop ferroelectric tunnel junctions which has been subject of investigation.<sup>9</sup> Ferroelectric tunnel junctions (FTJ), which are composed of two metal electrodes separated by an ultrathin ferroelectric barrier, are considered as promising candidates for non-volatile resistive memories. The Figure 1.5 shows atomic force microscopy results of a tunneling heterostructure composed of a metal-ferroelectric-semiconductor configuration ( $\text{Pt}/\text{BaTiO}_3/\text{Nb}:\text{SrTiO}_3$ ) produced by pulsed laser deposition (PLD), where the height and the width of the barrier can be electrically modulated as a result of a ferroelectric field effect that leads to a greatly enhanced tunneling electroresistance.<sup>9</sup> The author argues that the giant tunneling electroresistance, reliable switching reproducibility and long data retention observed in this configuration suggest a great potential in non-destructive readout non-volatile memories.

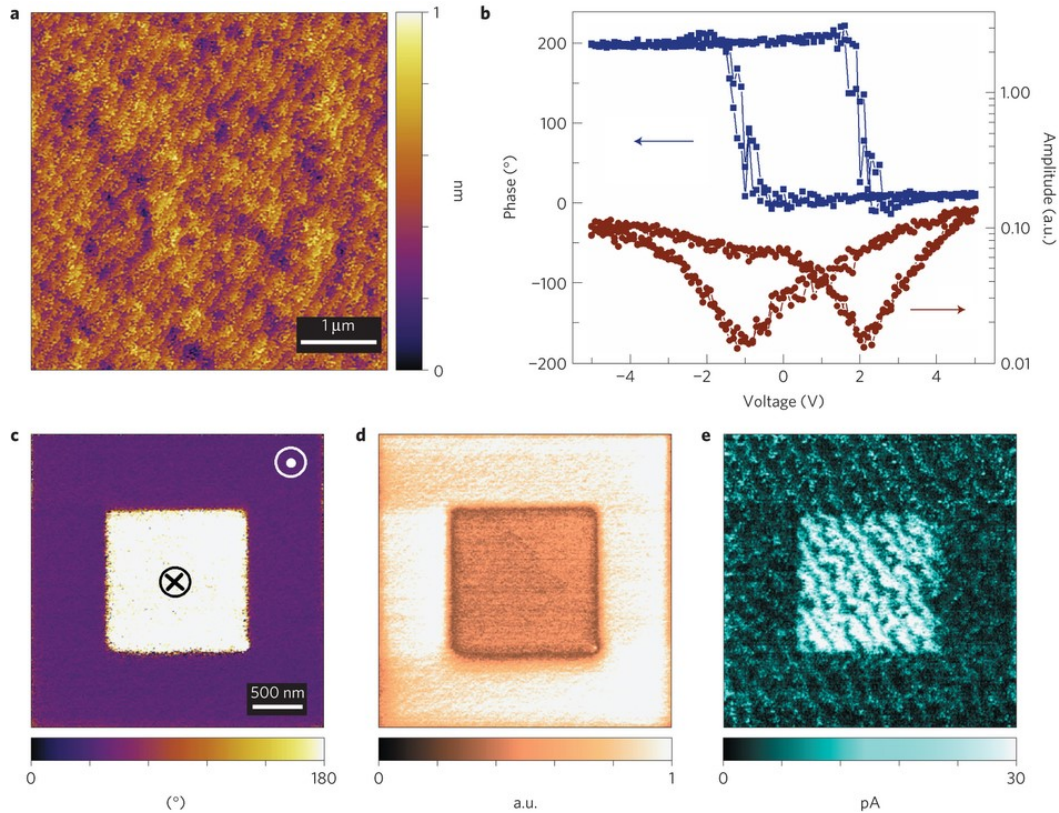


Figure 1.5: a), morphology of a  $\text{BaTiO}_3$  surface on  $\text{Nb:SrTiO}_3$  semiconductor substrates. b), local Piezoresponse Force Microscopy hysteresis loops: top, phase signal; bottom, amplitude signal. c,d, PFM out-of-plane phase and amplitude images recorded after writing an area of  $3 \times 3 \mu\text{m}^2$  with  $-5 \text{ V}$  and then the central  $1.5 \times 1.5 \mu\text{m}^2$  square with  $+5 \text{ V}$  using a biased conductive tip. e, Current mapping over the same area shown in c),d),e), demonstrating the polarization direction-dependent resistance in the  $\text{BaTiO}_3/\text{Nb:SrTiO}_3$  heterostructure. Adapted from reference 9.

### 1.1.2. Bismuth ferrite ( $\text{BiFeO}_3$ )

Bismuth ferrite is a multiferroic material with polar and magnetic ordering coexisting at room temperature.<sup>28,29</sup> It has a rhombohedral perovskite structure in bulk (monoclinic in thin films) with bismuth atoms located at the corners of the cell, iron at the center, and oxygen at the face centers.<sup>22</sup> It has excellent ferroelectric and piezoelectric properties and it is considered to be a suitable material for high-temperature applications thanks to its ferroelectric Curie temperature ( $T_c$ )  $\sim 830 \text{ }^\circ\text{C}$  and Néel temperature ( $T_N$ )  $\sim 370 \text{ }^\circ\text{C}$ .<sup>23</sup> Facing an increasing demand for alternative

and renewable energy sources, researchers have begun to screen a broader spectrum of photovoltaic materials. Complex oxide compounds can be inexpensive and stable, and their properties can be tuned in order to be applied for photovoltaic applications.<sup>24</sup> The low mobility of charge carriers and the large band gap have so far impeded the use of bulk-photovoltaic materials in solar cells and their use might indeed be in optoelectronic sensor applications instead. The conversion process of light energy to electrical energy in conventional solar cells, e.g. silicon based devices, relies on the charge separation using the potential developed at the p–n junction.<sup>25</sup> The electrons increase the minority carrier density in the p-type region and the holes in the n-type region respectively. The minority excess lowers the potential at the junction, which might be compensated by a current to the electrodes.<sup>24,26</sup> In contrast to p-n junctions, photocurrent and photovoltage in polar materials have been found to arise from the inherent non-centrosymmetry in the bulk material by exhibiting an intrinsic electric field due to their crystal structure. This field can give rise to a charge separation of photo-excited electron-hole pairs. When these charges reach external electrodes, an electrical current is generated. This phenomenon is known as the bulk photovoltaic effect (BPVE).<sup>26-28</sup> The main characteristics of this effect are its large, non-equilibrium photovoltage and its small photocurrent, which is oriented according to the polarization direction and charge-carrier separation in homogeneous media.<sup>26,27</sup> The mechanism by which the anisotropic properties of the dipole excitations can be analyzed is represented by the photovoltaic tensor described in equation 1.2 which expresses the details of the response of the current density  $J_i$  to the light intensity  $I$ , where the components  $e_k e_l^*$  represent unit vectors of the light electric field and  $\beta_{ikl}$  is a third rank complex tensor which expresses the relation of the squares of the incident photon electric fields  $E \cdot E^*$ , although this mechanism is not fully understood<sup>29</sup>. Nevertheless, polar materials with large bandgap tend to have a fast carrier recombination having a detrimental effect on the short current, making them unattractive for photovoltaic applications.

$$J_i = \beta_{ikl} e_k e_l^* \cdot I \quad \text{Equation 1.2}$$

When a ferroelectric in an open circuit is illuminated by ultraviolet light (UV), for example, a high photovoltage, much larger than the band gap, has been observed in the direction of the electric polarization<sup>35,36</sup>. The magnitude of this photovoltage is directly proportional to the crystal

---

length in the polarization direction. The photovoltaic effect has been studied in ferroelectric BiFeO<sub>3</sub> since 2009 when Choi et. al<sup>30</sup>, reported single ferroelectric domain BiFeO<sub>3</sub> crystals exhibiting a diode-like effect where the forward direction of the diode was determined by the direction of the electric polarization, and the directionality of the diode could be reproducibly switched by large external electric fields. Associated with the diode effect, a substantial zero-bias PV current was induced by visible light. Its relatively small band gap of ~2.74 eV makes it an interesting candidate for high performance photovoltaic and optoelectronic applications<sup>26</sup>.

### 1.2. Thin film epitaxy

An appropriate understanding of the thin film growth process is required to produce high quality epitaxial thin films on single crystalline substrates. Crystal growth modes (Figure 1.6), as well as the atomistic model to describe the processes for the film growth are discussed in this section. Figure 1.6a corresponds to the layer-by-layer, or Frank-Van der Merwe (FM) growth mode which is observed when atoms are more strongly bounded to the substrate than to each other. When there is no firm bonding between the substrate and the arriving particles, three dimensional island growth can be observed as depicted in Figure 1.6b called Volmer-Weber (VW) mode. Finally, Figure 1.6c describes the layer by layer plus island growth, or Stranski-Krastanov (SK), which is an intermediate mode. After the first or a few monolayers subsequent layer growth is unfavorable and islands are formed on top of this 'intermediate' layer.

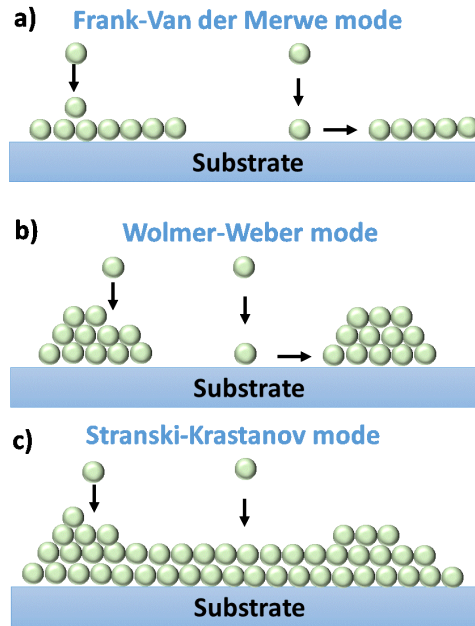


Figure 1.6: Film growth modes: a) layer-by-layer Frank-Van der Merwe, b) island Volmer-Weber, (c) Stranski-Krastanov.

The specific growth mode conditions can be understood in terms of surface or interface energy ( $\gamma$ ), which is the free energy (per unit area) to create an additional surface or interface as shown in Figure 1.7.

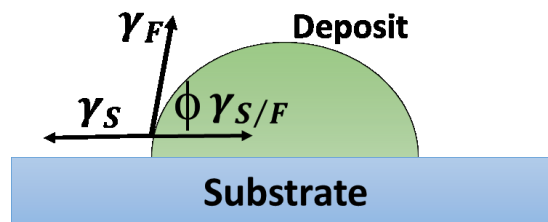


Figure 1.7: Schematic representation of the surface energy related to the thin film growth.

Since  $\gamma$  can be interpreted as a force per unit length of boundary, force equilibrium at a point where substrate and 3D island of the deposited film are in contact requires:

$$\gamma_S = \gamma_F + \gamma_{S/F} \cos \Phi \quad \text{Equation 1.3}$$

where  $\gamma_S$  is the surface tension of the substrate,  $\gamma_F$  corresponds to the one of the film, and  $\gamma_{S/F}$  to that of the substrate/film interface. By employing the *Equation 1.3*, the (layer-by-layer, FM) and (islanding, VW), can be distinguished by the wetting angle  $\Phi$  as follows.

$$FM: \quad \Phi = 0, \quad \gamma_S \geq \gamma_F + \gamma_{S/F} \quad \text{Equation 1.4}$$

$$VW: \quad \Phi > 0, \quad \gamma_S < \gamma_F + \gamma_{S/F} \quad \text{Equation 1.5}$$

Stranski-Krastanov (SK) corresponds to a mixed growth mode and it can be explained by assuming that there is a lattice mismatch between the deposited film and the substrate. The lattice of the film tries to adjust to the surface, but at the expense of the elastic deformation energy thus leading to a strained film. The film grows in a layer-by-layer mode until a certain critical thickness and it is when 3D islands are formed<sup>31</sup>.

The growth modes are a thermodynamic approach to crystal growth. Kinetic effects have to be considered in the hydrothermal process. The individual atomic processes responsible for adsorption and crystal growth on the surface are illustrated by supplies of single atoms (number density  $n_1(t)$ ) on a substrate with  $N_0$  sites per unit area, making the single-atom concentration  $n_1/N_0$ . These atoms may then diffuse over the surface until they nucleate or re-dissolve, as seen on Figure 1.8. Atoms or clusters can be captured at defect sites such as steps or nucleate in new 2D or 3D clusters. Each of these processes will be governed by characteristic times, dependent on the single-atom concentration and/or coverage.

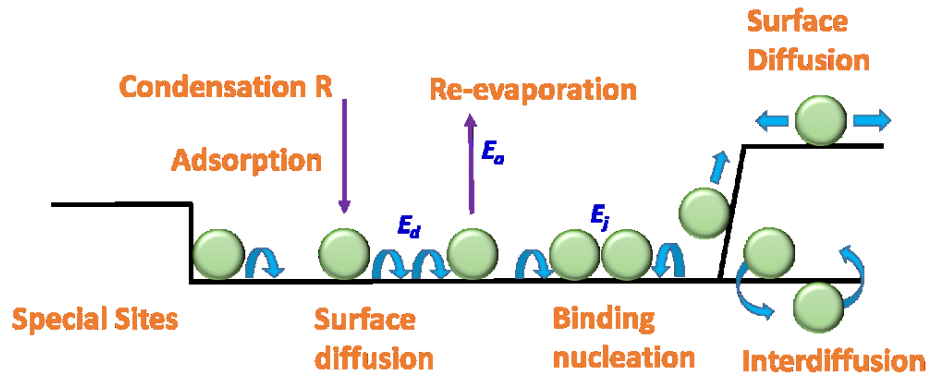


Figure 1.8: Schematic diagram of processes and characteristic energies in nucleation and growth on surfaces, adapted from reference 32

The nucleation density,  $N_x$ , of clusters is determined by the amount of particles arriving on the surface,  $R$  (deposition rate) and the distance an atom can travel on a flat surface, the diffusion length.

$$l_d = \sqrt{D_S \tau} \quad \text{Equation 1.6}$$

$\tau$  is the residence time before re-evaporation or incorporation.  $D_S$  the diffusion coefficient defined as:

$$D_S = va^2 \exp\left(-\frac{E_A}{K_b T}\right) \quad \text{Equation 1.7}$$

$E_A$  being the activation energy for diffusion,  $v$  the attempt frequency and  $a$  the characteristic jump distance. From Equation 1.5 it is clear that the deposition temperature (substrate temperature) is important, influencing the  $l_d$  and with that the nucleation density.<sup>32</sup>

### 1.2.1 Substrate selection

A successful realization of an epitaxial growth of thin film on any single crystal substrates requires a thorough consideration to choose the proper single crystal substrate<sup>33,34</sup>. Figure 1.9 shows the lattice match/or mismatch between some of the single crystal substrates with multiferroic thin films.

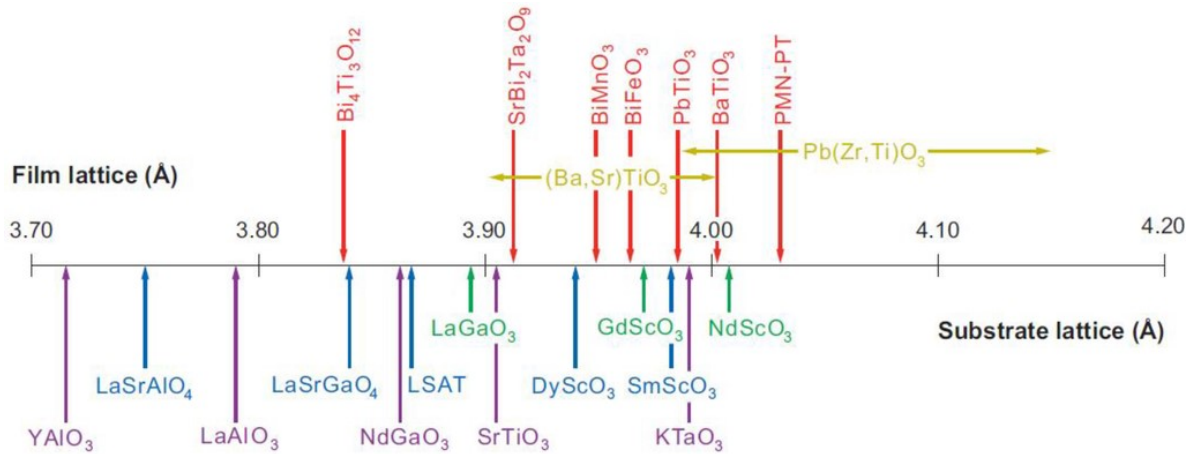


Figure 1.9: Commercially available perovskite substrates to show compatible lattice matching adapted from reference 35

Perovskite strontium titanate, which has a cubic room temperature structure with  $a = 3.905 \text{ \AA}$ , is a key player and is widely used as a substrate material for hetero-epitaxy, as well as an active player in various interface controlled phenomena. The selection of  $\text{SrTiO}_3$  as a substrate for the hetero-epitaxial growth of multifunctional perovskites was due to (i) its structural compatibility in terms of the lattice matching, (ii) its thermal stability at very high deposition temperatures, and (iii) its chemical robustness in highly reactive or corrosive ambient. *Figure 1.10* depicts an epitaxial perovskite heterostructure. Single crystal  $\text{SrTiO}_3$  can be made electrically conductive by doping Niobium (Nb) into the lattice in order to create additional energy levels. Doping concentration (0.1 ~ 1 wt. %) change resistivity from  $10^{-1}$  to  $10^{-3} \text{ Ohm-cm}$  by partially substituting  $\text{Ti}^{4+}$  by  $\text{Nb}^{5+}$ , and such substrates are useful for many epitaxial thin film applications, which require a conducting or semiconducting bottom electrode. Epitaxial perovskite ferroelectrics and multiferroics on semiconducting  $\text{SrTiO}_3$  substrates have recently proven to be advantageous for ferroelectric tunnel junctions. Hence, doped  $\text{SrTiO}_3$  substrates are widely used as bottom electrode for the heteroepitaxial growth of  $\text{BaTiO}_3$  and  $\text{BiFeO}_3$  thin films.

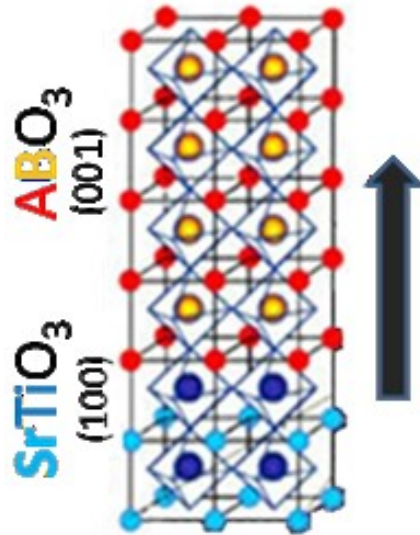


Figure 1.10: Highly oriented epitaxial perovskite films are of particular interest since its physical properties are directly linked to the direction of the crystallographic orientation. Adapted from reference 36.

### 1.2.2 Substrate surface preparation

The surface morphology of the substrate is an important aspect to be studied in order to determine and understand the thin film growth. Another important aspect is to procure a best possible interface quality by proper preparation of single chemically terminated surfaces. The (100) oriented SrTiO<sub>3</sub> single crystal is non-polar in nature containing a sequence of charge neutral sheets of SrO and TiO<sub>2</sub> along the (100) direction with an interplanar spacing of  $\frac{a}{2}$ . On the other hand, SrTiO<sub>3</sub> oriented in the (110) direction corresponds to a polar surface containing a sequence of charged sheets of SrTiO<sup>4+</sup> and O<sub>2</sub><sup>4-</sup> with an interplanar spacing of  $\frac{a}{2\sqrt{2}}$ .<sup>37</sup> In the case of a (111) oriented crystal, alternately stacked cationically different (SrO<sub>3</sub>)<sup>4-</sup> and Ti<sup>4+</sup> charged sheets with interplanar spacing of  $\frac{a}{2\sqrt{3}}$  exist. SrTiO<sub>3</sub> orientations are discussed in detail in Chapter 3 in terms of the specific application and method used to prepare them. All the three crystallographic orientations of SrTiO<sub>3</sub> are of great importance in achieving heteroepitaxy and multilayer superlattices of many complex oxides targeted for various applications.<sup>38,39</sup> However, most of the commercially available single crystal SrTiO<sub>3</sub> surfaces contain terraces with different chemical

composition. The step height between them will remain the same after reconstruction and the terrace width is determined according to the equation 1.8 as function of the miscut angle,  $\alpha$  which is the angle at which the surface is slanted with respect to the specified crystal plane ( $0.05^\circ < \alpha < 0.3^\circ$ ),

$$\tan \alpha = \frac{3.905}{\text{terrace width}} \quad \text{Equation 1.8}$$

Surface reconstruction plays an important role that can affect the nucleation mechanisms in thin film growth and may induce different physical properties from those of the bulk<sup>40</sup>. For example, according to preparation and ambient conditions, at least 8 different reconstructions and relaxations have been reported for the SrTiO<sub>3</sub> (100) surface being (1 x 1) one of the most energetically favorable with TiO<sub>2</sub> termination<sup>40</sup>.

For the SrTiO<sub>3</sub> (110) surface under oxidizing conditions, (3 x 1), (4 x 1), (5 x 1) and (6 x 1) reconstructions have been observed and appear to be related<sup>41</sup>. A reconstruction on the (110) surface is termed ( $n \times m$ ) indicating that it has dimensions of  $n$  times the bulk unit-cell length in the (110) direction. These  $n \times 1$  ( $n = 3 - 6$ ) reconstructions show similar features in scanning tunneling microscopy and can evolve from one to the next often with two being present at the same time<sup>41</sup>.

In the case of (111), the presence of a perpendicular dipole causes the surface energy of the termination to be infinite and the dipole can be removed via four mechanisms: by changing the surface stoichiometry, by redistribution of electrons in the surface region, adsorption of atoms or molecules, and faceting. These mechanisms allow a large number of reconstructions to be formed, with variable compositions and surface chemistry. It has been found that when polished and unspattered SrTiO<sub>3</sub> (111) samples are annealed in ultrahigh vacuum (UHV) at 850 °C for 30 min, a surface with coexisting domains of ( $\sqrt{7} \times \sqrt{7}$ ) R19.1° and ( $\sqrt{13} \times \sqrt{13}$ ) R13.9° reconstructions are formed<sup>42</sup>. Few other reconstructions on (111) have been reported; for example, a Ti<sup>4+</sup>-rich (4 x 4) reconstruction by annealing in UHV at 1200 °C for 5 min and studied the influence of using different atmospheres finding that annealing in O<sub>2</sub> the surface was more Ti enriched than annealing in Ar<sup>42</sup>.

---

In order to get uniform substrate/film interfaces, the substrate surface should be single chemically terminated, i.e. it should be either SrO or TiO<sub>2</sub> for (100), (SrTiO) or (O<sub>2</sub>) for (110) and (SrO<sub>3</sub>) or Ti for (111) orientations. The practical importance of obtaining this step-terrace on the surface, which is unavoidable when the single crystals are cut and polished at some controlled 'miscut' angle, a few fractions of a degree off with respect to the nominal orientation of the crystal lattice, are very important in realizing epitaxy as steps often act as nucleation sites during the film growth. Control of this step density and knowing the surface prior to deposition is important to obtain reproducible epitaxy under identical experimental conditions. Thus surface step morphology is used as a parameter to optimize subsequent thin film growth.<sup>43</sup> It is essential to carefully control the substrate surface to control the nucleation and improve the quality of thin films.

The most common procedure to obtain atomically flat step-and-terrace structures with single chemical termination is by immersion of the SrTiO<sub>3</sub> substrate in a buffered hydrofluoric (HF) solution followed by an O<sub>2</sub> annealing at elevated temperatures.<sup>44,45</sup> Not only does the HF treatment impose severe safety precautions, it is also environmentally hazardous. It has been shown that HF etching promotes incorporation of F within the top layers of TiO<sub>2</sub> (an average of ~ 13 % of the O anions are replaced by F) which results in lower electron mobility at complex oxide hetero-junctions due to impurity scattering.<sup>46</sup> This fluorine contamination can be avoided by replacing HF with boiling DI H<sub>2</sub>O and optimizing the time-temperature product of the annealing step, respectively.<sup>39</sup> An approach that substantially reduces the processing time and achieves surfaces of equal quality as under buffered HF treatment without the possibility of fluorine contamination is of utmost importance and hence a novel approach is necessary. Since SrO is a basic oxide (metal oxidation state < +4, forms a base with water) and TiO<sub>2</sub> is an acidic oxide (metal oxidation state > +4; forms an acid with water), the control of the pH of the wet etch solution provokes either SrO or TiO<sub>2</sub> termination.<sup>44</sup> Water adsorption and dissociation studied by density functional theory supported the experimentally observed selective hydroxylation of the SrO-termination in the regime of low water partial pressures.<sup>47</sup> This Sr-hydroxide complex improves the solubility of SrO layer under hydrothermal conditions compared to the TiO<sub>2</sub> layer. Hence hydrothermal etching of SrTiO<sub>3</sub> in water and alkaline medium is of great interest.

The simplest way to approach the problem of surface roughening is to consider the surface of a Kossel crystal, which leads to the so-called TSK (Terrace, Step, and Kink) model for the surface (Figure 1.11). The crystal is made by piling together cubic unit cells which interact through their lateral faces with an energy. The ground state of a crystal surface is obtained when the cubes form a close-packed arrangement with every square face lying in the same plane. When the temperature is raised, thermal excitations can appear. These are point defects: adatoms, forbidden vacancies and kinks on steps or collective defects forming steps which can eventually isolate closed flat domains. All of these defects lead to what we shall call atomic roughness.

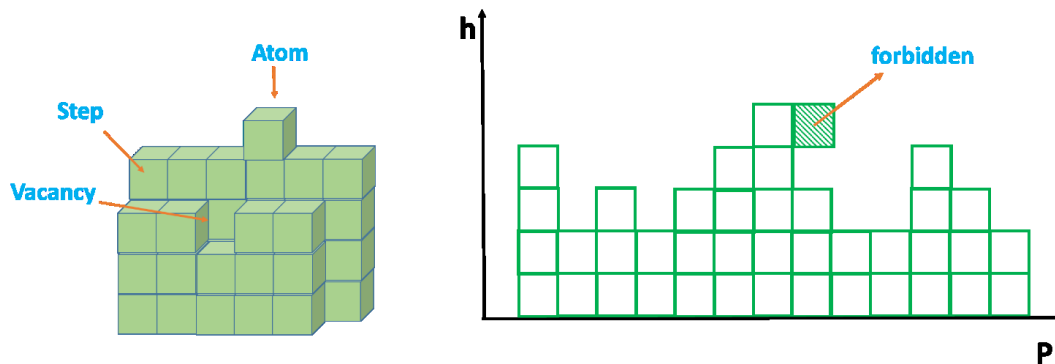
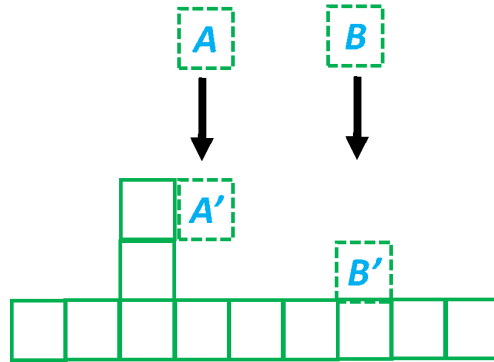


Figure 1.11: Kossel crystal (left) and Solid on solid (SOS) model (right).

In order to characterize this roughness more quantitatively, we shall restrict the model somewhat using the SOS assumption (Solid-On-Solid). As far as vacuum/solid interfaces are concerned, this hypothesis is generally quite well verified. Then any surface configuration can be characterized by a set of integers which represents the height of columns above the reference plane.<sup>32</sup> The surface morphology and the dynamics of growth after the formation of interfaces and surfaces can be described in microscopic detail through discrete growth models. In the ballistic deposition model (BD), the particles rain down vertically onto a  $d$ -dimensional substrate and aggregate upon first contact. It uses simple basic laws to determine these surface characteristics on a lattice (Figure 1.12) by generating a non-equilibrium interface that exemplifies many of the essential properties of a growth process.



*Figure 1.12: The ballistic model (BD) with the nearest-neighbor, illustrating two sticking possibilities for the newly deposited particles.*

A particle is released from a randomly chosen position above the surface, located at a distance larger than the maximum height of the interface. The particle follows a straight vertical trajectory until it reaches the surface whereupon it sticks. The deposited particles form a cluster or an aggregate with a very particular geometry. In this work we use the height to height correlation function (HHCF) to quantify the roughness.

### 1.2.3 Deposition technique

The hydrothermal method can be effectively used for the surface preparation of  $\text{SrTiO}_3$  single crystals and for the thin film deposition of  $\text{BaTiO}_3$  and  $\text{BiFeO}_3$  multiferroic materials. Epitaxial thin films of  $\text{BaTiO}_3$  and  $\text{BiFeO}_3$  are typically produced by means of physical methods such as radio frequency sputtering, pulsed laser deposition (PLD) or molecular beam epitaxy (MBE); and chemical techniques such as chemical vapor deposition (CVD), sol-gel, atomic layer deposition (ALD) or hydrothermal processes.<sup>2,48,49</sup> Most of these methods require relatively expensive setups, as well as high temperature processes, except for the sol-gel, ALD and the hydrothermal method which correspond to low energy processes. As reported in literature, sol-gel depends upon a subsequent annealing step to achieve the necessary crystallinity, whereas in the case of ALD, which certainly provides a crystallinity to the product, a thermal treatment could be required to enhance it. The use of the term “hydrothermal” was initiated in the middle of 19<sup>th</sup> century by geologists to describe the action of water at an elevated temperature and pressure to

---

create changes in the earth's crust leading to the formation of various minerals.<sup>50</sup> The hydrothermal method is considered as a mild and low temperature process. It is defined as any chemical reaction in presence of aqueous solvents conducted at autogenous pressure in a closed system. This pressure (> 1 atm.) is generated by the vapor pressure above room temperature and below the critical point ( $25\text{ }^{\circ}\text{C} < T < 370\text{ }^{\circ}\text{C}$ , in the case of water). The use of mineralizers could be required to promote the solubility.<sup>51-53</sup> This technique has gained interest among researchers because of an increase of the development of new materials, primarily ceramic oxides that can be prepared under mild conditions. The *Figure 1.13* shows the vapor pressure diagram of water as function of temperature. When getting close to the critical point of water, at approximately  $374\text{ }^{\circ}\text{C}$ , the dielectric constant of water decreases dramatically, thus water can act as organic solvent.

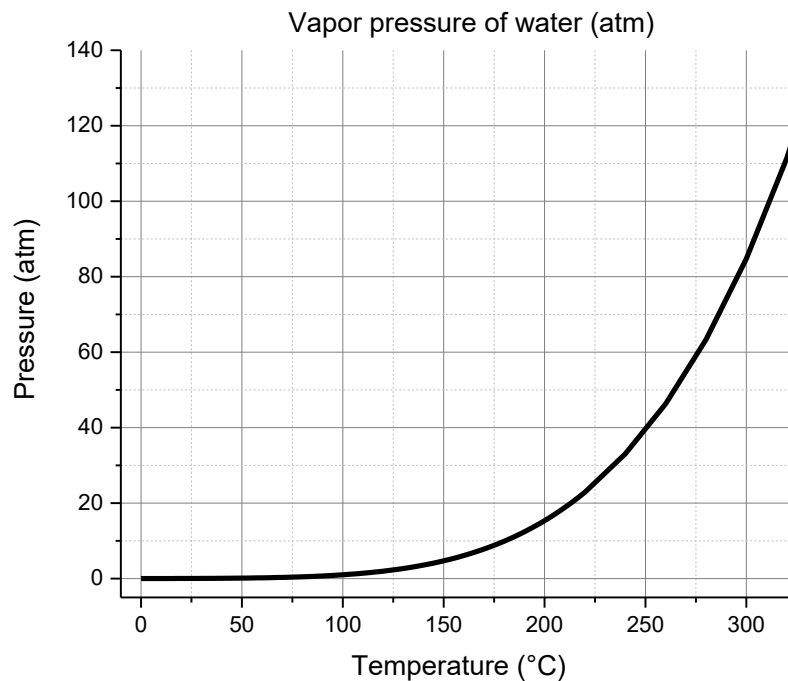


*Figure 1.13: Vapor pressure diagram of water as function of temperature.*

More recently, the addition of microwave energy into hydrothermal process has added the convenience of producing thin films and nanostructures with comparable improvement in crystallinity with respect to a conventional hydrothermal process while requiring significantly less time and reducing the cost of energy by about thousands of times<sup>54,55</sup>. Metallic surfaces are good reflectors of microwaves; however, electrically semi-conductive materials as Nb doped  $\text{SrTiO}_3$

allow microwave to pass through them with very little absorption and thus, the heating effect directly depends on the microwave radiation on water.

### 1.3 Research objectives

BaTiO<sub>3</sub> and BiFeO<sub>3</sub> are the model perovskite oxide systems that exhibits ferroelectric and multiferroic properties, respectively. Epitaxial thin films of ferroelectric BaTiO<sub>3</sub> and multiferroic BiFeO<sub>3</sub> are very interesting for the non-destructive readout non-volatile memories and photovoltaic applications, respectively. A successful realization of an epitaxially growth thin film requires a proper single crystal substrate. Single crystal SrTiO<sub>3</sub> is widely used as a substrate material for hetero-epitaxy, as well as an active player in various interface controlled phenomena. In order to get a uniform epitaxial interface between the substrate and the film, the SrTiO<sub>3</sub> surface should be single chemically terminated prior to the film deposition, i.e. it should be either SrO or TiO<sub>2</sub> for the (100); SrTiO<sup>4+</sup> or O<sub>2</sub><sup>4-</sup> for the (110); and SrO<sub>3</sub><sup>4-</sup> or Ti<sup>4+</sup> for the (111) crystallographic orientations. The main goal of this research is to investigate the realization of pure and Nb doped SrTiO<sub>3</sub> substrate surface with single chemical termination; and to address challenges in fabricating BaTiO<sub>3</sub> and BiFeO<sub>3</sub> thin films on single chemically terminated Nb:SrTiO<sub>3</sub>(100) substrates with low electric leakage which might be influenced by the hydrogen from the hydrothermal process or by impurities coming from mineralizers. The use of hydrogen peroxide as a strong oxidizer (hydrogen scavenger) is also discussed.

The specific objectives of the thesis are:

- Preparation of single chemically terminated pure and Nb doped SrTiO<sub>3</sub> substrate surface with a novel, fast and environmentally benign hydrothermal etching method.
- Synthesis of BaTiO<sub>3</sub> and BiFeO<sub>3</sub> thin films by conventional and microwave assisted hydrothermal methods
- Characterization of the substrate surface with atomic force microscopy and x-ray photoelectron spectroscopy.
- Study the structure, microstructure and ferroelectric properties of BaTiO<sub>3</sub> and BiFeO<sub>3</sub> epitaxial films on single chemically terminated Nb:SrTiO<sub>3</sub> substrates.

## 2. Characterization tools

The work presented in the thesis consist of single chemically terminated surface preparation of pure and Nb doped  $\text{SrTiO}_3$  substrates by a microwave assisted hydrothermal method. Similarly, thin film preparation of  $\text{BaTiO}_3$  and  $\text{BiFeO}_3$  multifunctional oxides on  $\text{Nb:SrTiO}_3$  were also realized by a microwave assisted and conventional hydrothermal technique. The experimental details of the hydrothermal method used for the surface preparation and thin film deposition are discussed in chapter 3 and 4, respectively. The different orientations of  $\text{SrTiO}_3$  surfaces and properties of multifunctional oxides were characterized with various tools and that are discussed here.

### 2.1. Atomic Force Microscopy

Atomic Force Microscopy (AFM) is a technique that allows to obtain topographic images by using a sharp tip at the end of a cantilever that is scanned over a surface.<sup>14</sup> The AFM is equipped with piezoelectric crystals that control the movement of the tip relative to the sample. The cantilever acts as an optical lever arm reflecting a laser beam onto a four sector photodiode which measures the deflection of the beam and thereby the deformation of the cantilever in interaction with the surface (Figure 2.1). The measured deflection gives a topography image of the sample to estimate the thickness of a film by doing a line profile of the cross section between an edge of the film and the substrate. Depending on the type of sample, the probe and/or set up experiment, ferroelectric or photoconductive measurements can be also determined as explained in 2.1.1 and 2.1.2 of the present document.

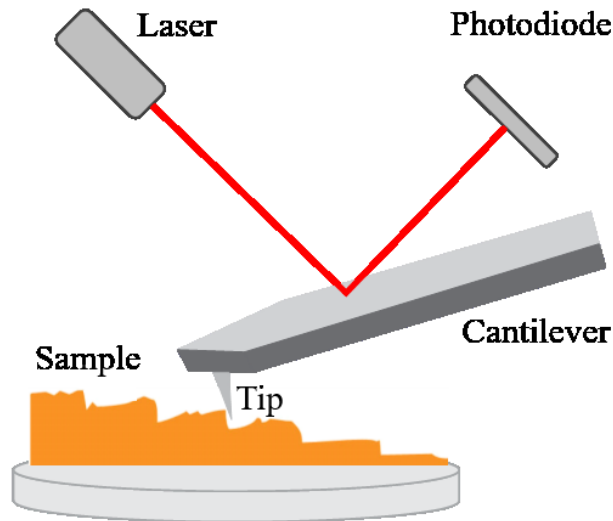


*Figure 2.1: Principle of Atomic Force Microscopy. The cantilever reflects a laser beam, and the movement is detected by a four sector diode.*

The principle of atomic force microscopy is the atomic interaction of the tip with the surface of the material in question. Figure 2.2 shows the Lennard-Jones potential in which at very small tip-sample distances (a few angstroms) a very strong repulsive force appears between the tip and sample atoms due to the overlap of the electronic orbitals at atomic distances. When this repulsive force is predominant, the tip and sample are considered to be in “contact”. An instantaneous polarization of an atom induces a polarization in nearby atoms and therefore an attractive interaction due to Van der Waals forces.

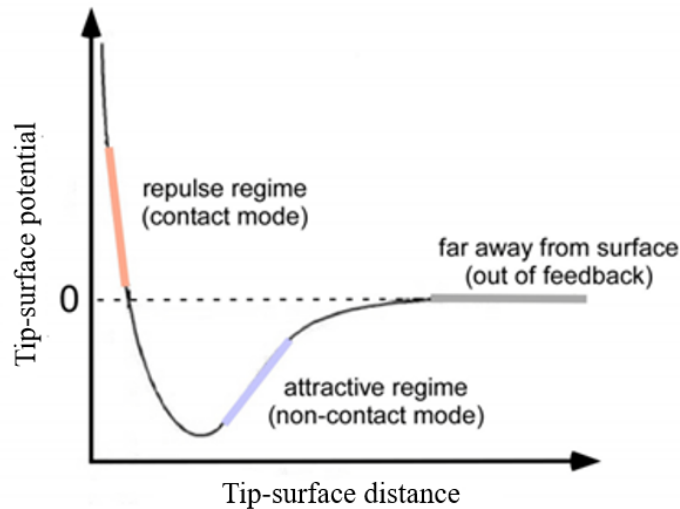


Figure 2.2: Atomic interaction at different tip-surface distances.

AFM images can be obtained by two main regimes: The contact mode where the deflection of the cantilever is maintained constant, and the non-contact regime where the tip is oscillated at the resonance frequency and the amplitude of the oscillation is maintained constant. A combination of these two modes leads to a semi-contact or tapping mode where only intermittent touching occurs on the sample. Hence, the dragging forces during scanning are greatly reduced leading to less damage of the sample. During oscillation, the tip goes through both the attractive and the repulsive regimes of the tip-sample force field and it provides a higher resolution. In the present work we kept the focus on the semi-contact mode, except for the case of photovoltaic measurements where contact mode was employed.

In the semi-contact mode, three different images are obtained simultaneously. One that corresponds to the topography, the second one to the phase image which depicts the phase lag between the signal that drives the cantilever to oscillate by a piezoelectric driver, and the cantilever oscillation output signal. In phase image, a contrast can be interpreted by variations in surface properties as adhesion<sup>14</sup>; and an error signal image. The morphological analysis of the substrate surface and the thin film was carried out using atomic force microscopy (AFM, Smart SPM1000-AIST-NT Inc.) and silicon probes (Nanosensors, PPP-NCHR).

### 2.1.1. Piezoresponse Force Microscopy

Piezoresponse Force Microscopy (PFM) is a tool that has been extensively employed to characterize materials in the nanometer scale allowing to evaluate the ferroelectric properties by the inverse piezoelectric effect.<sup>14</sup> Ferroelectric properties of the films were investigated by means of a PFM module coupled to the AFM system (AFM, Smart SPM1000-AIST-NT Inc.) by using a soft conductive probe (HQ:NSC15/Pt-MikroMasch) as top electrode and a semi-contact technique called Top-PFM developed by AIST, where the probe is gently “scanned” over the sample surface in the semi-contact mode, applying an AC signal only when the tip is in “touch” with the sample generating an electric field under the tip which excites the ferroelectric domains locally due to the inverse piezoelectric effect. Top-PFM technique limits damage to both the sample and the probe by avoiding friction force. The piezoelectric response of the material leads to a mechanical movement of the cantilever and, taking into account the configuration previously shown in Figure 2.1, the laser will be reflected and detected by the photodiode.

### 2.1.2. Photoconductive Atomic Force Microscopy

In order to study the photovoltaic properties for the case of BiFeO<sub>3</sub>, photoconductive atomic force microscopy (PCAFM) was conducted using a conductive probe (HQ:NSC15/Pt-MikroMasch) in contact mode by illuminating the sample locally with a UV laser (355 nm) in order to read the photo-generated currents by the short circuit current (when the voltage is zero). The setup is shown in Figure 2.3.

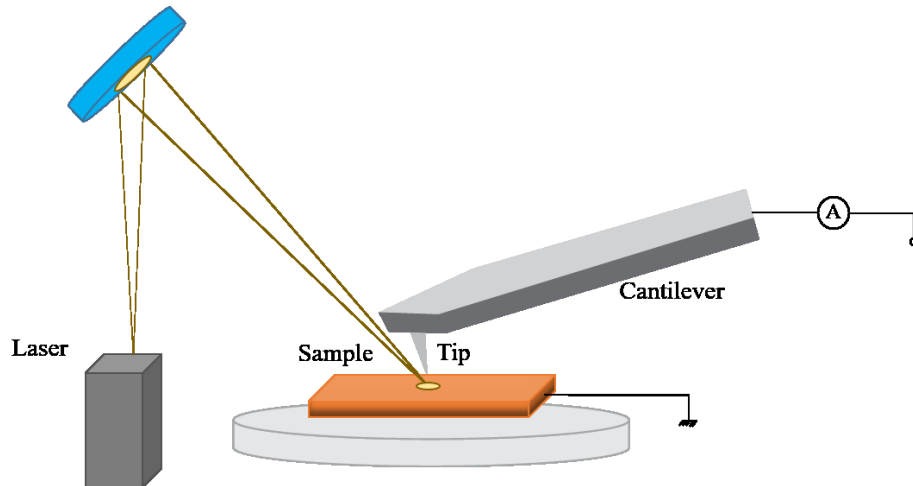


Figure 2.3: Setup for photovoltaic characterization (PCAFM); adapted from reference 56.

## 2.2. X-Ray Diffraction

Crystalline properties of the film were measured utilizing X-ray diffraction (XRD, Panalytical Xpert Pro, Cu  $K_{\alpha}$  radiation) in  $\theta$ - $2\theta$  mode and epitaxial character can be evaluated by means of  $\varphi$  scan mode. The crystallite size was calculated using Scherrer equation and lattice parameter out-of-plane was determined using the Nelson Riley extrapolation function.<sup>57</sup>

## 2.3. X-Ray Photoelectron Spectroscopy

X-ray photoelectron spectroscopy (XPS) is a very surface sensitive characterization tool which provides valuable quantitative and chemical state information from the variations in binding energies, or chemical shifts within a depth of 3 to 10 nm, and the identification of the elements in the sample can be made directly from the kinetic energies of the ejected photoelectrons:

$$E_K = h\nu - E_B - \phi \quad \text{Equation 2.9}$$

where  $E_K$  corresponds to the kinetic energy of ejected photoelectron,  $\phi$  the spectrometer work function,  $h\nu$  is the photon energy and  $E_B$  is the binding energy of the initial state of the electron<sup>58</sup>.

### 3. Strontium titanate surface preparation

This chapter discusses the existence of different chemical terminations on single crystal strontium titanate ( $\text{SrTiO}_3$ ) substrates and to realize single chemical termination on its surface to address epitaxial oxide thin film growth with uniform interface. In the case (100) oriented  $\text{SrTiO}_3$ , alternating layers of (SrO) and ( $\text{TiO}_2$ ) are separated by  $d_{100}/2$  ( $a/2=0.2$  nm) existing along  $\langle 100 \rangle$  direction and equivalent (SrO) or ( $\text{TiO}_2$ ) stacks separated by  $d_{100}$  ( $a/1=0.3905$  nm), where ‘ $a$ ’ is the lattice constant (0.3905 nm) of  $\text{SrTiO}_3$ . Similarly, in the case of (111) orientation alternately stacked layers ( $\text{SrO}_3$ ) $^{4-}$  and  $\text{Ti}^{4+}$  separated by  $d_{110}/2$  ( $a/2\sqrt{3}=0.113$  nm) exist along  $\langle 111 \rangle$  direction) and the equivalent ( $\text{SrO}_3$ ) $^{4-}$  or  $\text{Ti}^{4+}$  stacks separated by  $d_{111}$  ( $a/\sqrt{3}=0.225$ nm). In both (100) and (111) orientations, two adjacent layers contains either Sr or Ti only, even though the composition of the layers (in terms of O coordination) is different. However, in the case of (110) orientation, equivalent stacks are separated by  $d_{110}$  ( $a/\sqrt{2}=0.276$ nm) and adjacent ( $\text{SrTiO}$ ) $^{4-}$ - ( $\text{O}_2$ ) $^{4-}$  stacks separated by  $d_{110}/2$  (0.138 nm); suggesting both Sr and Ti exist together in one of the adjacent layers. In terms of polarity of the surface (110) and (111) are similar as they are charged polar surface, whereas (100) is a neutral surface. The aforementioned layers are restricted to the out-of-plane direction, i.e. direction perpendicular surface. The in-plane layers are discussed now as it concerns the morphology of surface, very important for the thin film deposition. In ideal cases, when the miscut angle is zero, which is the angle at which the surface is slanted with respect to the specified crystal plane, the cleaved single crystal surface is terminated with one of the layers and hence it will be always single chemically terminated allowing a uniform epitaxial interface. However, the substrate miscut is unavoidable when a single crystal is cut for a particular orientation and polished, with the macroscopic top surface misoriented (in-plane as well as out-of-plane) with respect to the closest low index (hkl) plane.<sup>59</sup> So in real case, single crystal substrate surfaces are composed of step-terrace features as can be seen in Figure 3.1. For a surface with terraces of average width  $L$  and separated by steps of height  $H$ , the out-of-plane miscut angle (so-called: miscut angle,  $\alpha$ ) is defined as  $\alpha = \text{atan}(H/L)$  and the in-plane miscut angle (so-called: miscut direction,  $\phi$ ) is defined azimuth angle  $\phi$  of the step with respect to the closest crystal direction with lower step energy, which are schematically shown in Figure 3.1.<sup>59</sup>  $H$  is the multiple of interplanar distance ( $d_{hkl}/2$ ) along the  $[hkl]$  direction, the value of which determine the difference

---

or the similarity of the chemical composition of two adjacent terraces and in short the surface termination in general as discussed below.

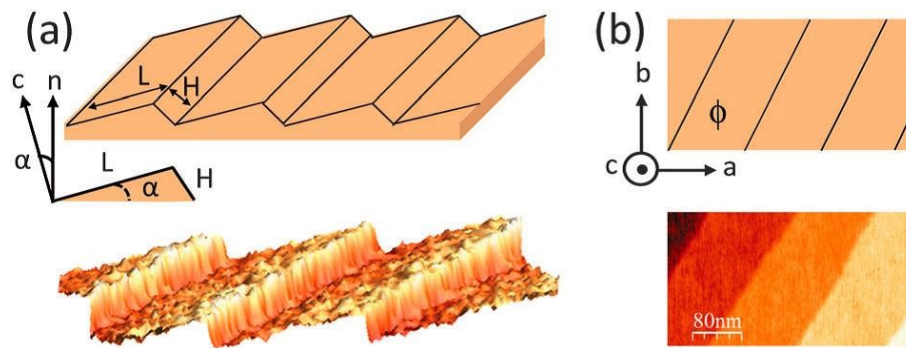


Figure 3.1: Sketch of a miscut substrate. (a)  $L$ ,  $H$  and  $\alpha$  are the terrace width, step height, and miscut angle respectively. (b) Sketch of a vicinal surface where the steps present an overall in-plane misorientation  $\phi$  with respect to the main crystallographic direction parallel to “a” axis. Adapted from reference 59.

$\text{SrTiO}_3$  substrates with low miscut angle ( $0.05^\circ < \alpha < 0.3^\circ$ ) corresponding to terrace widths in the 70-500 nm) are available. As we know, one of the prerequisites for high quality epitaxial thin film growth on  $\text{SrTiO}_3$  substrate with uniform interfacial properties is the realization of single-termination and atomically flat surfaces. As-received low miscut angle  $\text{SrTiO}_3$  substrates from the vendor consist of mixed termination and are characterized with  $d_{hkl}/2$  step height between adjacent terraces (or odd multiple of  $d_{hkl}/2$ ). A step height of  $a$ ,  $a/\sqrt{2}$  and  $a/\sqrt{3}$  (or multiples of them) for (100), (110) and (111), respectively, ensure single termination on the surface.

Figure 3.2 depicts the three different crystallographic orientations of  $\text{SrTiO}_3$ , (100), (110) and (111) with interplanar spacing of  $a$ ,  $a/\sqrt{2}$ , and  $a/\sqrt{3}$  corresponding to single termination for the two different chemical terminations.

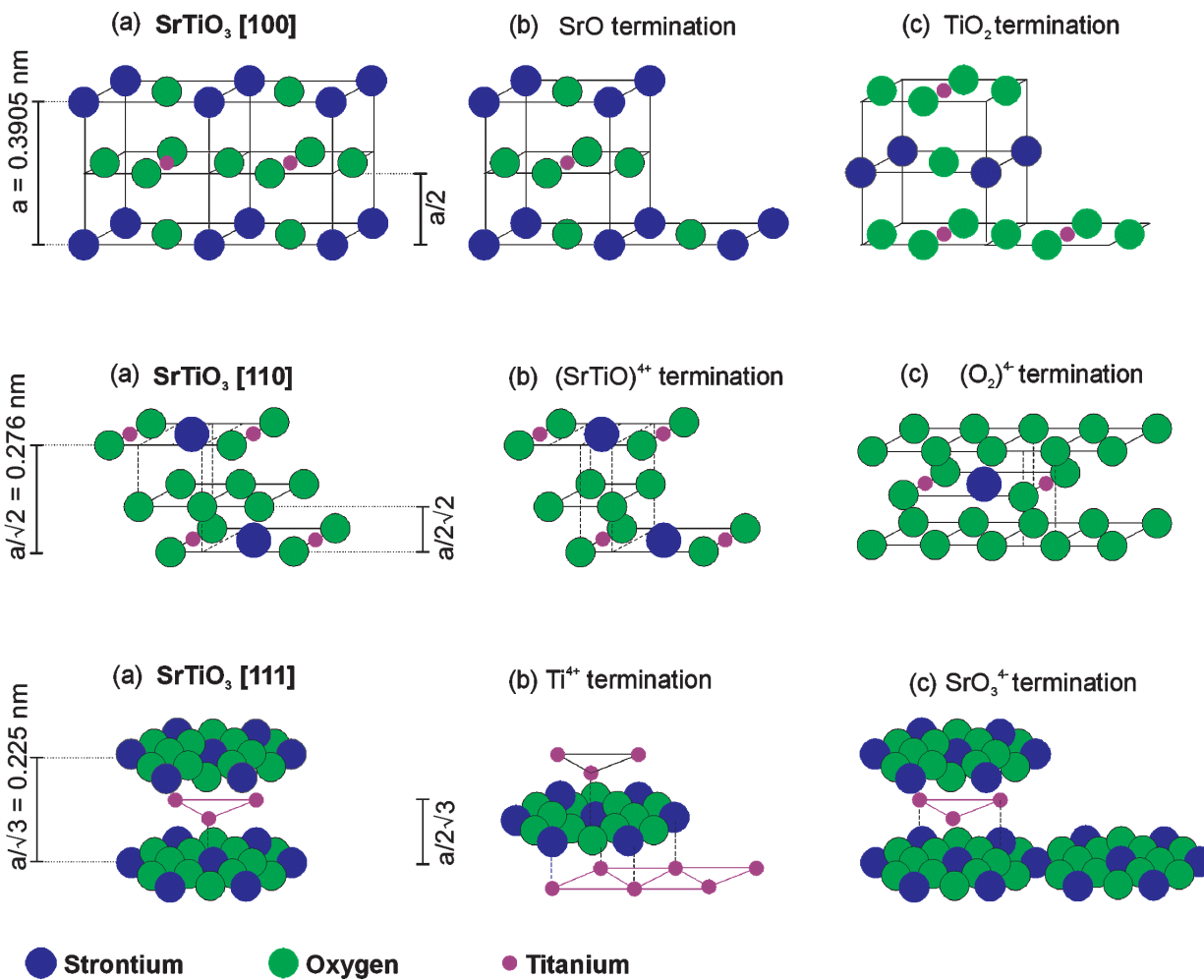


Figure 3.2: Depicts the three different crystallographic orientation of  $\text{SrTiO}_3$ , [100], [110] and [111] with interplanar spacing of  $a$ ,  $a/\sqrt{2}$ , and  $a/\sqrt{3}$ , where  $a = 0.3905 \text{ nm}$ .

Out of the three aforementioned surfaces, the orientations that allow selective chemical etching to realize single termination are [100] and [111] due to the fact that each alternate layer contains either Sr or Ti compounds. In contrast,  $\text{SrTiO}_3$  (110) contains  $(\text{SrTiO})^{4+}$  and  $(\text{O}_2)^{4-}$  stacks normal to the (110) plane, and hence preferential etching may not serve the purpose in comparison to the (100) and (111) surfaces. This chapter discusses a novel route for the preparation of such

surfaces on pure and Nb doped SrTiO<sub>3</sub> substrates of all three orientations. The preparation consists of a two-step process: a chemical etching followed by an annealing in O<sub>2</sub> atmosphere which minimize reduction and the atomic arrangement for thermodynamic equilibrium on the surface and the step edge can be uniform.

### 3.1. Experimental details

A microwave assisted hydrothermal etching technique was adopted for the surface preparation as a safer and less expensive alternative to the standard procedure that consisted in the immersion of the substrate in a buffered-HF<sup>44</sup>. The schematic diagram of the microwave compatible hydrothermal reactor used for the SrTiO<sub>3</sub> substrate etching is shown in Figure 3.3. It consist of a polytetrafluoroethylene (PTFE) cup (from Parr Instrument) which is the container for the etching medium and a home built substrate holder (custom designed for holding multiple substrates) which is attached to the lid of the aforementioned cup. This substrate holder/etchant cup assembly ensured stable positioning of the substrate at one specific distance from the bottom of the cup during the entire hydrothermal processing. One side polished pure and Nb (0.5 wt. %) doped SrTiO<sub>3</sub> single crystal substrates (5 × 5 × 0.5 mm, miscut angle < 0.3° from Crystec GmbH) were used. Both, neutral (deionized water, pH 7) and basic (10% ammonium hydroxide (Sigma-Aldrich >99.99%) solution, pH 10), conditions were used. Substrates were kept inside the PTFE cup at a distance of 1 cm from the bottom with the polished side facing down. This face down positioning reduces particle contamination and re-adsorption on the surface. The Teflon O-ring attached to the cup cover develops and maintains a tight seal without heavy pre-loading. This sealed cup/substrate assembly was then housed into a polymer autoclave (microwave digestion bomb from Parr Instrument: Model 4781) to ensure overpressure while heating the solution with microwave energy. The temperature and pressure generated within a microwave bomb are solely depended upon the filling level, time of exposure and the power level. In the present case, the volume fill factor of the etching media was fixed at 66% of the total volume of the cup. The microwave oven used for the heating was a commercial kitchen microwave (Panasonic Inverter) which provides a continuous microwave irradiation (non-duty-cycle). Duty cycling the power ON and OFF is a common low cost method in most of commercial microwave ovens in which the power level is always at maximum power during the ON time<sup>60</sup>. The average power level is based

---

on the amount of ON time vs. OFF time and this power control is not good in the case of the hydrothermal process since, as shown in *Figure 1.13*, small changes in temperature would represent a big variation in the pressure and the process would not be uniform. The vessel is always placed in the center of the rotating plate with an output power level was fixed at 360 W and time of microwave exposure was 3 and 4 minutes, respectively, for the ammonium hydroxide solution and for DI water (Resistance > 10 M $\Omega$ ) media. The reactor was kept in the microwave oven after the heating cycle for a period to allow the internal pressure to drop significantly and to then submerge the lower part of the reactor in water to accelerate cooling down to room temperature.

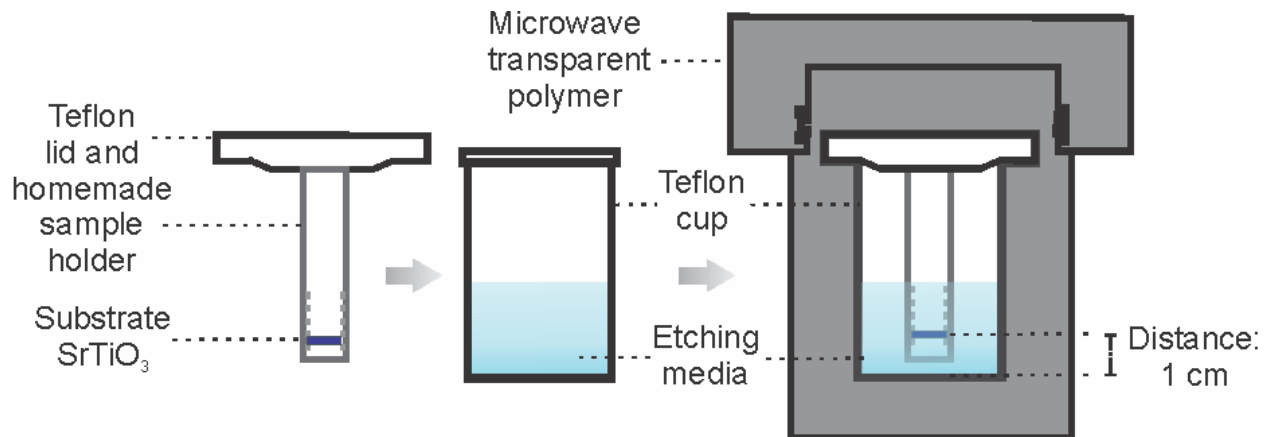


*Figure 3.3: Experimental setup showing a cross-section of the microwave-compatible hydrothermal reactor.*

Eventually the etched substrates were annealed at 1000°C-1100°C for various time in a programmable tube furnace (from MTI Corporation) under oxygen flow of 80 sccm and allowed furnace cooling to room temperature. The topography of the substrate was then analyzed by Atomic Force Microscopy, AFM (Smart SPM1000-AIST-NT Inc.) in tapping mode. Silicon cantilever tips (Model PPP-NCHR from NANOSENSORS™) with typical tip radius < 8 nm, length 125  $\mu\text{m}$  and tip height 10-15  $\mu\text{m}$  have been used. Sr and Ti contents on the substrate surface were determined with X-ray photo-electron spectroscopy (VG Escalab 220i XL) using Al K $\alpha$  (1486.6 eV) radiation from a monochromatic x-ray source operating at 400 W. Spectra were calibrated using carbon by assigning the binding energy of 284.6 eV to the C1s peak position to

compensate for a possible shift in the peak position due to charging effects.<sup>61</sup> Commercially available (100, 110 and 111) oriented SrTiO<sub>3</sub>, pure and 0.5 % wt. Nb doped SrTiO<sub>3</sub> single crystal substrates of 5 x 5 x 0.5 mm, (CrysTec GmbH, miscut angle < 0.3°) were used for the present study.

### 3.2. SrTiO<sub>3</sub> (100)

SrTiO<sub>3</sub> with the crystallographic direction (100) is widely used as a substrate for the heteroepitaxial growth of high T<sub>C</sub> superconductors<sup>62</sup>, colossal magneto-resistance manganites<sup>63</sup>, multiferroics<sup>64,65</sup> and other complex perovskite oxides<sup>66,67</sup>. Recent discoveries of various electronic properties<sup>35,68,69</sup>, 2D electron gas (2DEG)<sup>70</sup>, superconductivity<sup>71</sup>, ferromagnetism and magnetoelectric effects at the interface of complex oxides<sup>72,73</sup> stimulated additional research in this field. One of the procedures to obtain atomically flat step-and-terrace structures with single chemical termination is by immersion of the SrTiO<sub>3</sub> substrate in a buffered hydrofluoric (HF) solution to selectively remove one chemical termination, followed by an O<sub>2</sub> annealing at elevated temperatures to obtain a sharp well-arranged single chemically terminated surface.<sup>44,45</sup> Another method avoids this fluorine contamination by replacing HF with boiling DI H<sub>2</sub>O and optimizing the time-temperature product of the annealing step.<sup>39</sup> Ohnishi et al.<sup>74</sup> have reported an enrichment in Sr close to the surface layer upon heating to 1000°K in air by means of electron spectroscopy resulting in a possible partial coverage of the surface with SrO. Direct investigations of the (100) surface by atomic force microscopy<sup>75</sup> however revealed that even at 1600°K, the surface had to be exposed for 12 to air in order to achieve a partial SrO termination and 72h for a complete SrO termination.

Figure 3.4 depicts the evolution of surface morphology as revealed by the AFM of the undoped SrTiO<sub>3</sub> (100) single crystal substrate at different stages of the microwave-induced hydrothermal etching and annealing processes. As can be seen from Figure 3.4a, the sample surface of the as-received substrate is featureless due to physisorbed contamination. Figure 3.4b depicts the surface topography of the substrate after the hydrothermal etching. Terraces with  $3.90 \pm 0.1 \text{ \AA}$  in height, corresponding to one unit cell within experimental errors, are observed. For the aforementioned reasons, we presume that the given conditions strongly favour a TiO<sub>2</sub> termination.

Figure 3.4c illustrates the AFM surface topography of the substrate, which undergoes microwave-induced hydrothermal etching in water for 3 min followed by the oxygen annealing at 1000°C for 10 min. As can be seen from this subfigure, the topography shows a clear step-terrace structure with sharp steps of  $3.90 \pm 0.1 \text{ \AA}$  in height and smooth step edges. Additionally, the phase image of the same scan of the topography shows uniform contrast, and hence confirms one chemical termination (Figure 3.4d).

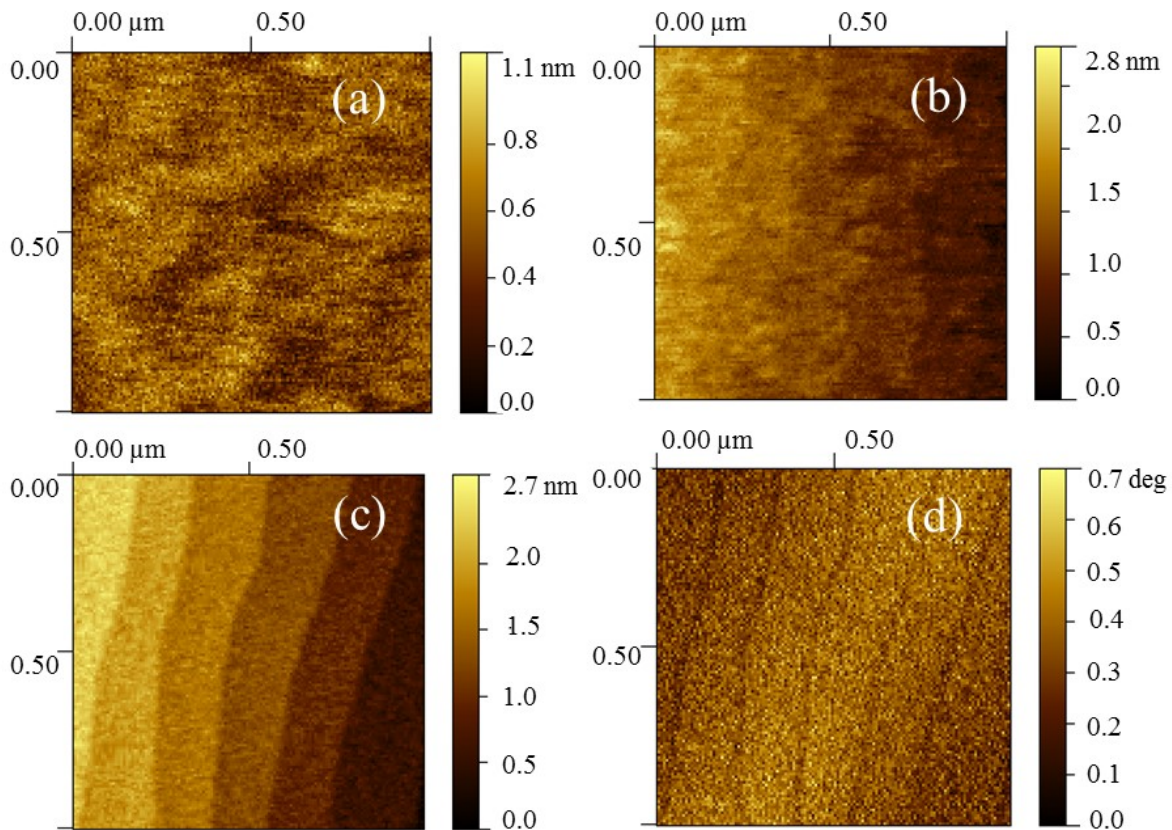


Figure 3.4: (a)  $\text{SrTiO}_3$  (100) single crystal substrate as-received; (b) hydrothermally etched in water; (c) hydrothermally etched in water followed by an annealing step, and (d) its corresponding phase image depicting single chemical termination.

We further extended this preparation procedure to niobium doped (0.5 wt. %)  $\text{SrTiO}_3$  (100) substrates as well. This metallic/semiconducting substrate is of substantial technological interest as conducting bottom electrode for many applications and in itself still subject of intense

research.<sup>76</sup> Figure 3.5 depicts the evolution of the surface topography of SrTiO<sub>3</sub>:Nb (100) substrates at various stages of the surface preparation processes obtained by means of AFM in tapping mode. As can be seen from Figure 3.5a, for the as-received sample, no surface features are detectable, similar to the undoped SrTiO<sub>3</sub> (Figure 3.4a) surface. Figure 3.5b shows the substrate surface after etching alone, and the result is again similar to the undoped SrTiO<sub>3</sub> (Figure 3.4b) with a step height of approximately 0.4 nm. Finally, Figure 3.5c, which corresponds to the substrate surface that was hydrothermally etched in water and subsequently annealed, shows the final result, a step height of  $4.0 \text{ \AA} \pm 0.1$  and smooth terrace edges. The slight increase in the step height compared to the undoped SrTiO<sub>3</sub>, is attributed to an increment of the lattice parameter upon niobium doping. The AFM phase image (Figure 3.5d) of the same scan shows uniform contrast, which independently confirms single termination. Undoped and niobium-doped SrTiO<sub>3</sub> (100) surfaces have thus been treated by this technique.

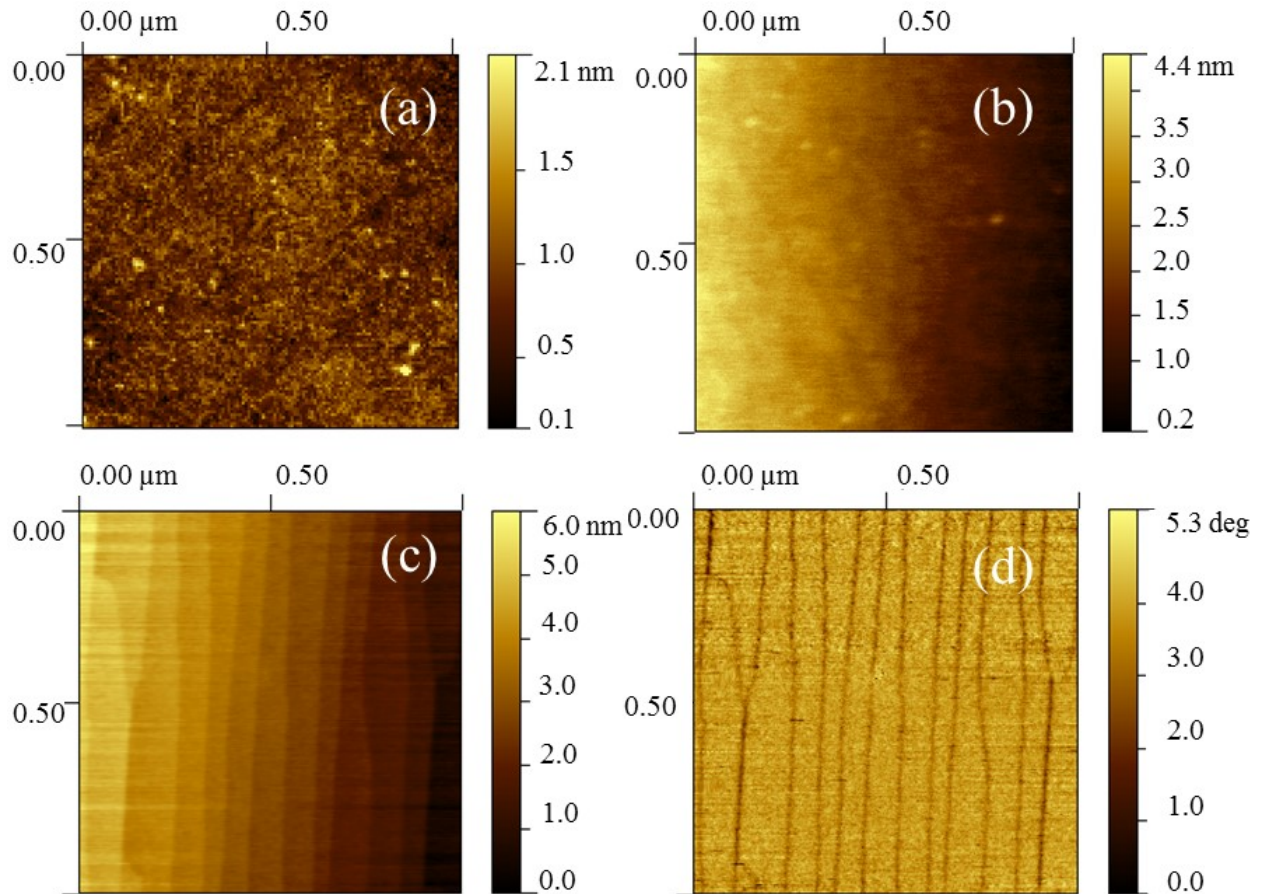


Figure 3.5: (a)  $\text{SrTiO}_3\text{:Nb}$  (0.5 wt. %) (100) as-received; (b) hydrothermally etched in water only; (c) hydrothermally etched in water after thermal treatment and (d) its corresponding phase image depicting single termination.

For comparison, a  $\text{SrTiO}_3\text{:Nb}$  (0.5 wt. %) (100) single crystal substrate was also processed in boiling water following the recipe of Chambers, et al<sup>46</sup>. However, instead of using 30 min as they suggested, we used 3 min for direct comparison with the microwave-induced hydrothermal etching in order to see the effect of processing time on the surface evolution. In this case, the observed step height was  $2.0 \text{ \AA} \pm 0.1$ , which corresponds to half a unit cell, indicating incomplete etching. This comparative study shows the effectiveness of microwave treatment in water through a substantially reduced etching time thus making the  $\text{SrTiO}_3$  substrate cleaning process faster.

### 3.3. SrTiO<sub>3</sub> (110)

Even though less used for the epitaxial growth of multifunctional oxides, (110) oriented SrTiO<sub>3</sub> substrates are gaining importance in Josephson junctions, controlling the magnetic anisotropy and stabilizing the charge-ordered phases.<sup>77-79</sup> More specifically, SrTiO<sub>3</sub> (110) substrates ensure (110) growth of YBCO high temperature superconducting films, important for the fabrication of superconducting/normal-conducting/superconducting Josephson junctions because of the longer coherence length parallel to the CuO/(001) planes which are then normal to the interface.<sup>80</sup> It can also be used in controlling interface states arising from polarity discontinuities in Perovskite heterostructures, e.g. SrTiO<sub>3</sub>/LaAlO<sub>3</sub>.<sup>81</sup> Again, the misfit dislocations of anisotropic magneto-resistant Nd<sub>0.45</sub>Sr<sub>0.55</sub>MnO<sub>3</sub> thin films grown on SrTiO<sub>3</sub> (110) substrate, modulate the properties of manganite films, which enables the tuning of Jahn–Teller distortion and thereby manipulate the metal–insulator transition.<sup>79</sup> Also, higher polarization of ~80 μC/cm<sup>2</sup> of (101) oriented BiFeO<sub>3</sub> thin films epitaxially grown on (110) oriented SrTiO<sub>3</sub> single crystal substrates has been reported, compared to the remnant polarization ~55 μC/cm<sup>2</sup> of (001) oriented BiFeO<sub>3</sub> films.<sup>82</sup> Hence, anisotropic polar SrTiO<sub>3</sub> (110) serves as a promising function tunable substrate for many technological applications.

As discussed before, SrTiO<sub>3</sub> (110) contains (SrTiO)<sup>4+</sup> and (O<sub>2</sub>)<sup>4-</sup> stacks normal to the (110) plane, and hence preferential etching may not serve the purpose in comparison to the (100) and (111) surfaces. However, atomically flat (110) SrTiO<sub>3</sub> surface with 0.27 nm step height were realized by annealing with and without the etching step.<sup>39,83-85</sup> The recipe which used annealing at 1000°C in reducing ultra-high vacuum (UHV) atmosphere showed terraces with surface steps of  $a/\sqrt{2}$ . However, other step heights, suggesting non-equivalent surface terminations have also been found.<sup>85</sup> In the case of air annealing above 1000 °C, zig-zag step step-terrace emerged with (110) unit cell heights and SrO segregation, which are increased in density with annealing temperature.<sup>84</sup> However, annealing in a vacuum chamber with low oxygen partial pressure ( $PO_2 = 5 \times 10^{-7}$  Torr) at 1000 °C for 1 h, and quenching down to room temperature to freeze the surface structure, resulted in straight step edges.<sup>84</sup> The recipe which considered chemical etching, used buffered acidic medium (Hydrofluoric acid solution) for selective etching (for 30 min) and that resulted SrTiO<sub>3</sub> (110) surfaces with a clear step-terrace structure upon annealing at 1000°C for 2-3 hrs.<sup>39</sup> The aforementioned recipes use ultra-high vacuum and long annealing time or hazardous HF acid. So

---

it will be interesting to find a method which does not require an ultra-high vacuum, long annealing time and avoiding F contamination on the surface.

Figure 3.6 and Figure 3.7 show the surface morphology of pure SrTiO<sub>3</sub> (110) substrates which had undergone a microwave assisted hydrothermal etching in water as well as in ammonia solution and O<sub>2</sub> annealing at various temperature and time.

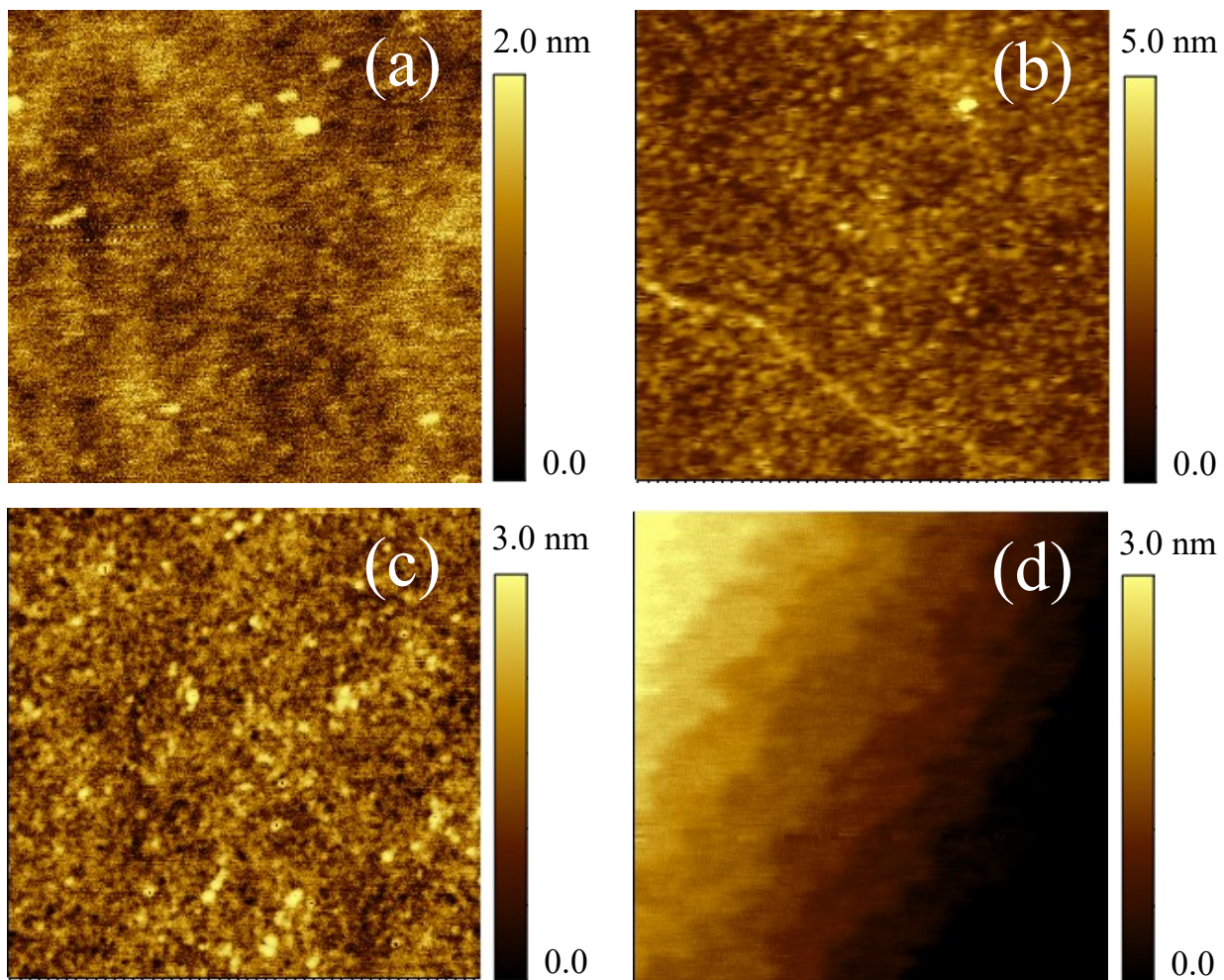


*Figure 3.6: AFM surface morphology ( $1 \times 1 \mu\text{m}^2$ ) of pure (110) SrTiO<sub>3</sub> surface; (a) as-received substrate, (b) annealed at 1000°C for 10 min; (c) after etched in DI water and (d) after annealing 'c' at 1000°C for 10 min.*

AFM studies revealed feature-less surface morphology with an average root-mean-square roughness around 7 and 9 Å (Figure 3.6a and Figure 3.7a) for the as-received pure SrTiO<sub>3</sub> (110) substrates. A direct annealing at 1000°C for 10 min (Figure 3.6b) and 30 min (Figure 3.7d) in oxygen atmosphere do not reveal either single-termination (step height=0.276 nm) or mixed termination (step height=0.138 nm), contrary to the zig-zag step like structures emergence with (110) unit cell heights (0.276nm) reported for single termination.<sup>84</sup> In fact after this annealing, the surface became rougher with some granular features, compared to the pristine sample, with the root mean square (RMS) roughness around 13 Å and 19.9 Å (Figure 3.6b and Figure 3.7b) for the film annealed at 1000°C for 10 min and 30 minutes, respectively. In order to understand the composition of this granular structures we performed XPS analysis on the surface corresponding to Figure 3.7b.

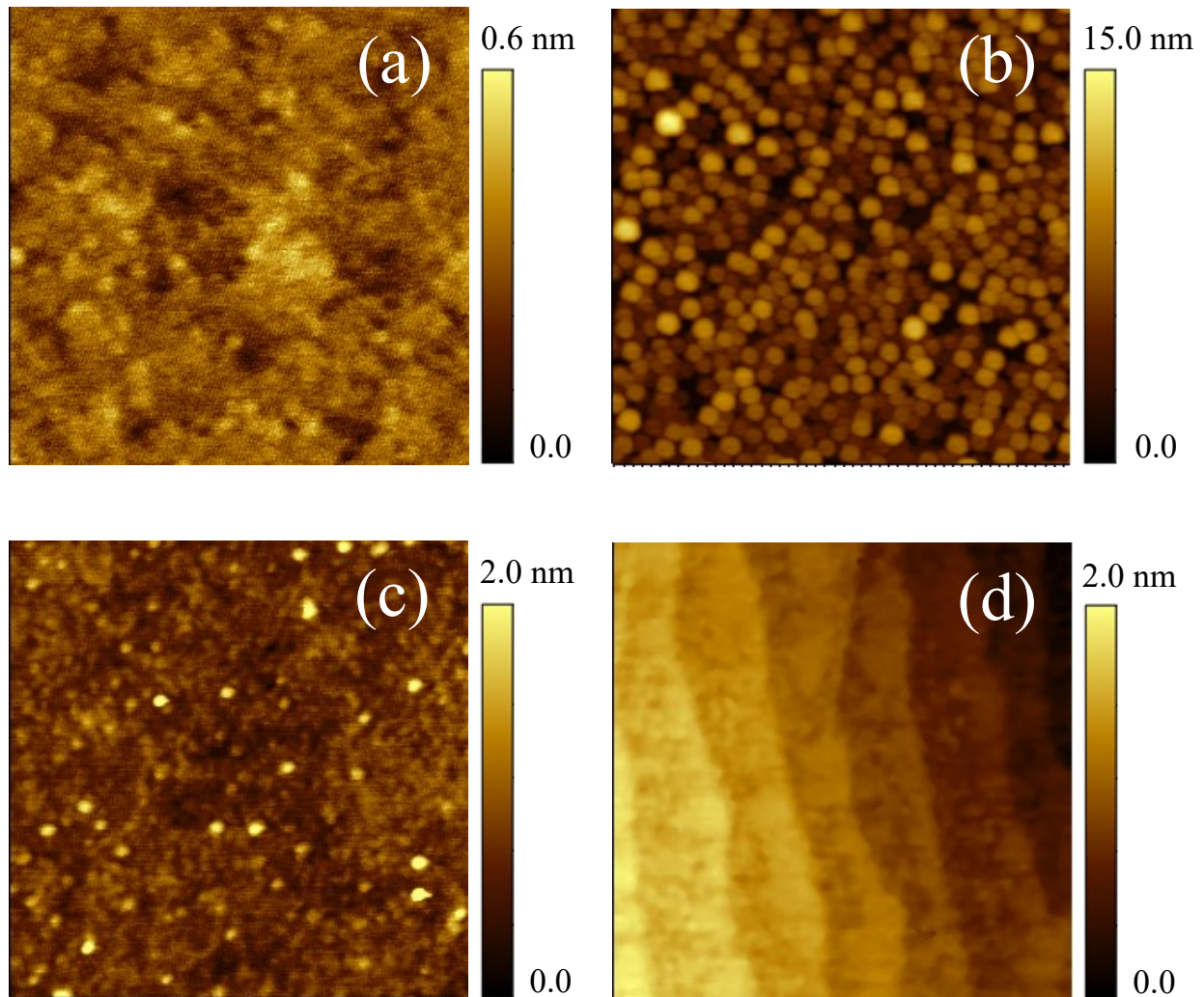


Figure 3.7: AFM surface morphology ( $1 \times 1 \mu\text{m}^2$ ) of pure (110)  $\text{SrTiO}_3$  surface (a) as-received substrate; (b) annealed at  $1000^\circ\text{C}$  for 30 min; (c) after etched in ammonia solution and (d) after annealing 'c' at  $1000^\circ\text{C}$  for 10 min.

A survey scan (Figure 3.8a) from 1300 eV to 0 eV revealed the presence of Sr, Ti, O and C (contaminant) at the substrate surface that went for an annealing at  $1000^\circ\text{C}$  for 30 minutes. Additional high resolution scans (Figure 3.8b, Figure 3.8c and Figure 3.8d) were performed in the selected binding energy ranges for  $\text{Ti}_{2p}$ ,  $\text{Sr}_{3d}$  and  $\text{O}_{1s}$  to determine the elemental composition on the substrate surface. No curve fitting was necessary. As it can be seen from Figure 3.8b, Ti  $2p$  consists of two peaks of Ti  $2p_{3/2}$  (457.8 eV) and Ti  $2p_{1/2}$  (463.5 eV) due to Ti-O bonds. In

Figure 3.8c, the two peaks, which are observed at 132.8 and 134.4 eV are due to Sr  $3d_{5/2}$  and Sr  $3d_{3/2}$ , respectively due to the Sr-O bonds. The peak at 530 eV in Figure 3.8d is attributed to the main peak of O ( $1s$ ) atoms in the lattice of SrTiO<sub>3</sub> and the peak at 532.3 eV can be attributed to the chemically adsorbed O<sup>86</sup>. The atomic concentrations were determined based on the peak areas and the relative sensitivity factors 5.05, 7.81 and 2.93 of Sr $3d$ , Ti  $2p$  and O $1s$ , respectively.

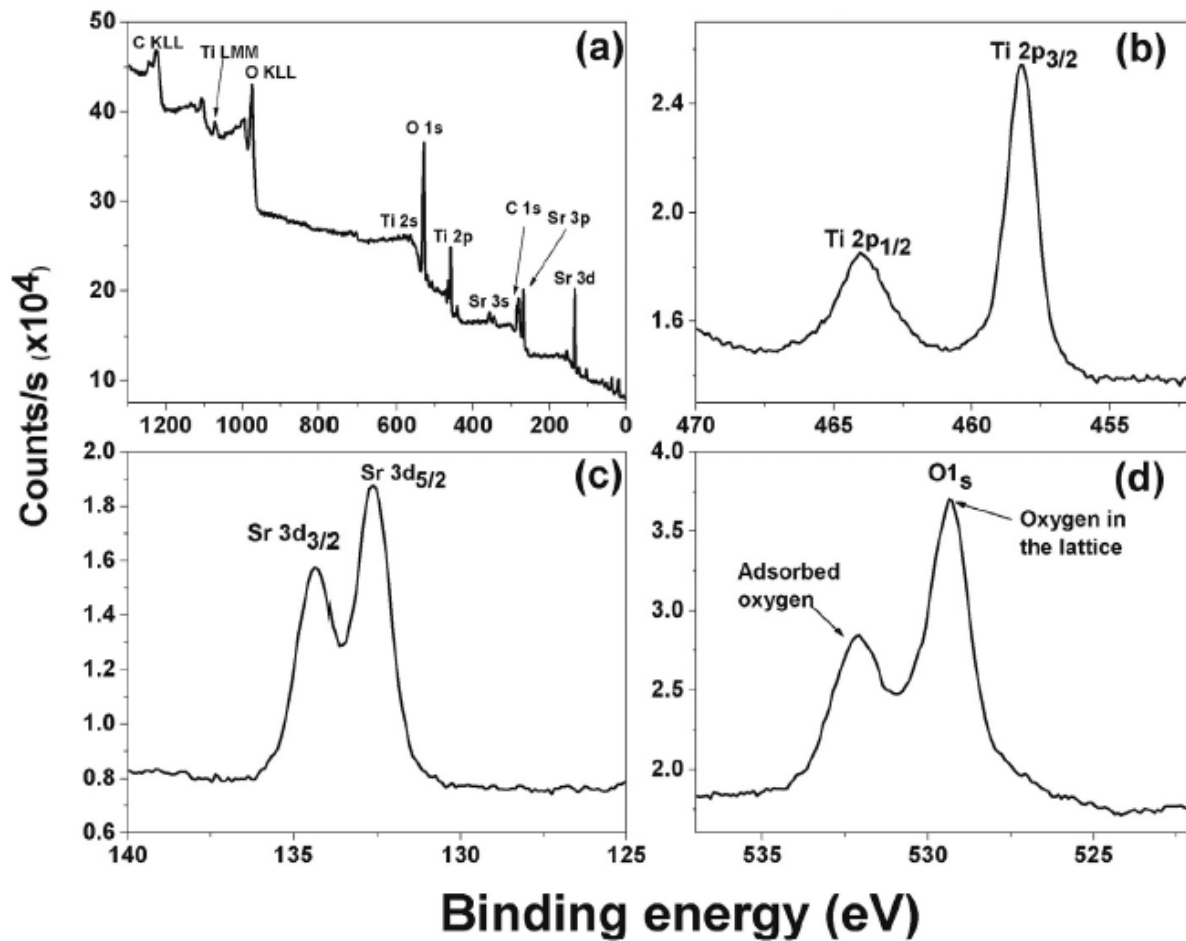


Figure 3.8: XPS spectra of SrTiO<sub>3</sub> (110) substrate annealed at 1000 °C for 30 min: (a) survey, (b) Ti 2p, (c) Sr 3d and (d) O 1s

The Sr/Ti ratio on the surface of this annealed SrTiO<sub>3</sub> (110) surface with granular features were ~ 1.5; thus showing a significant Sr enrichment on the surface. Also, it has been reported that a relatively higher amount of oxygen is adsorbed on the BaO surface compared to the TiO<sub>2</sub> surface in BaTiO<sub>3</sub>.<sup>86</sup> So based on the presence of higher Sr content on the surface and a higher amount of

chemically adsorbed O, we can explain the surface morphology as follows. During heat treatment in oxygen-rich atmospheres, SrO phases appear on top of these surfaces<sup>87</sup> and growth of this phase may be responsible for the observed granular features on the (110) surface. Our efforts in increasing the temperature resulted in enhanced granular growth and hence restricted the temperature to 1000°C for pure STO (110) substrates.

As the next step, hydrothermal etching in DI water and ammonia solution were performed on the pristine samples and corresponding surface morphology is depicted in Figure 3.6c and Figure 3.7c. Such etching procedures selectively etch SrO rich phases and suppress/reduce the granular growth of the same during annealing. Surface morphology has not changed much from the virgin substrate surface except for an increase in the RMS roughness around 1.8-2.6 Å (Figure 3.6c and Figure 3.7c). The higher roughness might be due to the selective removal of one of the cation compound from the surface, presumably Sr compound, as the solubility of the Sr containing compound is higher in hydrothermal condition compared to Ti containing compounds.<sup>88</sup> In fact such an etching of (100) resulted in steps with 0.3905 nm (single terminated TiO<sub>2</sub> surface) in height even though the terrace was not fully formed or clear, suggesting varying reaction of (100) and (110) with the etchant.<sup>88</sup> However, an annealing in oxygen atmosphere at 1000°C for 10 min results in the appearance of zig-zag steps with a height of  $\sim a/\sqrt{2}$  Å, indicate that the surface has one termination, either (O<sub>2</sub>)<sup>4-</sup> or (SrTiO)<sup>4+</sup> layers. Figure 3.6d and Figure 3.7d show these results with DI water and ammonia solution etching medium. As can be seen from the figure under identical processing conditions, the ammonia medium resulted in clearer step-terrace features compared to the DI water etched sample. The SrO segregation may be the reason for this contrasting behaviors for the water etched and ammonia etched substrates.<sup>84</sup>

The observed favorable features of ammonia based etching route is due to more SrO removal compared to DI water based etching route and that in turn reduces SrO granular growth or its segregation. It seems a SrO depleted surface layer prior to annealing is necessary for the termination of (SrTiO)<sup>4+</sup> or O<sub>2</sub><sup>4-</sup> phase at the surface in the case of (110) oriented SrTiO<sub>3</sub> crystals. Also, alkaline medium is more preferable since SrO is a basic oxide (metal oxidation state < +4,

forms a base) and easily dissolve in water under hydrothermal condition. Compared to the pure and Nb doped SrTiO<sub>3</sub>(100) surface preparation<sup>88</sup>, the same experimental conditions and parameters resulted in single termination in the case SrTiO<sub>3</sub>(110) substrates also. However, in the case of Nb-SrTiO<sub>3</sub> (110), as can be seen below, the same conditions did not result in single termination.

Figure 3.9 and Figure 3.10 show the AFM surface morphology evolution of 0.5 wt.% Nb doped SrTiO<sub>3</sub> (110) substrates which had undergone a microwave assisted hydrothermal etching in water as well as in ammonia solution, respectively, and O<sub>2</sub> annealing at various temperature and time.

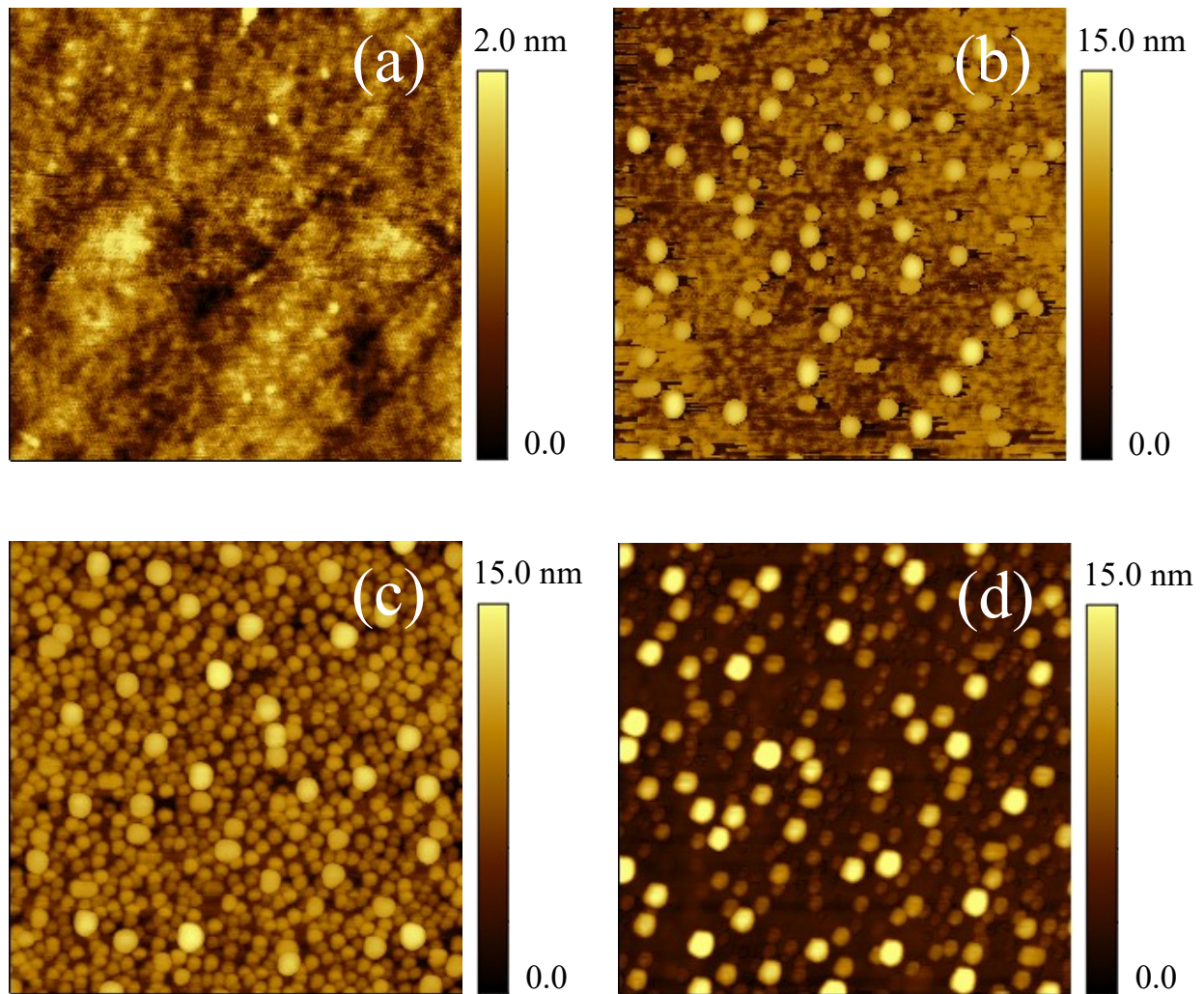
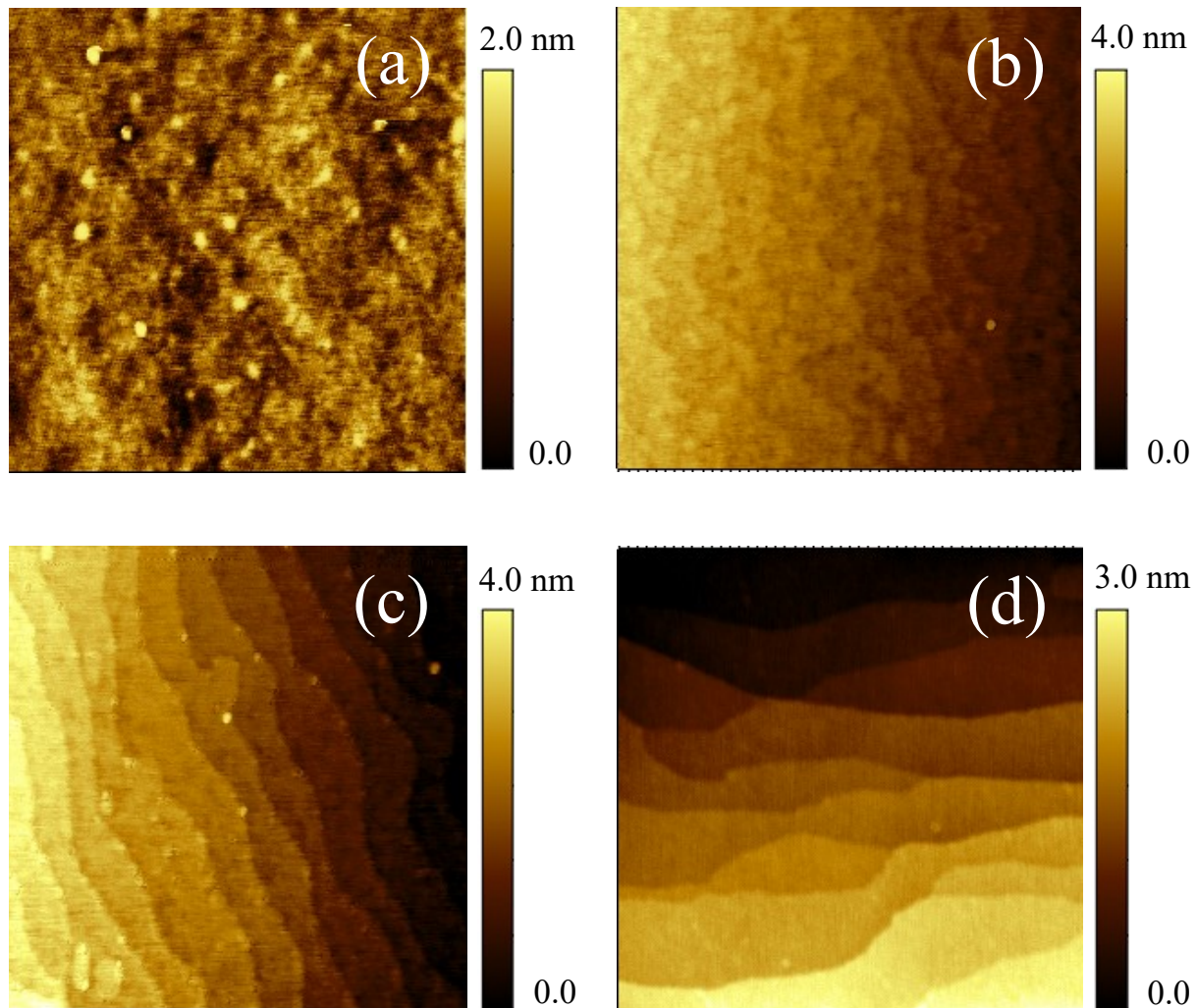


Figure 3.9: AFM surface morphology ( $1 \times 1 \mu\text{m}^2$ ) of Nb doped (110)  $\text{SrTiO}_3$  surface; (a) as-received substrate, (b) and (c) water etched substrate annealed at  $1000^\circ\text{C}$  for 10 min and 30 min, respectively, (d) water etched substrate annealed at  $1100^\circ\text{C}$  for 30 min.

As-received substrates (Figure 3.9a) have featureless surfaces with an RMS roughness around  $1.1 \text{ \AA}$  like undoped  $\text{SrTiO}_3$  (110) discussed before. But, unlike pure  $\text{SrTiO}_3$  (110) substrates, water etching and annealing does not result in the formation of step-terrace features at the surface of Nb doped  $\text{SrTiO}_3$  (110). Topographies of the water etched samples after annealing in  $\text{O}_2$  ambient at various temperature and time are depicted in Figure 3.9b to Figure 3.9d. SrO diffusion and grain growth occurred at  $1000^\circ\text{C}$  and that resulted in rougher surface with a RMS

roughness around 19.3 Å. The RMS roughness was determined by using the height to height correlation function (HHCF).



*Figure 3.10: AFM surface morphology ( $1 \times 1 \mu\text{m}^2$ ) of Nb doped (110)  $\text{SrTiO}_3$  surface (a) ammonia solution etched; after annealing 'a' at (b)  $1000^\circ\text{C}$  for 10 min, (c)  $1000^\circ\text{C}$  for 30 min and (d)  $1100^\circ\text{C}$  for 30 min.*

An increase of annealing time to 30 min at the same temperature resulted in more uniform circular grain growth with RMS roughness round  $20\text{\AA}$  (Figure 3.9c). Surprisingly, as the temperature further increased to  $1100^\circ\text{C}$  for 30 min (Figure 3.9d) some of the grain disappeared and new one start to grow on the surface, and that suggests that it is difficult to realize step-terrace

---

features on Nb-SrTiO<sub>3</sub> (110) surface with water etching and annealing. These observations were very different from what we had seen with undoped SrTiO<sub>3</sub> (110) discussed before (Figure 3.6) and Nb-SrTiO<sub>3</sub> (100) surface preparation<sup>88</sup>, where single termination was realized in water etched substrates. In fact, by Nb doping in SrTiO<sub>3</sub> system, Nb<sup>5+</sup> substitutes Ti<sup>4+</sup>, bringing more electrons into the system which improve the conductivity<sup>89</sup>. It is reported that in the case of donor doping in SrTiO<sub>3</sub>, Sr vacancies are predominant due to SrO phase segregation.<sup>90</sup> The complete failure of realizing the step-terrace structure in water etched Nb:SrTiO<sub>3</sub>(110) substrate surface and enhanced granular growth upon annealing might be the effect of SrO segregation discussed before. Excessive SrO phase on the surface restricts the restructuring of the surface upon annealing at elevated temperatures and it adversely affects the step-terrace formation. So the ammonia etching of Nb:SrTiO<sub>3</sub>(110) single crystal substrates can eliminate the possibility of excessive SrO on the surface prior to the annealing step and it will be discussed below.

Figure 3.10a to Figure 3.10d shows the results on etching in ammonia solution and annealing. As-etched sample did not show any particular features on the surface except an increase in the surface roughness compared to the as received substrate. Upon annealing this etched substrate at 1000°C for 10 min, a step-terrace feature started to form on Nb SrTiO<sub>3</sub> substrate (Figure 3.10b) with a step height 0.28 nm as expected for the (110) substrate with single termination. An annealing at the same temperature for 30 min resulted on even clearer step-terrace structure with a step height of 0.28nm. However, SrO segregation is also visible in this case (Figure 3.10c). A final annealing at 1100°C for 30 min (Figure 3.10d) was required to get sharper step and cleaner step and terrace structure, and less SrO segregation and resulting in a step height 0.28 nm with nearly perfect single termination in the case of Nb-SrTiO<sub>3</sub> (110) substrates, like pure SrTiO<sub>3</sub> (110). So the donor doping in SrTiO<sub>3</sub> enhances SrO segregation in the case of (110) Nb-SrTiO<sub>3</sub> surface compared to (100) Nb-SrTiO<sub>3</sub> and hence etching in ammonia and a higher annealing temperature and time are required for high quality single termination.

Polar strontium titanate (110) surface has non-zero dipole moment normal to the surface causing the (110) surface to have a diverging electrostatic surface energy and hence be unstable. Since truncation of the surface with either (SrTiO)<sup>4+</sup> or (O<sub>2</sub>)<sup>4-</sup> is energetically unfavorable, the surface has to undergo many changes with time to achieve a more stable, lower energy state. In order to understand the stability of the single-terminated surface we have studied the surface

---

morphology of the SrTiO<sub>3</sub> (110) surface (Figure 3.10d) and compared with the granular surface morphology (Figure 3.7b and Figure 3.9d) after 6 months.

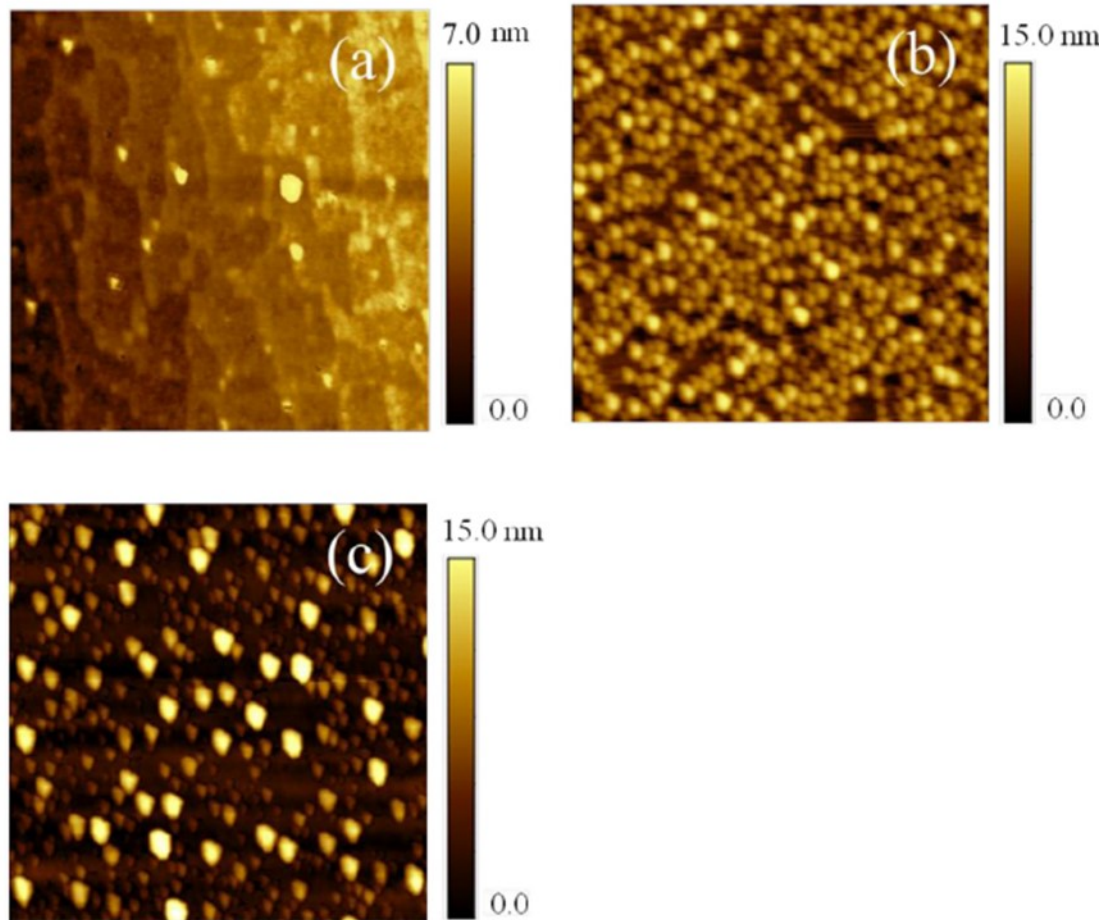


Figure 3.11: AFM surface morphology ( $1 \times 1 \mu\text{m}^2$ ) of the corresponding substrates of (a) Fig. 3.11d, Nb doped (110) SrTiO<sub>3</sub>; (b) Fig. 3.8b, (110) SrTiO<sub>3</sub>; and (c) Fig. 3.10d, Nb doped (110) SrTiO<sub>3</sub> surfaces after six months of storing in ambient atmosphere.

As can be seen from the Figure 3.11a, the ideal step-terrace surface feature obtained for the Nb:SrTiO<sub>3</sub> (110) is lost over this period of storing. However, the surface with granular features remained the same without much modification. XPS analysis showed the same Sr/Ti ratio (1.5) for the surfaces in Figure 3.11b and Figure 3.11c compared to the 6 month old surface (Figure 3.7b and Figure 3.9d), suggesting no stoichiometry or morphology changes with time. In contrast, for

---

the singly terminated surface, Sr/Ti changed to  $\sim 1.3$  from  $\sim 1$  suggesting stoichiometric changes with Sr enhancement on the surface and a significantly altered step-terrace morphology.

### 3.4. SrTiO<sub>3</sub> (111)

The SrTiO<sub>3</sub> (111) surface is ideal to grow metastable multiferroic phases, e.g. in GaFeO<sub>3</sub>-type AlFeO<sub>3</sub>, because the arrangement of oxygen ions along c-axis is similar to that for SrTiO<sub>3</sub> (111).<sup>91</sup> Epitaxial growth of SnO<sub>2</sub> films was realized on SrTiO<sub>3</sub> (111) and this perovskite wide band semiconducting binary oxide combination may give rise to the feasibility of hybrid device design.<sup>92</sup> In the case of epitaxial metallic film, SrTiO<sub>3</sub> and Pt have FCC stacking of the close-packed layers along the (111) directions that facilitates heteroepitaxial growth of Pt on SrTiO<sub>3</sub> (111).<sup>93</sup> (111)-oriented SrTiO<sub>3</sub> has also been successfully employed in creating 2DEGs at the interface with LaAlO<sub>3</sub> epilayer and high mobility of the confined electrons at the interface ensure faster nano-electronic devices.<sup>94</sup> Furthermore, the most important crystalline orientation in the perovskite system, in terms of the ability to use strain engineering and to fabricate superlattices, is the (111) direction as substrate and its single chemically terminated surface preparation are of utmost importance in the emerging field of oxide electronics. SrTiO<sub>3</sub> (111) surface with identical chemical termination on the terraces was realized mainly by two methods; (i) annealing at high temperature alone and (ii) chemical etching and subsequent annealing. Initial studies considered Ar-ion bombardment on the SrTiO<sub>3</sub> (111) single crystal and subsequent annealing under ultra-high vacuum (UHV) for realizing clean SrTiO<sub>3</sub> (111) substrate surface.<sup>95,96</sup> Annealing in UHV without any Ar<sup>+</sup> bombardment was considered next and that resulted in two different terminations; at a temperature  $\sim 1180^\circ\text{C}$ , the terminating layer was SrO<sub>3</sub> and at  $1220^\circ\text{C}$ , the outermost layer was Ti.<sup>97,98</sup> Also, in the case of annealing at  $1000^\circ\text{C}$  for 10h in oxygen atmosphere (no UHV), AFM observations suggested single termination (i.e. either SrO<sub>3</sub><sup>4-</sup> or Ti<sup>4+</sup> layer) on the (111) surface and a mixed terminations on the surface for annealing in argon gas on Nb doped SrTiO<sub>3</sub> (111).<sup>99,100</sup> These studies confirm the realization of single termination in (111) direction either under UHV or O<sub>2</sub> atmosphere by selecting a proper temperature for annealing and the polarity of (111) surface was discussed theoretically soon after.<sup>101</sup> However, (111) surface obtained after annealing under reducing/oxidizing conditions did not show a well-defined step-and-terrace structure. Also terrace and step-heights were not atomically smooth and uniform, respectively, and are characterized by

---

many triangular features.<sup>97,100</sup> Chemical compositions of the layers in the (111) direction are  $(\text{SrO}_3)^{4-}$  and  $\text{Ti}^{4+}$ , similar to SrO and  $\text{TiO}_2$  in the (100) direction (in terms of layers with the cation presence), where selective etching and annealing in  $\text{O}_2$  atmosphere resulted in atomically flat terraces with clear steps.<sup>39,88,102-104</sup> This combined procedure used for the (100) oriented  $\text{SrTiO}_3$  was applied to the (111) oriented  $\text{SrTiO}_3$  and that resulted in an atomically flat single chemically terminated (111) surface, and adopted as a standard recipe for the surface preparation.

The morphological evolution of  $\text{SrTiO}_3$  (111) surface towards the realization of step-terrace structure were systematically studied with atomic force microscopy. Surfaces of the as-received pure and Nb (0.5 wt. %) doped  $\text{SrTiO}_3$  (111) single crystal substrates after cleaning were imaged with AFM first and the results are shown in Figure 3.12a and Figure 3.12c. Both images revealed a featureless surface morphology with a root mean square (RMS) roughness about 0.1 nm, indicating an amorphous surface contamination. Growing films on such an ill-defined surface results in serious problems for the reproducibility and quality of the epitaxial oxide growth. Reproducible surface conditions of the substrate are the first step towards achieving epitaxy. As can be seen from Figure 3.12b and Figure 3.12d after annealing in  $\text{O}_2$  atmosphere at  $1000^\circ\text{C}$  for 10 min, step-terrace structure (typical roof-tile features) emerged on the surface with a step height of 0.115 nm and 0.112 nm, respectively, for  $\text{SrTiO}_3$  and Nb: $\text{SrTiO}_3$  substrates. Removal of the adsorbed layer along with the mobility and diffusion of surface atoms to obtain a lowest energy state leads to these configurations. However, in the case of single termination (identical chemical termination for all terraces) the expected step height is  $d_{111}=a/\sqrt{3}=0.225\text{nm}$ . Step-profile line scan shows adjacent terrace structures are having an average step height of 0.113 nm. This height is equal to  $d_{111}/2$ , corresponding to the transition between two different chemical terminations,  $(\text{SrO}_3)^{4-}$  and  $\text{Ti}^{4+}$  layers in the present case. Even though one could obtain step-terrace features with an RMS roughness  $\sim 40\text{pm}$  in the each terrace on the surface with annealing alone, the surface has a bimodal distribution of composition. Additionally, the observation of terraces with various width depends on the miscut angle as mentioned in equation 1.8.

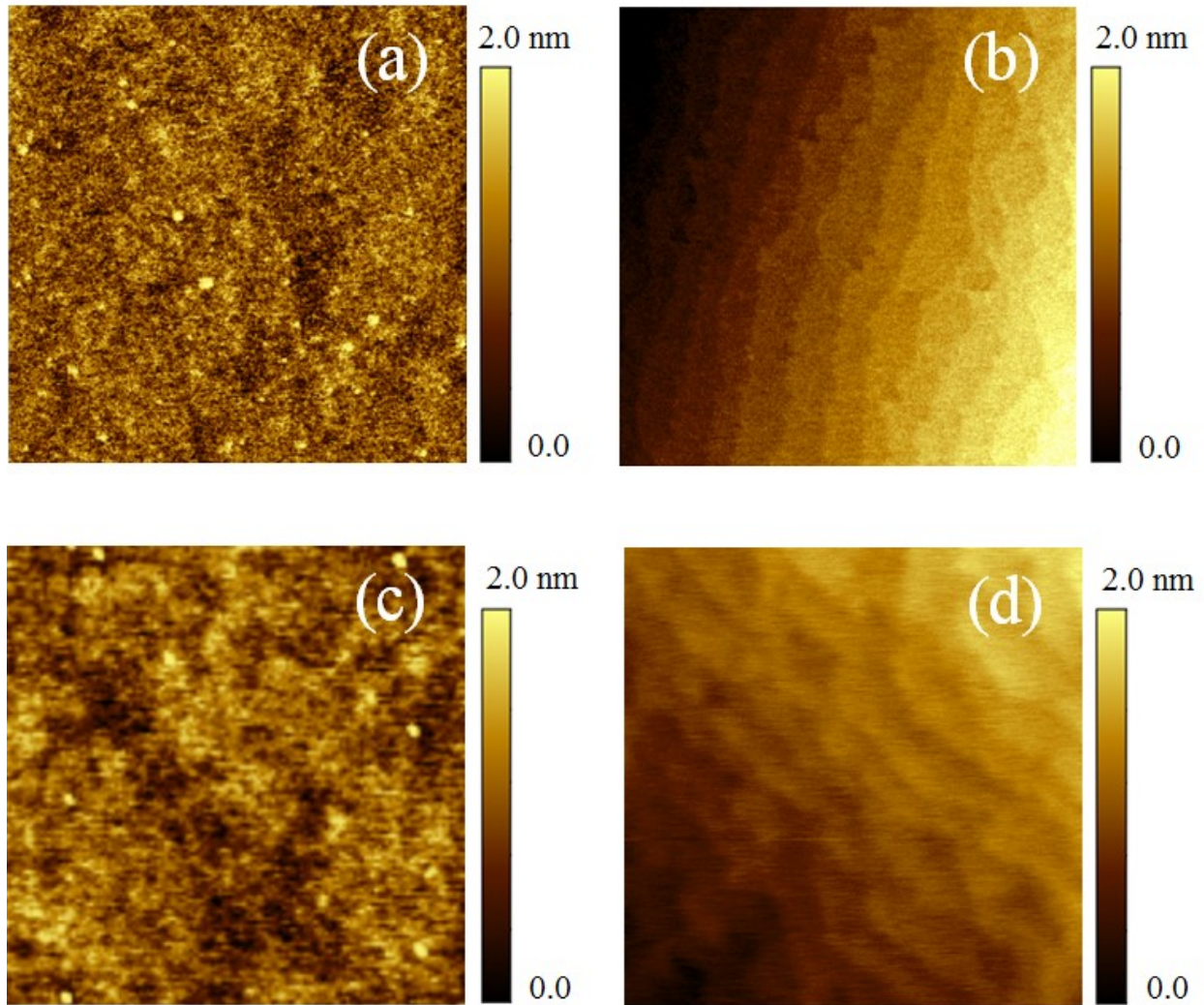


*Figure 3.12: AFM micrographs ( $1 \times 1 \mu\text{m}^2$ ) of the surface (a) as received  $\text{SrTiO}_3$  (111), (b) annealed at  $1000^\circ\text{C}$  for 10min; (c) as-received  $\text{Nb:SrTiO}_3$ (111), (d) annealed at  $1000^\circ\text{C}$  for 10 min.*

Figure 3.13 shows the surface morphology of the annealed  $\text{SrTiO}_3$  surface after etching in water and ammonia. These substrates were annealed at  $1000^\circ\text{C}$  for 10 min after the etching for 3 min and 4 min, respectively for ammonia and water etching media. We selected these optimized numbers based on a series experimental observation on substrates that undergone various etching and annealing time. The morphology of the surface shows a step height of 0.224 nm reveals a nearly perfect single termination of the atomically flat terraces with an RMS roughness  $\sim 40$  pm.

---

The larger number of terrace-step features in the case of ammonia etched substrate is due to the fact that this substrate had a larger miscut angle compared to the water etched one. Compared to Figure 3.12c, in Figure 3.12d step and terrace structure can be evidenced by more or less uniform terrace width. However, the edges were not straight as expected. Such observation of edges which are not parallel and with large density of kinks are due to high miscut direction (in-plane orientation of the steps).<sup>59</sup>

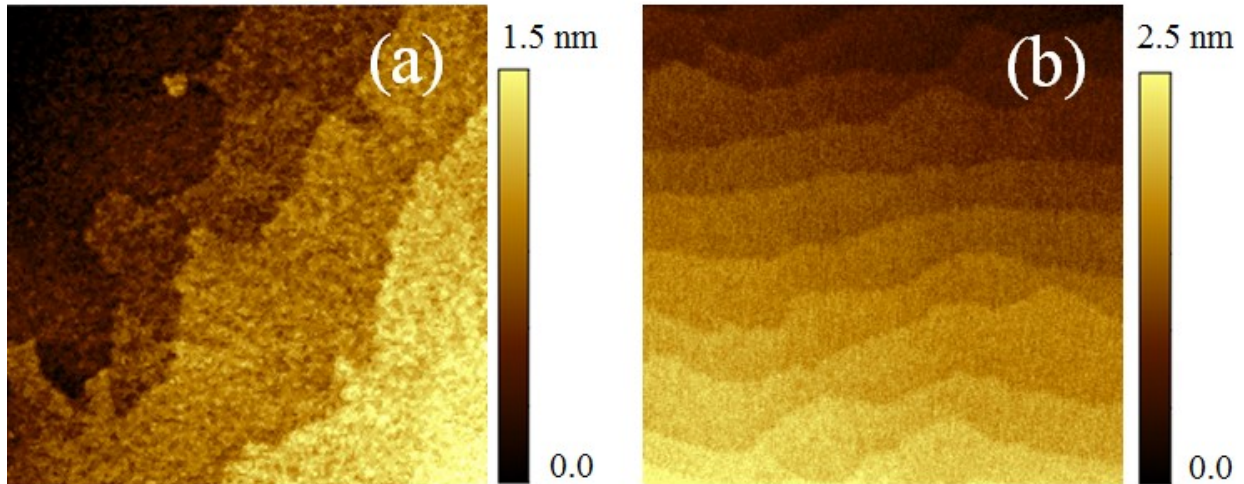
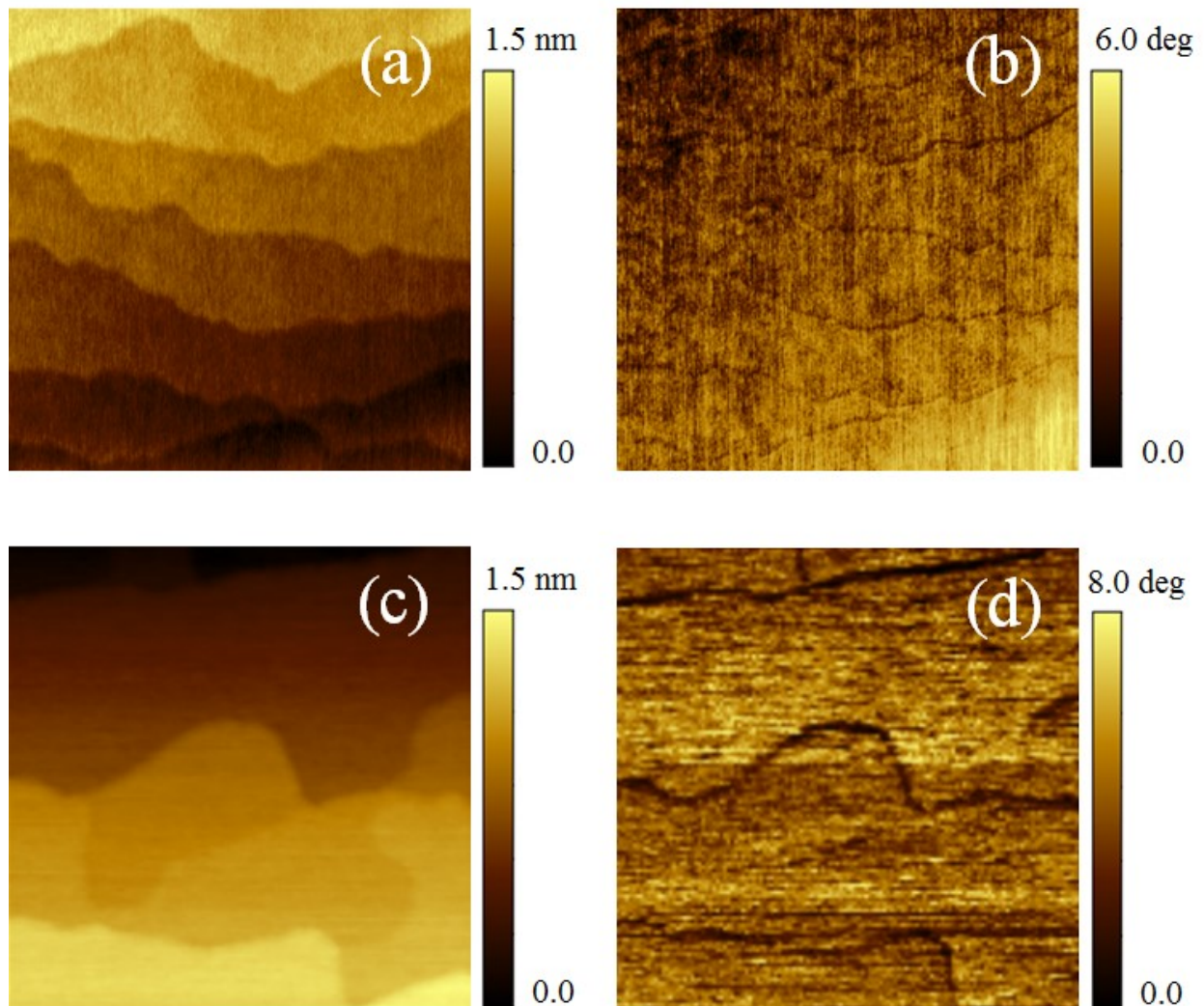


Figure 3.13:  $\text{SrTiO}_3$  (111) substrate surface ( $1 \times 1 \mu\text{m}^2$ ) annealed at  $1000^\circ\text{C}$  for 10 min after (a) etched in water and, (b) etched in ammonia.

So similar substrate preparation procedures, used for pure  $\text{SrTiO}_3$  (111), were also extended to the  $\text{Nb}:\text{SrTiO}_3$  substrate as well. Figure 3.14a and Figure 3.14c show the surface topography of  $\text{Nb}:\text{SrTiO}_3$  after annealing at  $1000^\circ\text{C}$  for 10 min for water and ammonia etched substrates, respectively. The line scan on this surface shows a step height of 0.23 nm as in the case of pure  $\text{SrTiO}_3$  (111) substrates, suggesting the realization of single termination on  $\text{Nb}:\text{SrTiO}_3$  substrate as well. The atomic flatness of the terraces is reflected in the obtained low RMS of roughness (30-40 pm) of the terraces. The phase in tapping mode is an indicator of adhesion forces on the surface and the contrast reflect different adhesion force due to different surface terminations. Phase scans in Figure 3.14b and Figure 3.14d of the corresponding topography scans show uniform contrast on the terrace, which independently confirms single termination. The observed phase

contrast at the edges is due to the step, a common artifact due to the sudden vertical movement of the tip to the next terrace.



*Figure 3.14: Surface morphology ( $1 \times 1 \mu\text{m}^2$ ) of Nb: SrTiO<sub>3</sub> (111) substrate annealed at 1000 °C for 10 min after (a) etched in water and, (b) shows the corresponding phase image; (c) etched in ammonia and (d) shows the corresponding phase image.*

### 3.5. Conclusion

A novel microwave-assisted hydrothermal etching was successfully applied to the surface preparation of pure and Nb-doped SrTiO<sub>3</sub> single crystals with (100), (110) and (111) orientations.

---

Without the possibility of fluorine contaminations from the Teflon liner and by avoiding the etching chemistry involved with HF widely used, the surface structure appears perfect within the limitations of the in-plane and out-of-plane miscut angles. These results indicate utilization of this method, without any corrosive chemicals during the preparation steps, to achieve atomically flat surface with single chemical termination of SrTiO<sub>3</sub> substrates. This technique is inexpensive, fast, safe, environmentally benign, compatible with batch processes, and showed remarkable reproducibility. Further, this method does not need an ultra-high vacuum environment and long annealing time at high temperatures. The possibility to reduce the etching time significantly avoids the formation of etch pits and holes on the substrate surface.

Pure and Nb-doped SrTiO<sub>3</sub> single crystal (100) substrates were singly terminated as evidenced by the step and terrace morphology with a step-height of  $d_{100}$  ( $a=0.3905$  nm) between two adjacent TiO<sub>2</sub> terraces, upon etching in water and annealing at 1000°C for 10 min. The shelf-time of this (100) surface is identical to that of HF-treated surfaces within experimental uncertainties. In the case of microwave hydrothermal process, the etching medium does not play a significant difference in the realization of single chemically terminated surfaces as both water and alkaline solution resulted in identical surfaces for (100). The importance of considering Nb doped SrTiO<sub>3</sub> substrates (metallic) is that is used as bottom electrode for metal-insulator-metal (MIM) configuration for vertical capacitor structures.

Pure and Nb doped SrTiO<sub>3</sub> single crystal substrates with (110) orientation, showed a step height  $\sim 0.276$  nm between adjacent terraces, a value matched very well to the  $d_{110}$  ( $a/\sqrt{2}$ ); suggesting identical chemical termination on the terraces. In the case of pure SrTiO<sub>3</sub> (110) substrates, etching in alkaline medium and annealing at 1000°C for 10 min resulted in better surface compared to the water based route. Interestingly, in the case of Nb doped SrTiO<sub>3</sub> (110) substrate step-terrace surface could not be realized with water based etching route at all, even at temperature as high as 1100°C. However, with etching in alkaline medium and annealing at 1100°C for 30 min, Nb doped SrTiO<sub>3</sub> (110) surface can also be made singly-terminated. Compared to the pure and Nb doped SrTiO<sub>3</sub>(100), the same experimental conditions and parameters resulted in single termination for SrTiO<sub>3</sub>(110) not in the case of Nb-SrTiO<sub>3</sub>(110). Etching medium, annealing temperature and time play a crucial role in the preparation of single chemically terminated pure and Nb doped SrTiO<sub>3</sub> (110) single crystals.

---

In the case of pure and Nb doped SrTiO<sub>3</sub> (111) surface, annealing of the as-received substrates resulted in alternate (SrO<sub>3</sub>)<sup>4-</sup> or Ti<sup>4+</sup> terminated terraces with a step height of 0.113 nm ( $d_{111}/2$ ). An etching process under microwave assisted hydrothermal condition in deionized water and ammonia solution selectively removed either (SrO<sub>3</sub>)<sup>4-</sup> layers or Ti<sup>4+</sup> chemical termination on all terraces. Subsequent annealing at 1000 °C improved the step and terrace structure to a great extent. Measured step height of 0.225 nm ( $d_{111}$ ) and uniform contrast in the phase image of the terraces confirms single termination in pure and Nb doped SrTiO<sub>3</sub> single crystal substrates. Unlike (110), (111) orientation resulted in single termination under the same experimental conditions and parameters used for pure and Nb doped SrTiO<sub>3</sub> (100).

However, the surface of SrTiO<sub>3</sub> is prone to reconstruction to reduce the surface energy and that significantly changes the surface co-ordination of atoms over the period of time, which is severe in the case of charged surfaces of (110) and (111) compared to neutral (100) surface. This aspect, which is independent of how the surface termination was achieved, affects the shelf-life of the single chemically terminated surface and is subject to further investigation. Since it is a field of its own and is discussed fairly in the literature for all the three orientations of SrTiO<sub>3</sub> surfaces with theoretical models<sup>40-42</sup>, it was not considered here. In short, epitaxial thin films growth of multifunctional oxides on these F- free single-terminated substrates may find new functionalities and interesting interface physical phenomena for novel applications discussed in Chapter 1 in the field of oxide electronics. However, in order to have reproducible deposition of thin films on the substrate with same orientation, miscut angle and direction must be same between substrates. This is because of the fact that nucleation and growth thin films on single crystal substrate greatly depends on the density of steps and kinks on the substrate surface. Along with the unavoidable dislocation/imperfections on the crystal, the obtained surface heavily depends on the history of the sample and the production batch it belongs to. So preparation of the surface and its characterization cannot be bypassed when the epitaxial thin film on single crystal SrTiO<sub>3</sub> is considered for any applications.

#### 4. Multifunctional barium titanate and bismuth ferrite thin films

The hydrothermal technique presents a feasible way to obtain high crystalline quality epitaxial multifunctional oxide thin films at low temperature compared to other techniques that usually require high temperature processes. This method can also be seen as a simple, inexpensive route to obtain highly textured thin films in quantities compatible with batch processing. However, the formation of several aqueous byproducts during the process represents a risk that could be deposited on the substrate surface, severely affecting the structural, dielectric, and electric properties. BiFeO<sub>3</sub> has a ferroelectric Curie temperature,  $T_C \sim 1100$  K, and Neel temperature,  $T_N \sim 640$  K, both are well above the room temperature. So BiFeO<sub>3</sub> is currently the only known multiferroic material with ferroelectric and (anti-) ferromagnetic ordering at room temperature. Furthermore, BiFeO<sub>3</sub> is a robust, environmentally benign ferroelectric material and has an additional advantage over Pb-based materials in future device applications. In this work, highly textured BaTiO<sub>3</sub> and BiFeO<sub>3</sub> thin films were successfully produced by hydrothermal synthesis that avoided to a great extent the hydroxyl group incorporation onto the grown film. The 0.5 % wt. Nb doped SrTiO<sub>3</sub> (100) substrates were served as the bottom electrode and the single termination on the surface of this substrate was realized prior to the deposition by the method discussed in Chapter 3.

##### 4.1. BaTiO<sub>3</sub> thin films

Excellent quality epitaxial BaTiO<sub>3</sub><sup>105-108</sup> thin films have been produced by several techniques such as pulsed laser deposition (PLD), metal-organic chemical vapor deposition (MOCVD), molecular beam epitaxy (MBE), or RF-sputtering. Gersten, *et al.* found that temperature required to synthesize single phase BaTiO<sub>3</sub> particles by hydrothermal process is 90°C. Below that temperature, the reaction is incomplete due to very slow reaction kinetics.<sup>109</sup> Chien *et al.*<sup>110</sup> measured the electrical properties of epitaxial BaTiO<sub>3</sub> thin films formed on SrRuO<sub>3</sub>/SrTiO<sub>3</sub> by conventional hydrothermal method<sup>111</sup> but did not report any polarization switching curves due to high electrical leakage caused by the presence of hydroxyl group incorporation and the deposition time was longer. The main source of this hydroxyl group is from the mineralizer, generally added to improve the solubility of the precursors under hydrothermal conditions.

However, BaTiO<sub>3</sub> can be produced without the addition of a mineralizer to promote the solubility, minimum by employing only Ba(OH)<sub>2</sub> to provide the basic solution. Yoshimura *et al.* utilized microwave assistance in order to produce polycrystalline BaTiO<sub>3</sub> thin films by reducing the process time from hours to minutes compared to conventional hydrothermal conditions.<sup>54</sup> Hence it will be interesting to utilize mineralizer free chemistry and microwave radiation assisted hydrothermal method for the BaTiO<sub>3</sub> thin films. Also, to the best our knowledge, epitaxial barium titanate thin films by microwave-assisted hydrothermal have not been reported so far.

### 4.1.1 Experimental details

Microwave assisted and conventional hydrothermal deposition of BaTiO<sub>3</sub> thin films were realized on polycrystalline and single crystalline conducting substrates. The polycrystalline platinumized silicon substrates (Pt/Al<sub>2</sub>O<sub>3</sub>/SiO<sub>2</sub>/Si) consist of a 100 nm thick platinum film on a 5 nm-thick Al<sub>2</sub>O<sub>3</sub> layer that improve the adhesion of platinum on the SiO<sub>2</sub>/Si substrates. Single crystalline substrates are the Nb:SrTiO<sub>3</sub> (5 × 5 × 0.5 mm, miscut angle <0.5°, 0.5 wt. %Nb) with (100) orientation from Crystec GmbH. Single termination of Nb:SrTiO<sub>3</sub> (100) surfaces and atomically flat surfaces are required for epitaxial growth and hence a method described in *chapter 3* was used to prepare the surface of the Nb:SrTiO<sub>3</sub> (100) substrate. Measured step height of 0.39 nm between the adjacent terraces in the observed surface topography by atomic force microscopy matches with the lattice parameter ‘a’ of cubic SrTiO<sub>3</sub>. In the case of (100) oriented surfaces this is equal to the inter-planar distance (d<sub>100</sub>) between two identical surfaces and that suggests single chemical termination on the surface in the present case (Figure 4.1a).<sup>88</sup> The RMS roughness on the terraces were in the pm range as the z-range shown in the figure exactly correspond to the height difference between the first and last terraces (5 x 0.39 nm) and is due to the miscut angle of the single crystal.<sup>59</sup> As received Pt/Al<sub>2</sub>O<sub>3</sub>/SiO<sub>2</sub>/Si substrates were cleaned in ultrasonic bath with acetone and then annealed at 550°C to stabilize the Pt and suppress its grain growth during the hydrothermal deposition of BaTiO<sub>3</sub>. Figure 4.1b shows the AFM surface morphology of polycrystalline platinum surface (x-ray diffraction studies revealed Pt orientation along (111) direction, results not shown) with an RMS roughness of about 1.2 nm.

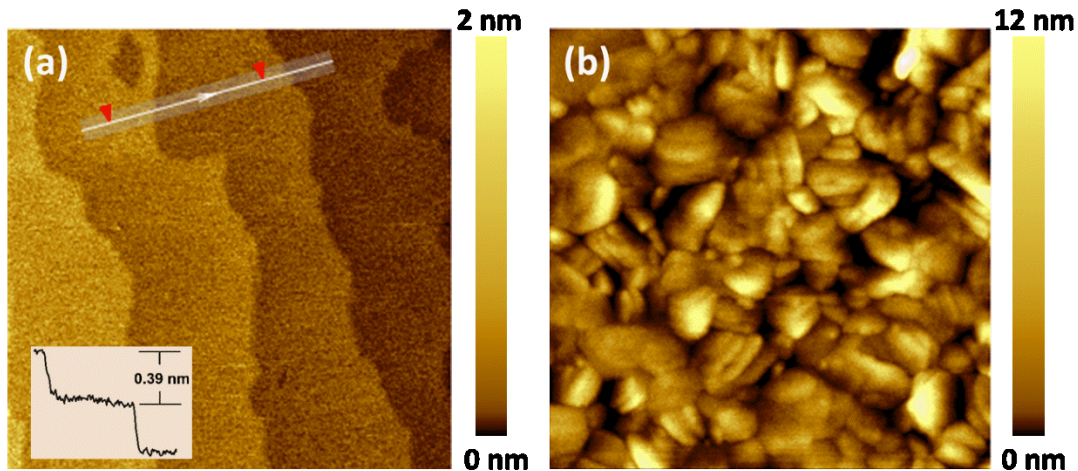
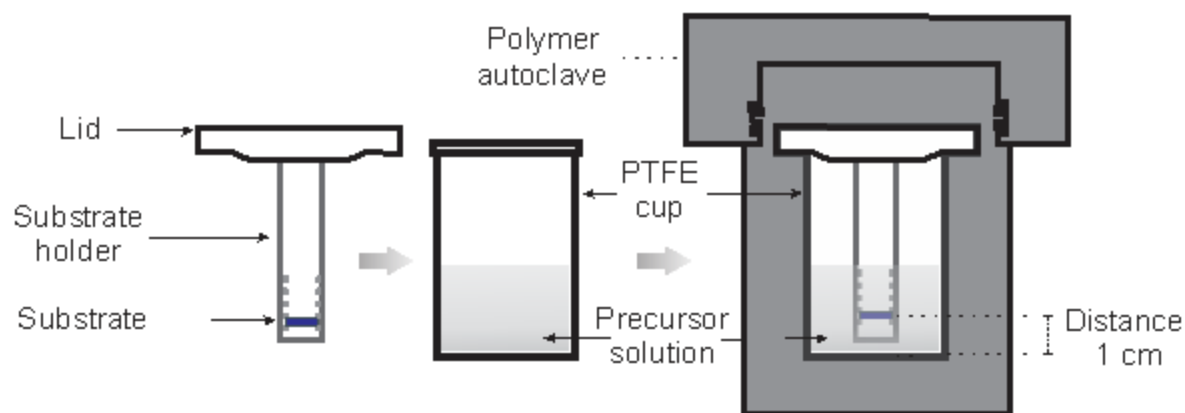


Figure 4.1: AFM Surface morphology ( $1 \times 1 \mu\text{m}^2$ ) of the substrates used for the  $\text{BaTiO}_3$  thin film deposition by hydrothermal method, (a) step-terrace surface of  $\text{Nb:SrTiO}_3$  (100) and (b) Pt surface of  $\text{Pt/Al}_2\text{O}_3/\text{SiO}_2/\text{Si}$ .

A schematic diagram of the microwave compatible hydrothermal reactor used for the  $\text{BaTiO}_3$  deposition is shown in Figure 4.2. It consists of a Teflon® cup (from Parr Instrument) and a custom designed Teflon® substrate holder attached to the lid of this cup. This assembly ensured stable positioning of the substrate at one specific distance from the bottom of the cup during the entire hydrothermal process. In the present case, substrates were kept at a distance of 1 cm from the bottom, polished side facing down in the case of  $\text{Nb:SrTiO}_3$  and Pt surface facing down in the case of  $\text{Pt/Al}_2\text{O}_3/\text{SiO}_2/\text{Si}$  to avoid sedimentation of reaction products from liquid so the deposition of the film occurs by convection material transport. This face down positioning reduces particle sticking on the surface and ensures atom by atom deposition. The equimolar  $\text{Ba(OH)}_2 \cdot 8\text{H}_2\text{O}$  granules (Sigma-Aldrich 99.995 %), and  $\text{TiO}_2 < 25\text{nm}$  nanoparticles (Sigma-Aldrich 99.7 %), were added to the Teflon® cup to form an aqueous suspension in deionized water. Teflon® O-ring attached to the lid develops and maintains a tight seal without heavy pre-loading. Water of hydration of the Ba-salt was also taken into consideration while determining the concentration of the precursor solution and to maintain the molar ratio with  $\text{TiO}_2$  for the stoichiometric  $\text{BaTiO}_3$  formation of the film on the substrate as well as the  $\text{BaTiO}_3$  powder. In the case of synthesis with  $\text{H}_2\text{O}_2$ , 10%  $\text{H}_2\text{O}_2$  was added (while maintaining concentration at 0.5M) and that in fact replaced corresponding volume of deionized water. This sealed cup/substrate assembly was then housed

into a polymer autoclave (microwave digestion bomb from Parr Instrument: Model 4781) to ensure overpressure while heating the solution with microwave energy. The temperature and pressure generated within a microwave bomb are solely depended upon the filling level, time of exposure and the power level. In the present case, the volume fill factor of the precursor solution was fixed at 66% of the total volume of the Teflon® cup. The microwave oven used for the heating was a commercial kitchen microwave (Panasonic Inverter). Film growth were carried out at 120 W of output power for 10 min and the process was cycled until the completion of the reaction as evidenced by the single-phase formation of tetragonal BaTiO<sub>3</sub> by Raman scattering studies.

Topography of the substrate and the films were analyzed with help of an AFM (SMART-AIST). Theta-2 theta scan with X-Ray Diffraction (Panalytical Xpert Pro) was used to study the epitaxial and crystalline properties of the film. Raman scattering measurements (Horiba spectrometer laser source, iHR320 solid-state Cobolt 04-01 series at 473.2 nm, 400 mW) were also used to study the crystallinity to optimize the reaction time and number of cycles. Ferroelectric switching of the films were studied with piezoresponse force microscopy (PFM, Smart SPM1000-AIST-NT Inc.) by studying the phase- voltage and phase-contrast characteristics at room temperature.



*Figure 4.2: Schematic of the microwave reactor used for the deposition of BaTiO<sub>3</sub> thin film deposition by hydrothermal method. In the case of conventional hydrothermal polymer autoclave was replaced with a stainless steel autoclave.*

#### 4.1.2. Surface coverage

The effect of  $\text{H}_2\text{O}_2$  on the  $\text{BaTiO}_3$  film formation on  $\text{Nb}:\text{SrTiO}_3$  (100) substrates was studied first for the optimization process. Figure 4.3a and Figure 4.3b show the surface morphology of  $\text{BaTiO}_3$  films as studied by the AFM. Equimolar  $\text{Ba}(\text{OH})_2 \cdot 8\text{H}_2\text{O}$  and  $\text{TiO}_2$  were mixed with de-ionized water in Teflon cup and final concentration of the solution was 0.5M and that filled ~66% of the reactor-cup volume. In this experiment, substrate and precursor were exposed to the microwave radiation for 10 min at a power level of 120 W and kept in the oven for 2 h before cooling down to room temperature by immersing the reactor assembly in water. As can be seen from the Figure 4.3a, in the case of hydrothermal deposition of  $\text{BaTiO}_3$  without the addition of  $\text{H}_2\text{O}_2$  in the precursor solution, under identical condition, thin film coverage on the  $\text{Nb}:\text{SrTiO}_3$  substrate was very low compared to the precursor solution with 10%  $\text{H}_2\text{O}_2$ .  $\text{BaTiO}_3$  nucleation occurred at the substrate-solution interface at specific sites on the  $\text{Nb}:\text{SrTiO}_3$  surface in the case of solution without  $\text{H}_2\text{O}_2$  and further growth was restricted to the film-solution interface. Other regions of the substrate is nothing but bare surface as it still showed step-terrace features of the virgin substrate (Figure 4.3 b). However, with 10%  $\text{H}_2\text{O}_2$  (replaced with same volume of water to keep the filling factor 66%) addition, uniform nucleation of  $\text{BaTiO}_3$  over the entire  $\text{Nb}:\text{SrTiO}_3$  substrate surface occurred and growth continued at the film-solution interface as well and completely masked step-terrace signature morphology of the single chemically terminated surface. This observation underlines the influence of  $\text{H}_2\text{O}_2$  (a strong oxidant) in the formation of  $\text{BaTiO}_3$  thin films that promotes wetting by modifying the pH and hence the charge neutrality point to favor the reaction of  $\text{Ba}(\text{OH})_2$  and  $\text{TiO}_2$  to form  $\text{BaTiO}_3$  all over the surface. With this observation we have used 10%  $\text{H}_2\text{O}_2$  in the precursor solution containing barium hydroxide, titanium dioxide and de-ionized water for the subsequent deposition of  $\text{BaTiO}_3$  on  $\text{Pt}/\text{Al}_2\text{O}_3/\text{SiO}_2/\text{Si}$  and  $\text{Nb}:\text{SrTiO}_3$  (100) substrates. Also, microwave radiation instantly heats the solution and pressure increases rapidly to accelerate the reaction to form  $\text{BaTiO}_3$  in the solution as well as on the substrate. In the case of conventional process, using stainless steel autoclave and Teflon cup, heating up the precursor solution is very slow due to the poor thermal conductivity of Teflon and hence time to reach the proper hydrothermal condition to start reaction between the precursors is very high. For comparison, conventional synthesis have been done and the results are shown in *Figure 4.4*. It took 24 hours for the synthesis of  $\text{BaTiO}_3$ . So, our process is very fast compared to a conventional

---

hydrothermal process where the processing time generally runs into days to complete the reaction.<sup>112</sup>

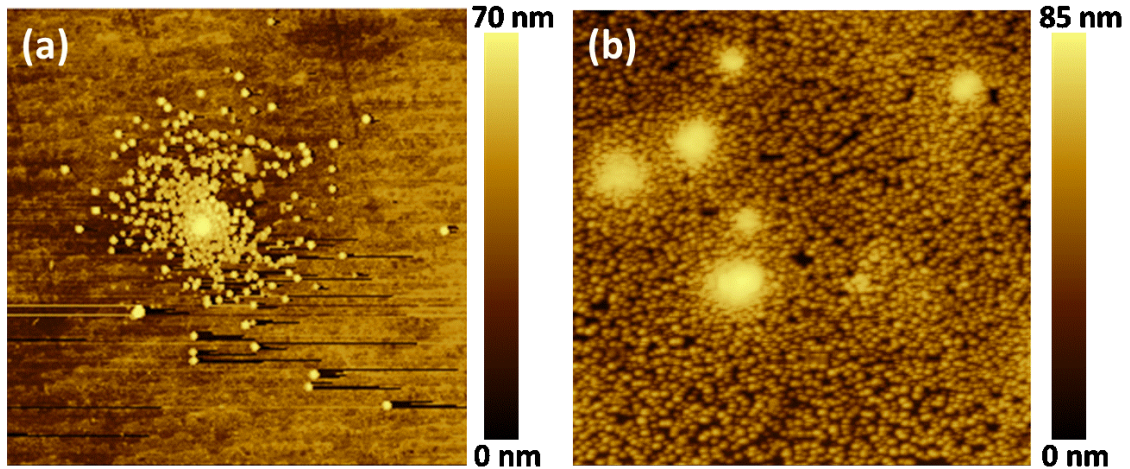


Figure 4.3: AFM Surface morphology ( $1 \times 1 \mu m^2$ ) of  $BaTiO_3$  thin film grown on  $Nb:SrTiO_3$  (100) substrates by microwave assisted hydrothermal method (a) without and (b) with  $H_2O_2$  in the precursor solution. Horizontal lines correspond to artifacts.

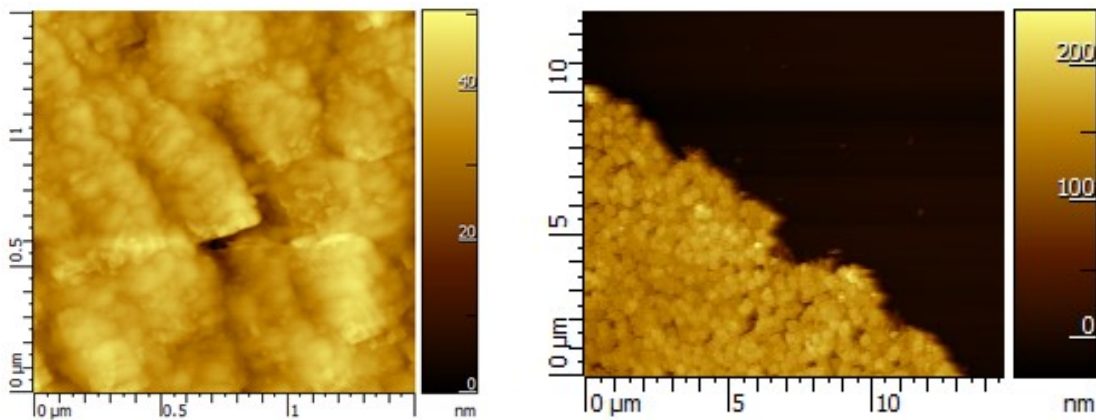


Figure 4.4: AFM non-contact tapping mode topographies (left), (center) of conventional hydrothermally synthesized  $BaTiO_3$  for 24h at  $90^\circ C$ .

#### 4.1.3. Reaction time and cycles

In the case of microwave assisted hydrothermal process, the time of radiation at a particular power should be optimized first for the safe operation of digestion reactor. The time was optimized at 10 min for an output power of 120 W. However, for the complete conversion of  $\text{TiO}_2$  particle to  $\text{BaTiO}_3$  film or powder by reacting with  $\text{Ba}(\text{OH})_2$  under hydrothermal condition depends on the reaction time and that may be much higher than the time 10 min mentioned before. In that case, the only option is by repeating the experiment after cooling the digestion bomb to a temperature as low as the temperature at which the first irradiation occurred. In the present case we performed the second cycle after a gap of 2 h by keeping the digestion bomb in cold water. This process was repeated until we got phase pure  $\text{BaTiO}_3$  thin film on the substrate. Figure 4.5 shows the surface morphology of  $\text{BaTiO}_3$  thin films on  $\text{Pt}/\text{Al}_2\text{O}_3/\text{SiO}_2/\text{Si}$  substrates deposited at various cycles. In the case of 1 cycle, a very uniform deposition of film was seen on all over Pt surface with an RMS 1.4 nm, comparable to the RMS roughness of Pt surface. In this case, grain growth of  $\text{BaTiO}_3$  was not visible, compared to 2 cycles (Figure 4.5b). In the case of 2 cycles, grainy feature of the films were clear and this grain growth resulted in higher surface roughness (2.4 nm). Similar behavior again observed in 3 cycle deposited film as well and it seems reaction is almost completed. In all cases, the morphology of the Pt surface was visible even after the deposition of  $\text{BaTiO}_3$  film due to the much lower grain size of  $\text{BaTiO}_3$  film on bigger Pt grains.

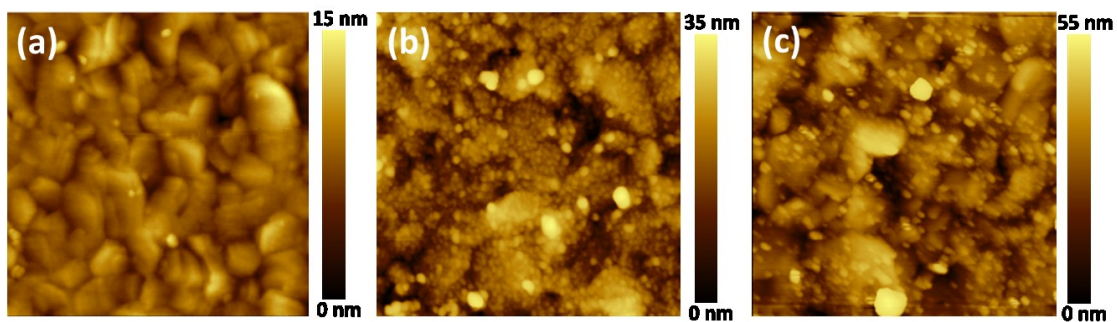


Figure 4.5: AFM Surface morphology ( $1 \times 1 \mu\text{m}^2$ ) of  $\text{BaTiO}_3$  thin film deposited on  $\text{Pt}/\text{Al}_2\text{O}_3/\text{SiO}_2/\text{Si}$  substrates (a) 1 cycle, (b) 2 cycles and (c) 3 cycles.

Raman spectroscopy is one of the most powerful techniques widely used to investigate the structure of a material. In the present case, in order to understand the phase evolution of tetragonal BaTiO<sub>3</sub> with the number of cycles (time of microwave radiation) we have performed Raman scattering studies on hydrothermally synthesized films. The selection of this substrate for the process optimization was due to the fact the Pt is Raman inactive strong signal from Si and other layers below Pt can be avoided and signal we get solely from the deposited film on the Pt surface. Also, if BaTiO<sub>3</sub> is deposited on SrTiO<sub>3</sub> film and studied with Raman scattering, the signals from both SrTiO<sub>3</sub> and BaTiO<sub>3</sub> are very difficult to differentiate and that bring ambiguity in the phase evolution studies. This is the reason for selecting Pt/Al<sub>2</sub>O<sub>3</sub>/SiO<sub>2</sub>/Si as the substrate for the process optimization. Raman spectra of the BaTiO<sub>3</sub> thin films as a function of number of cycles of microwave radiation are shown in Figure 4.6. As can be seen, films deposited with 1 and 2 cycle are diphasic as it contains TiO<sub>2</sub> anatase along with BaTiO<sub>3</sub> phases. In these spectra, three prominent peak at wave numbers, 144, 397 and 638 cm<sup>-1</sup> belong to the TiO<sub>2</sub> anatase phase.<sup>113</sup> We have used TiO<sub>2</sub> anatase nanoparticle as the source of Ti, hence it will be difficult to figure out whether it is a deposition of TiO<sub>2</sub> or the adhesion of TiO<sub>2</sub> nanoparticles onto the Pt surface. Based on the crystallography, Raman-active modes for tetragonal BaTiO<sub>3</sub> (*P4mm*) are; (i) E(TO1) at 38 cm<sup>-1</sup>, (ii) A (TO1) at 178 cm<sup>-1</sup>, (iii & iv) E(TO2) and E(LO1) at 180 cm<sup>-1</sup>, (v) A(LO1) at 189 cm<sup>-1</sup>, (vi) A(TO2) at 267 cm<sup>-1</sup> (vii-ix) E(TO3), E(LO2) and B1 at 308 cm<sup>-1</sup>, (x)E(LO3) at 466 cm<sup>-1</sup>, (xi) A1(LO2) at 473 cm<sup>-1</sup>, (xii) E(TO4) at 489 cm<sup>-1</sup>, (xiii) A(TO3) at 512 cm<sup>-1</sup>, (xiv)E(LO4) at 722 cm<sup>-1</sup> and (xv) A(LO3) at 740 cm<sup>-1</sup>.<sup>114</sup> Other peaks observed along with the anatase TiO<sub>2</sub> peaks at wave numbers 190, 280, 303 516 and 720 cm<sup>-1</sup> are hence due to the BaTiO<sub>3</sub>. The peak around 303 cm<sup>-1</sup> was is due to the overlap of *E*(TO3), *E*(LO2) and *B*1, and is the characteristic peak of tetragonal BaTiO<sub>3</sub>. Raman spectra of the film which undergone three cycles of microwave radiation was phase pure as it did not show the characteristics peaks of TiO<sub>2</sub> anatase and contained only peaks corresponding to the tetragonal BaTiO<sub>3</sub>. So the BaTiO<sub>3</sub> thin film is formed directly into the tetragonal phase by reacting with the excess TiO<sub>2</sub> already present on the substrate and 3 cycle of microwave radiation are required for this particular concentration of precursors and is expected to be more cycles if the concentration is increased further.

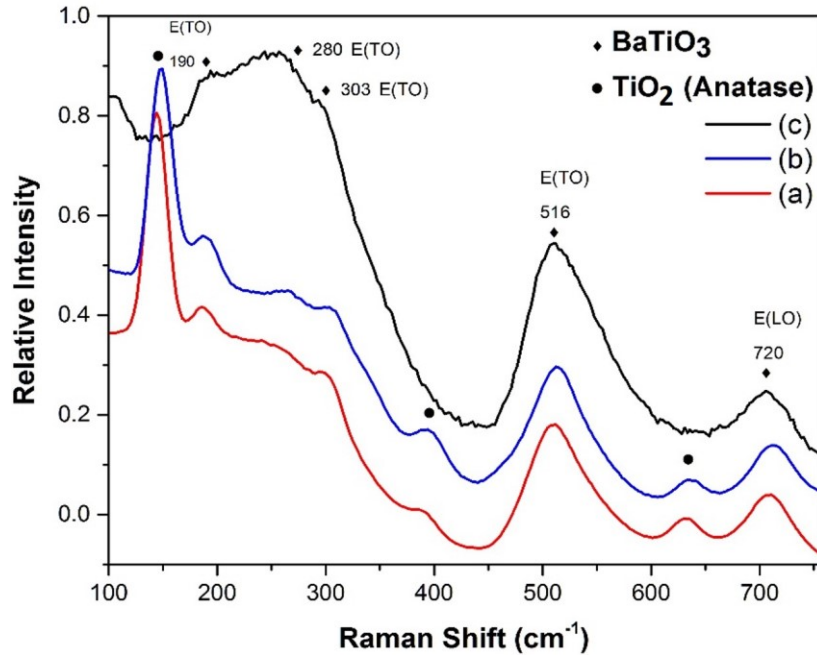
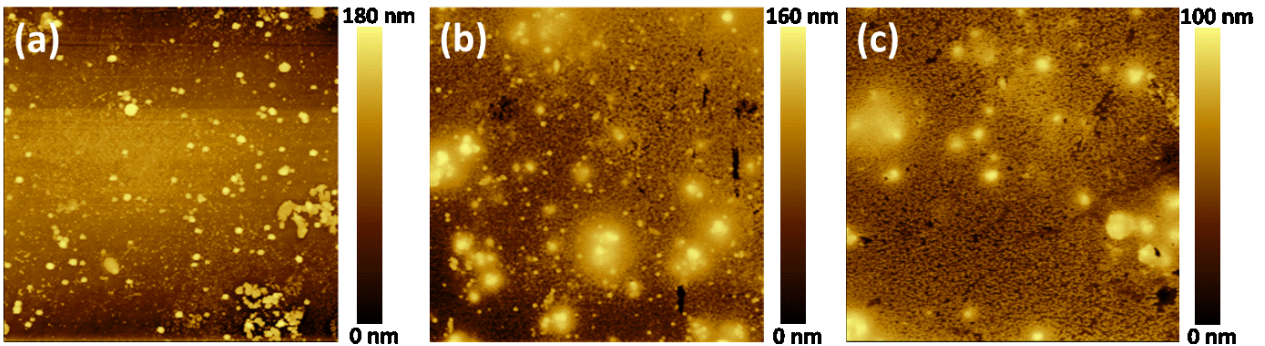


Figure 4.6: Raman spectra of  $\text{BaTiO}_3$  thin films on  $\text{Pt}/\text{Al}_2\text{O}_3/\text{SiO}_2/\text{Si}$  substrates, (a) 1 cycle, (b) 2 cycles, and (c) 3 cycles.

#### 4.1.4. Epitaxial $\text{BaTiO}_3$ on $\text{Nb}:\text{SrTiO}_3$ substrates

In order to understand initial stages of thin film growth, the surface morphology of the film on  $\text{Nb}:\text{SrTiO}_3$  (100) substrates was analyzed as a function of time of microwave radiation for the first cycle. Figure 4.7 shows the AFM surface topography ( $10\mu\text{m} \times 10\mu\text{m}$ ) of  $\text{BaTiO}_3$  film deposited on  $\text{Nb}:\text{SrTiO}_3$  (100) substrates with the microwave radiation for 2 min, 5 min and 10 min. In the case of 2 min of microwave radiation, uniform deposition of  $\text{BaTiO}_3$  at some regions on the substrate-solution interface by reacting Ba and Ti atoms on the substrate surface. However, particles with larger size can also be visible on the surface that might be due to the undissolved  $\text{TiO}_2$  nanoparticles adhered to the substrate surface and subsequent  $\text{Ba}^{2+}$  diffusion through it to form  $\text{BaTiO}_3$ . The later scenario need more time as the diffusion is slow process at this low temperature and that may be reason for seeing  $\text{TiO}_2$  phase in the film according to the Raman studies (Figure 4.6). In short, the former scenario favors the formation of layered structure and the later one favors the mixture phase. As the microwave radiation time is increased to 5 min, grain size increased along with more uniform thin film growth. With the present set-up we can increase the irradiation

time only up to 10 minutes due to the pressure safety valve of the reactor. As can be seen from Figure 4.7c, with this time of exposure the surface is much better compared to lower irradiation times and we fixed this time for continuous deposition of BaTiO<sub>3</sub> film at 120W of microwave power. However, Raman spectra of BaTiO<sub>3</sub> film showed (Figure 4.6a) anatase TiO<sub>2</sub> and tetragonal BaTiO<sub>3</sub> and hence further procedures are required to realize single phase tetragonal BaTiO<sub>3</sub> by microwave assisted hydrothermal method.



*Figure 4.7: AFM surface topography (10 μm x 10 μm) of BaTiO<sub>3</sub> film deposited on Nb:SrTiO<sub>3</sub> (100) substrates with the microwave radiation for: a) 2 min, b) 5 min and c) 10 min.*

Based on the Raman scattering results on BaTiO<sub>3</sub>/Pt/Al<sub>2</sub>O<sub>3</sub>/SiO<sub>2</sub>/Si substrates, we extended the number of cycles to 2, and corresponding surface morphology is shown in Figure 4.8. Surface morphology of 1 and 2 cycles were almost identical and upon third cycles (Figure 4.9a) coalescence of individual grain resulted in interlinked and continue films and this scenario provides improved conditions for realizing epitaxial BaTiO<sub>3</sub> on Nb:SrTiO<sub>3</sub>(100). Also films deposited with 3 cycles were phase pure without any TiO<sub>2</sub> phase and further used to improve the quality and will be discussed.

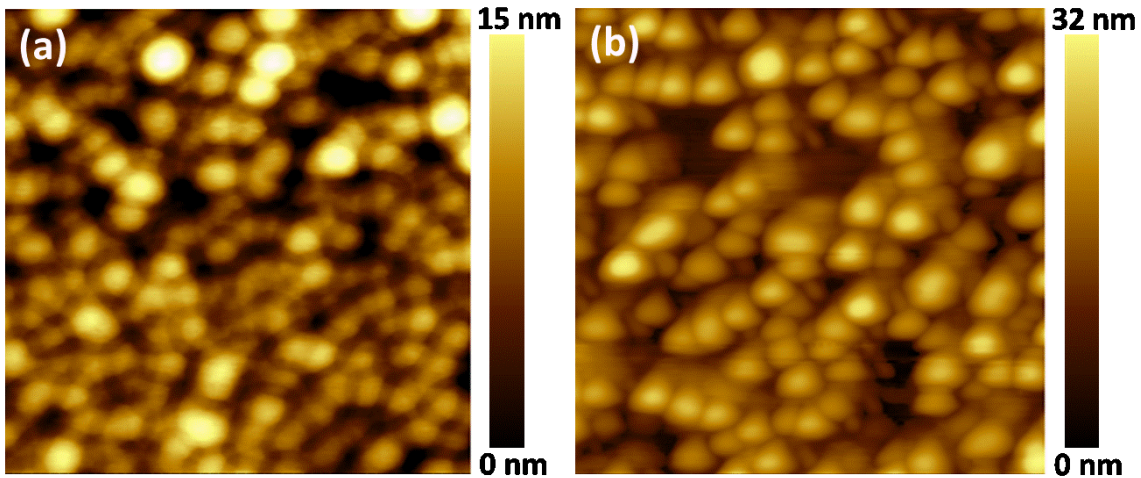


Figure 4.8: AFM surface morphology ( $1 \times 1 \mu\text{m}^2$ ) of the  $\text{BaTiO}_3$  thin film on Pt (a) 1 cycle and (b) 2 cycles of microwave radiation.

We already noticed complete reaction of all  $\text{TiO}_2$  and Ba to form single  $\text{BaTiO}_3$  upon 3 cycle of microwave radiation and hence proceeded two routes to improve the quality by reducing the grain boundaries. For that first we took out the sample from the reactor and introduced into the reactor with any precursor except water/ $\text{H}_2\text{O}_2$  solution and performed another microwave radiation for 10 min and the corresponding surface morphology is shown in Figure 4.9b. Unfortunately, this resulted in dissolution of  $\text{BaTiO}_3$  from the substrate surface and the substrate surface got exposed in most of the places. So we repeated the experiment to a 4<sup>th</sup> cycle without taking sample from the reactor and that resulted in more continues films with very few grain boundaries as can be seen from Figure 4.9c. This suggest lateral growth of the grain as there no further growth at the film-solution interface and hence ideal for the epitaxial deposition of  $\text{BaTiO}_3$  on Nb:SrTiO<sub>3</sub> (100) substrate.

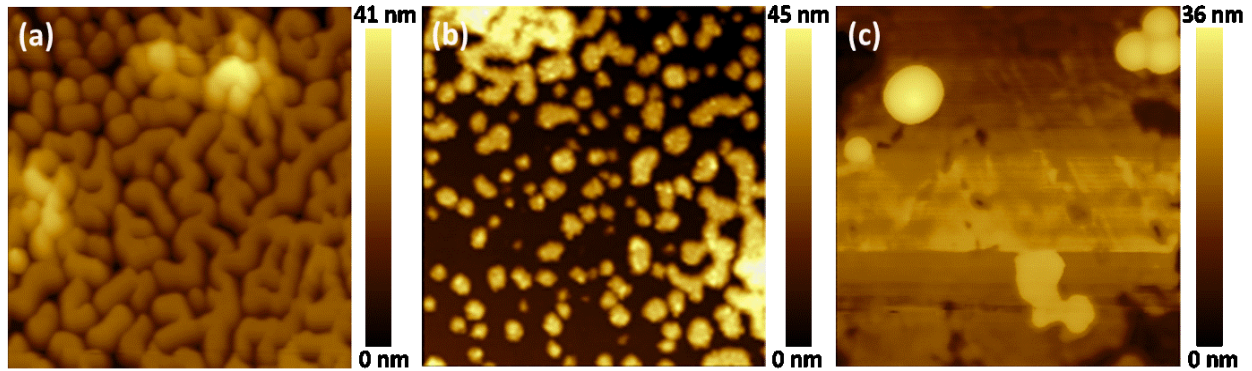


Figure 4.9: AFM surface morphology ( $1 \mu\text{m} \times 1 \mu\text{m}$ ) of the  $\text{BaTiO}_3$  film after (a) 3 cycle (b) 3 cycles and microwave radiation in  $\text{H}_2\text{O}_2/\text{water}$  solution. (c) 4 cycles

Crystalline structure of the  $\text{BaTiO}_3$  film was studied by  $\theta$ - $2\theta$  scans using a high resolution x-ray diffractometer. Monochromatic X-ray ( $\text{Cu K}\alpha_1$ , 0.154056 nm) was used. As can be seen from the Figure 4.10, the film had reflection only along (100) and (200) planes suggesting epitaxial growth on (100)  $\text{Nb:SrTiO}_3$  substrate. However, the corresponding splitting of (200)/(002) peak of the tetragonal  $\text{BaTiO}_3$  was not clearly visible. This must be due to the finer grains and lower thickness of  $\text{BaTiO}_3$ , which generally result in broad peak.<sup>115,116</sup> The lattice parameter out of plane was 4.123 Å which compared to the theoretical 4.036 Å, means that there is elongation along C axes. Also no traces of any impurity phases were present according to the XRD data. The square shaped islands on the  $\text{Nb:SrTiO}_3$  (100) surface underline fourfold symmetry as the consequence of ordered growth along the crystallographic axes of the substrate and hence epitaxial growth of  $\text{BaTiO}_3$  grains occurred. This morphology supports the x-ray diffraction data result as well. Similar surface morphology has been observed for  $\text{BiFeO}_3$  thin films by conventional hydrothermal<sup>117</sup> and  $\text{BaTiO}_3$  by RF-magnetron sputtering<sup>61</sup> on  $\text{Nb:SrTiO}_3$  (100), which has a cubic cell structure and lattice match with tetragonal  $\text{BaTiO}_3$ .

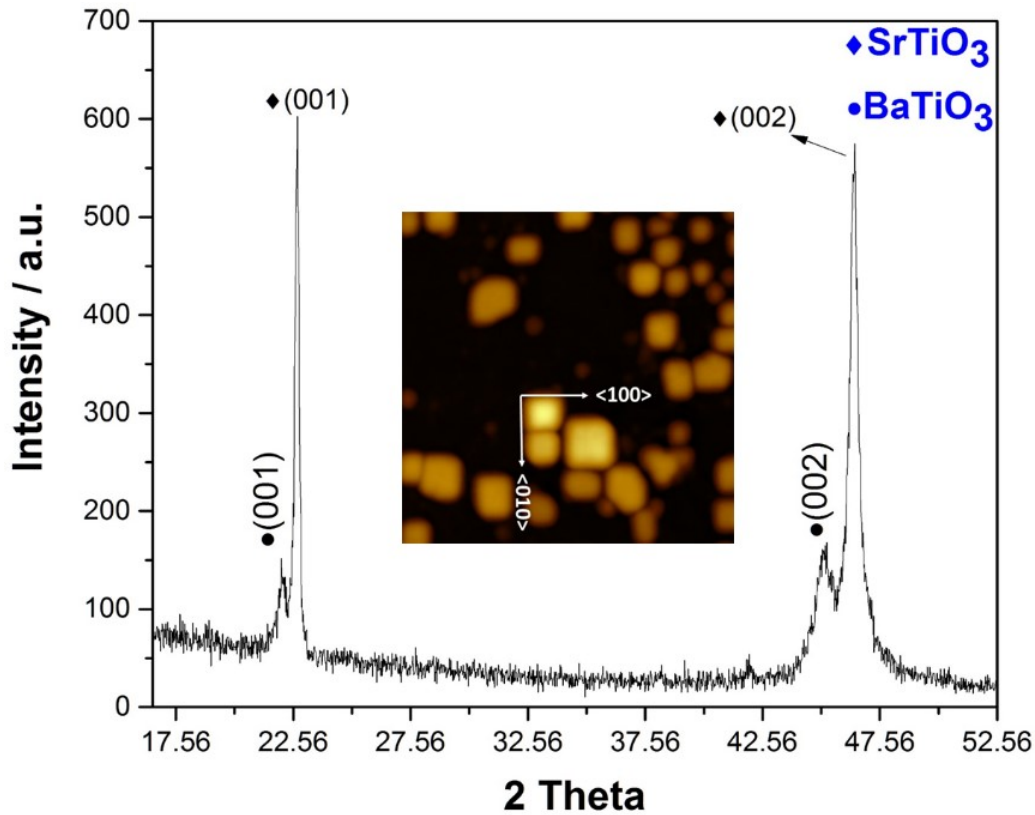


Figure 4.10: X-ray diffraction pattern of the 3 cycles microwave irradiated  $\text{BaTiO}_3$  film on (100) Nb doped  $\text{SrTiO}_3$  synthesized by the hydrothermal method. The lattice parameter out of plane was  $4.123 \text{ \AA}$  which compared to the theoretical  $4.036 \text{ \AA}$ , means that there is elongation along C axes. Inset shows nano-islands with long-range ordered fourfold symmetry.

In order to estimate the growth rate, the microwave radiation was emitted intermittently every minute. The Figure 4.11 (left and right) shows the non-contact tapping mode AFM topography and its corresponding line profile respectively where roughness calculated was  $0.2 \text{ nm}$  and the thickness estimated of  $25 \pm 5 \text{ nm}$ . The growth starts after 3 minutes of microwave radiation and the growth rate from the minute 4 to the minute 9 is  $0.8 \text{ nm/min}$ . After 10 min, the vessel reaches the maximum pressure that it can bear.

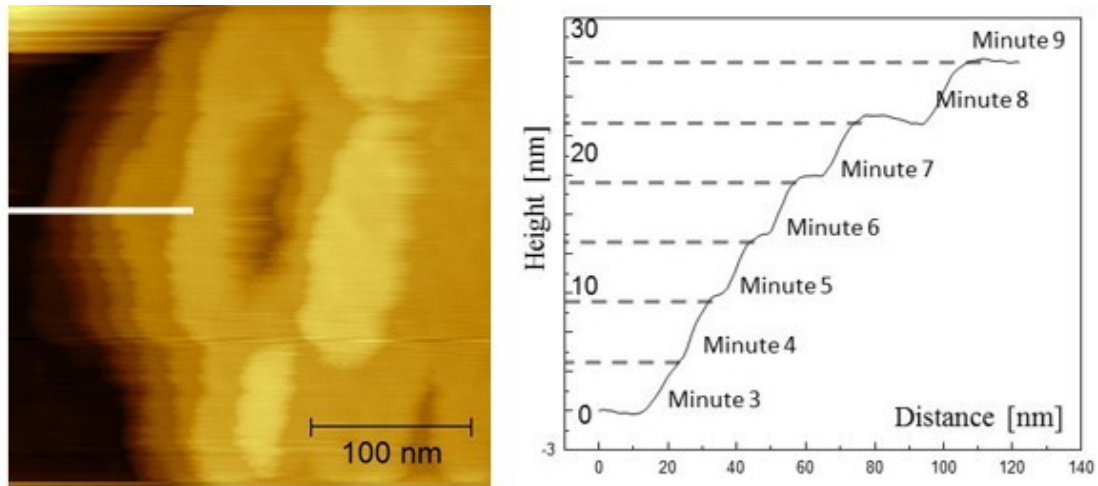


Figure 4.11: AFM non-contact tapping mode topography (left) and its line profile (right) of microwave-assisted hydrothermally synthesized  $\text{BaTiO}_3$  for 10 min discontinuously using 120 W output power.

#### 4.1.5. Ferroelectric properties

Polarization switching of hydrothermal synthesized  $\text{BaTiO}_3$  film was investigated by piezoresponse force microscopy (PFM). The piezoresponse was obtained by applying an AC voltage (51 kHz off-resonance) to the Ti-Pt layer coated silicon cantilever tip with respect to the bottom Nb:SrTiO<sub>3</sub> substrate. The amplitude and phase of the signal deflected from the cantilever were detected with a lock-in amplifier, which were used to evaluate the piezoresponse. AC voltages were applied in sequence while monitoring the piezoresponse.<sup>6</sup> For the current case, the voltage started at -8 V increasing by 1V steps to +8V and then back to -8 and the resulting hysteresis loop is shown in Figure 4.12. The Figure 4.12a and Figure 4.12c depict the local hysteresis curve of the  $\text{BaTiO}_3$  deposited in Nb:SrTiO<sub>3</sub> substrates with one cycle of microwave radiation at various time 2, 5 and 10 min did not show the hysteresis loop. Similar behavior again observed for the 2 cycles deposited  $\text{BaTiO}_3$  as well. This suggest that two cycles of microwave radiation are insufficient to realize ferroelectric properties by this processing. However, as the number of cycles of microwave radiation is increased to 3 times, typical hysteresis curves of ferroelectric  $\text{BaTiO}_3$  emerge and support the Raman scattering results which shows peaks corresponding to the tetragonal  $\text{BaTiO}_3$  only, a ferroelectric phase of  $\text{BaTiO}_3$  at room temperature.

However, compared to the local hysteresis of film obtained with 3 cycles of microwave radiation (Figure 4.12e), the 4<sup>th</sup> cycle resulted in a slimmer hysteresis window (Figure 4.12f). This observation can primarily be attributed to a different tip-sample contact resistance.

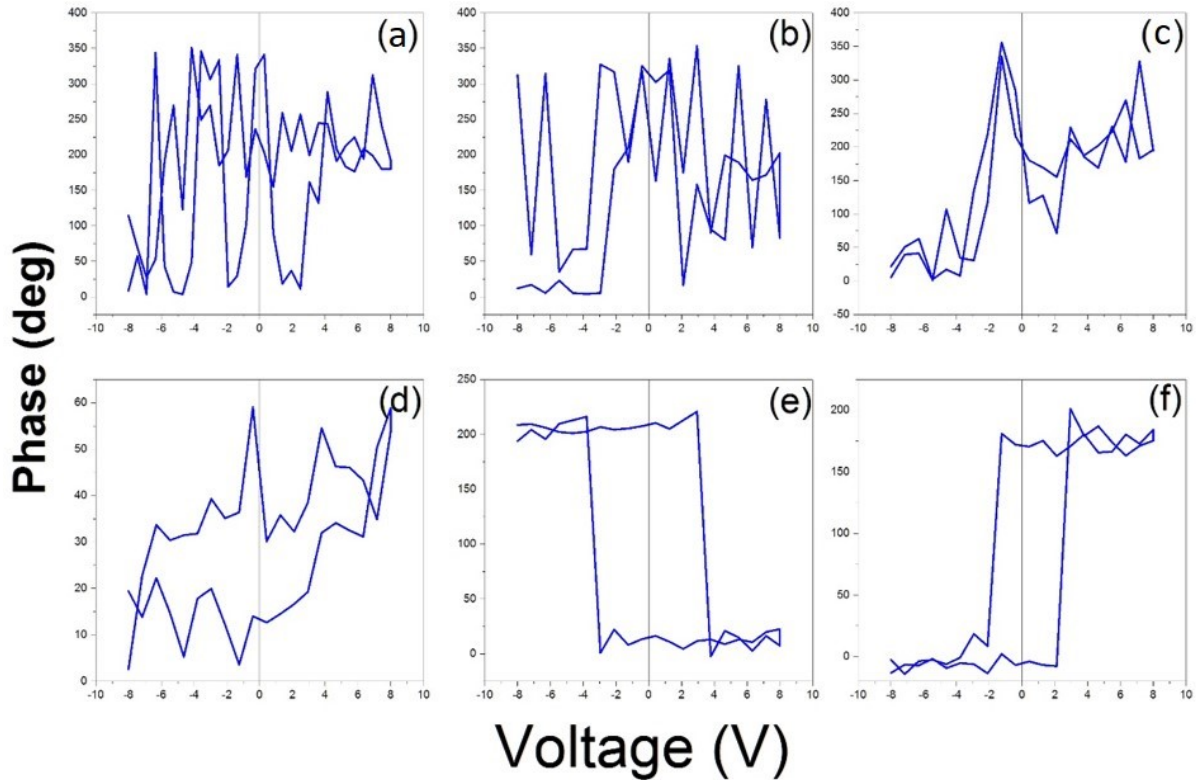


Figure 4.12: Local Phase hysteresis of  $\text{BaTiO}_3$  films on  $\text{Nb:SrTiO}_3$  substrate at various times and number of cycles.

#### 4.2. $\text{BiFeO}_3$ thin film

Multiferroic bismuth ferrite thin films have attracted considerable attention recently due to applications related to the bulk photovoltaic effect in which the direction of polarization determines the direction of the photocurrent and hence epitaxial growth is very important. Epitaxial  $\text{BiFeO}_3$  thin films have been produced by several techniques such as chemical solution deposition (CSD), pulsed laser deposition (PLD), metal-organic chemical vapor deposition (MOCVD), molecular beam epitaxy (MBE), or RF-sputtering etc.<sup>23,26,27,113</sup>. Hydrothermal technique has also already been employed to synthesize  $\text{BiFeO}_3$ <sup>118,119</sup> and it has not been

considered for bulk photovoltaic application presumably due to high electrical leakage current. With  $\text{BiFeO}_3$  being a wide-bandgap semiconductor, leakage originates from dopants that are introduced through the solvent (hydrogen from water in hydrothermal synthesis), other reaction promoters (catalysts, surfactants and mineralizers), and reaction by-products. These contributions should therefore be limited to the best possible extent during deposition.

### 4.2.1 Experimental details

$\text{BiFeO}_3$  thin films were produced only by conventional hydrothermal method.  $\text{Bi}(\text{NO}_3)_3 \cdot 5\text{H}_2\text{O}$  granules (Sigma-Aldrich >99.99 %) and  $\text{Fe}(\text{NO}_3)_3 \cdot 9\text{H}_2\text{O}$  granules (Sigma-Aldrich >98 %) were used as precursors and mixed at an equimolar concentration Bi and Fe. The concentration of the solution was 0.3 M and KOH (Sigma-Aldrich >99.995 %) was added as a mineralizer. In order to reduce leakage, we abstained from using surfactants and, most importantly, significantly reduced the concentration of potassium hydroxide (KOH) by a factor of 10 compared to reports in literature.<sup>118</sup> As mineralizer, KOH promotes solubility of reactants and considerably accelerates crystal growth; nevertheless, potassium is in a  $1^+$  state while all cations of  $\text{BiFeO}_3$  are in a  $3^+$  state. Potassium thus represents an aliovalent substitution that will induce substantial leakage acting as a dopant.<sup>120</sup> Another reason for reducing the KOH concentration is that potassium nitrate ( $\text{KNO}_3$ ) might be produced in a secondary reaction with the nitrite coming from the precursors.  $\text{KNO}_3$  is known to be a room temperature ferroelectric on its own.<sup>121</sup> Due to the reduction of mineralizer concentration, leading to less solubility of the precursors and decreasing the reaction rate, deposition time generally takes 24 h or more to get detectable thickness of the film on the substrate. A 0.5 % wt. Nb doped  $\text{SrTiO}_3$  (100) single crystal substrate (miscut angle  $< 0.3^\circ$ ), was positioned into a PTFE holder and the polished face is laid facing downwards in a PTFE liner 1 cm above the bottom in order to promote convection as the primary material transport mechanism for thin film growth. Single termination of this substrate was realized as discussed in Chapter 3. Reaction, nucleation, crystallization and film growth were then carried out in a general purpose reactor (Parr mod 4749) at a temperature of 200 °C employing a heating rate of 10 °C/min with a volume fill factor of 65 % in a Carbolite oven (model PN 30) and a cooling rate of 5 °C/min. The as grown films were annealed for 5 minutes at 500 °C under nitrogen flow for better crystallization and to remove hydrogen from the sample.

#### 4.2.2 Morphology and microstructure

An SEM cross section and top view of the synthesized  $\text{BiFeO}_3$  film are shown in Figure 4.13. The low concentration of the mineralizer KOH leads to less solubility of the precursors and decreases the reaction rate; 18 h were required to grow 40 nm thin films.

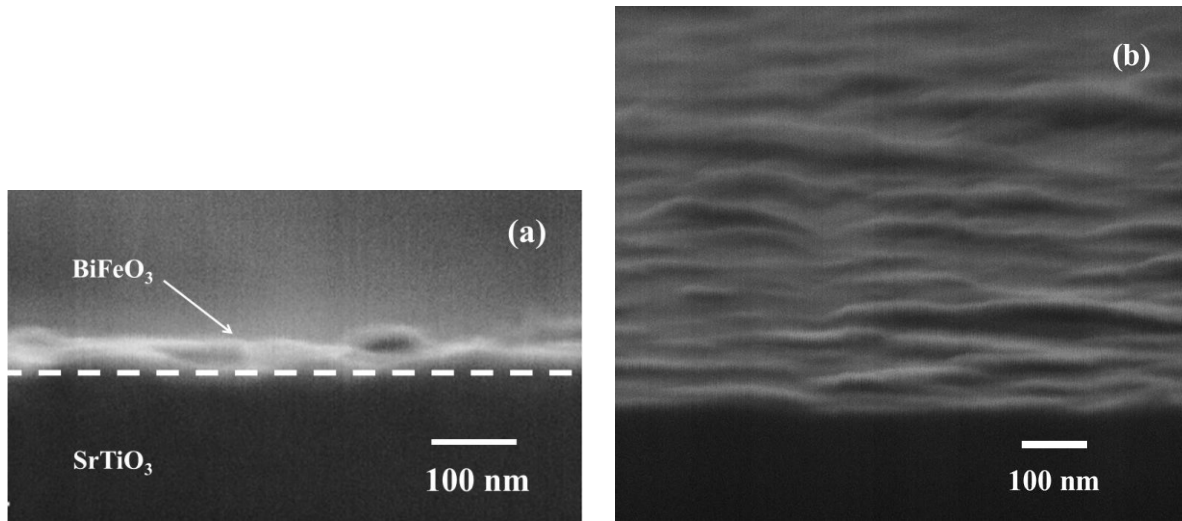


Figure 4.13: SEM images of the  $\text{BiFeO}_3$  film. (a) Cross section showing the substrate and the 40 nm thick film. (b) Top view showing the edge of the substrate that is covered by  $\text{BiFeO}_3$ .

The AFM topography is shown in Figure 4.14. The square shaped islands of up to 60 nm in height are attributed to an epitaxial growth of  $\text{BiFeO}_3$  on  $\text{SrTiO}_3$ , which has a cubic cell structure.

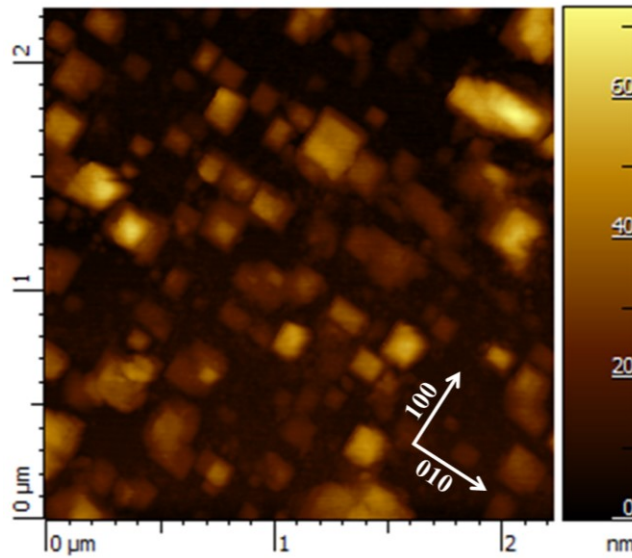


Figure 4.14: AFM topography image. A four-fold symmetry is clearly visible indicating an ordered growth along the crystallographic axes of the substrate.

The bismuth ferrite phase is verified in a high resolution semi-logarithmic theta-2theta diffractogram represented in Figure 4.15. The XRD scan was acquired with a (440) Ge monochromator in order to avoid secondary radiations from tungsten contamination ( $L_{\alpha}$ ) and secondary copper ( $K_{\alpha 2}$ ,  $K_{\beta}$ ) lines from source and cathode, respectively. The calculated out-of-plane lattice parameter is 4.16 Å and in good agreement with literature<sup>122</sup>. The crystallite size derived from the Scherrer equation is 37 nm. No traces of  $KNO_3$  were found by additional XRD measurements. Chien *et al.*<sup>110</sup> found that epitaxial growth initiates by the formation of islands along surface steps on the  $SrTiO_3$  substrate followed by growth and, when they reach sufficient size, they coalesce. After an initial film covers almost homogeneously the substrate, a new layer is formed on the first one.

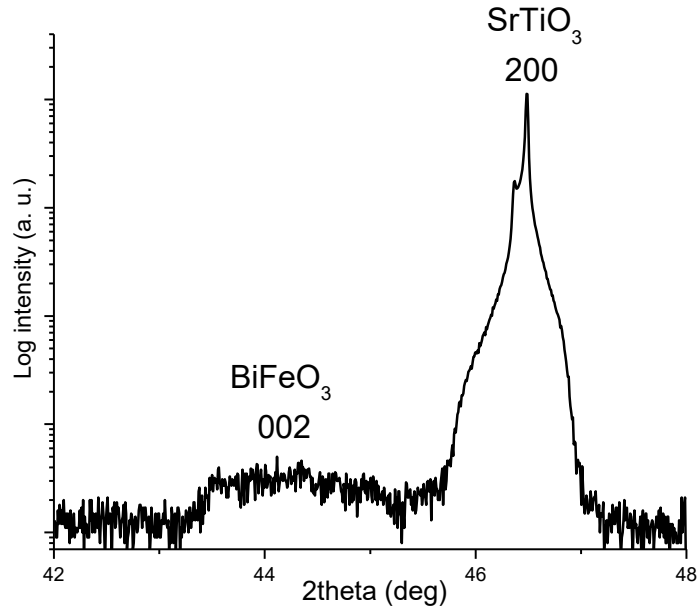


Figure 4.15: Semi-logarithmic  $\theta$ - $2\theta$  plot showing the  $\text{BiFeO}_3$  phase in (200) plane.

#### 4.2.3 Ferroelectric properties

Ferroelectric switching is shown for the first time in hydrothermally synthesized  $\text{BiFeO}_3$  thin films. Figure 4.16a shows a PFM phase-contrast image depicting an intentionally written ferroelectric pattern where some areas are poled “upwards” and some “downwards”. Using an AFM tip with a conductive coating and by applying an electrical bias potential, we poled three intersecting squares located from the top left to the bottom right with voltages of -8 V, 6 V and -8 V, respectively. The remaining area corresponds to the virgin state which exhibits a preferential upwards-orientation. The intersecting squares are showing the capability of the material to go through a full cycle of ferroelectric polarization switching. This is also confirmed in Figure 4.16b by a ferroelectric hysteresis loop between -10 V and 10 V where a phase shift of  $180^\circ$  out-of-plane is shown.

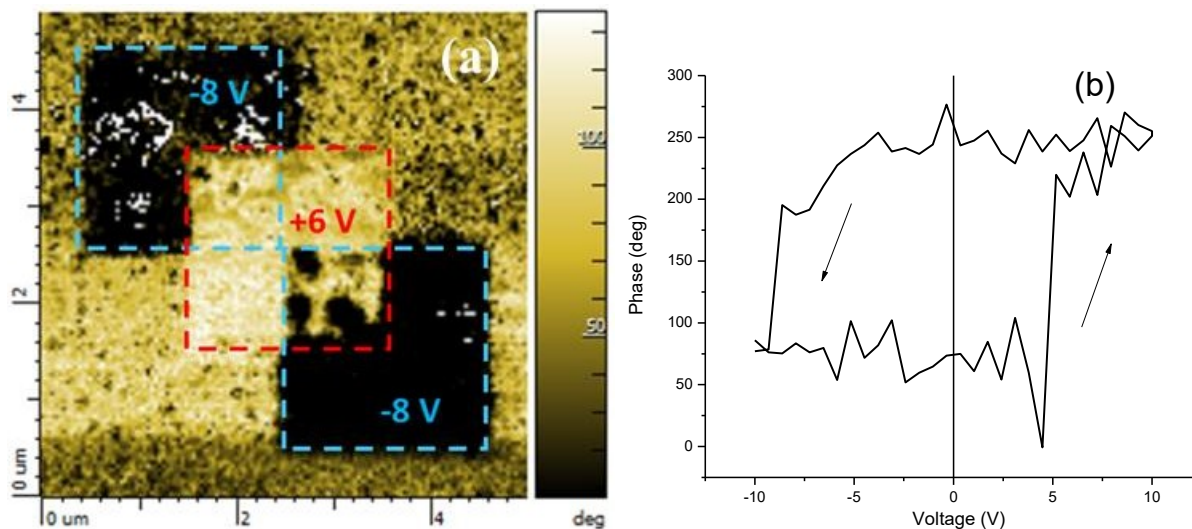


Figure 4.16: (a) PFM phase contrast image. (b) Local phase hysteresis showing  $180^\circ$  switching.

#### 4.2.4 Photocurrent

The bulk photovoltaic effect is shown in Figure 4.17, where (a) corresponds to the topography in contact mode, and (b) to the short-circuit photocurrent response generated by the incident light. Yang *et al*<sup>25</sup> has described a mechanism of charge separation and photo voltage generation that occurs exclusively at nanometer-scale ferroelectric domain walls in a model ferroelectric,  $\text{BiFeO}_3$ , under white-light illumination where the photo voltages were significantly higher than the electronic bandgap in comparison to the conventional semiconductor-based photovoltaics.<sup>25</sup> The topography scans in Figure 4.14 and Figure 4.17a show that the sample surface is not homogeneously covered by the  $\text{BiFeO}_3$  film. Although we assume that the substrate is homogeneously heated during growth, we do not control the direction of the convective flow, which will most likely be turbulent in a small vessel. It is worth mentioning that Figure 4.14 and Figure 4.17 were obtained on different areas of the same sample.

Due to the low concentration of the mineralizer KOH, up to 18 h were required to grow 40 nm thin films. This clearly represents a roadblock for industrial batch processing but recent experiments from our group with microwave-assisted hydrothermal synthesis of  $\text{BiFeO}_3$  nanoplates have shown the potential to decrease the reaction time to a few minutes.<sup>55</sup> Experiments to apply this technique to thin films are currently on the way.

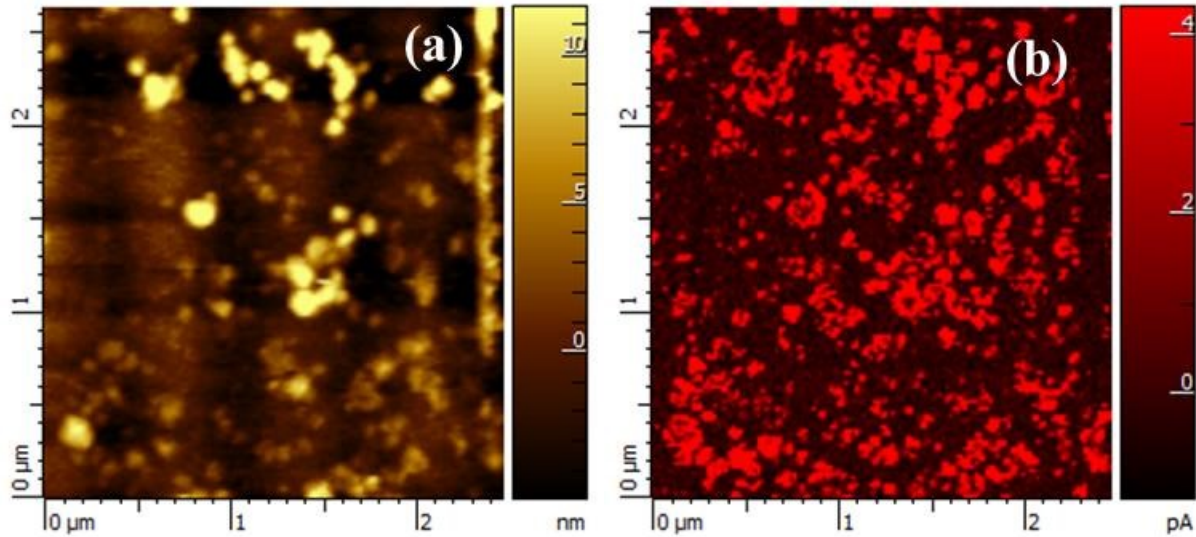


Figure 4.17: (a) AFM contact mode topography and (b) simultaneously measured photocurrent in short-circuit configuration under 355 nm excitation. Photovoltaic response is only observable in the presence of  $\text{BiFeO}_3$ .

Figure 4.18 presents the short circuit photocurrent and the open circuit photovoltage as a function of different UV light intensities. The maximum photocurrent corresponds well with values given in literature<sup>26</sup>. The straight line indicates the highest intensity which can be achieved before reaching the carrier generation saturation assuming an electric contact area of  $10 \text{ nm}^2$  under a light intensity of  $1 \text{ MWcm}^{-2}$ . The current density of  $0.8 \text{ A cm}^{-2}$ , which perfectly matches literature values for sputtered BFO films<sup>26</sup>, is a clear indication for the suitability of the hydrothermal method.

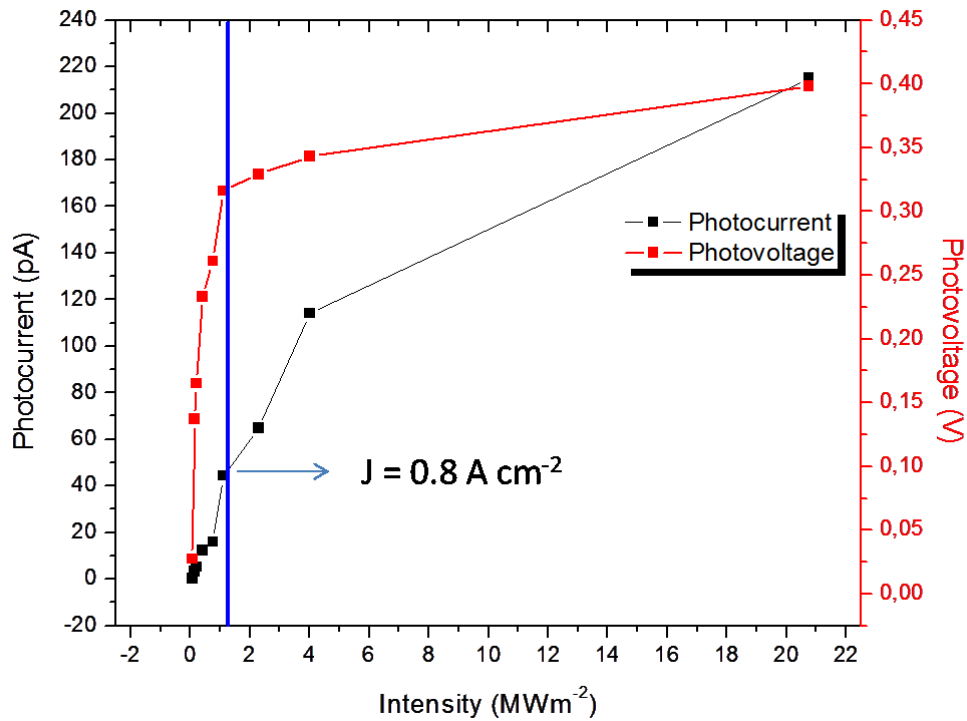


Figure 4.18: Short circuit photocurrent and open circuit photovoltage as function of different UV light intensities.

Figure 4.19 shows the photocurrent response as a function of the photovoltage obtained with a light intensity of  $1 \text{ MWcm}^{-2}$  which was employed to calculate a fill factor of 0.3 and its corresponding efficiency of  $\eta = 0.07 \%$ . The efficiency is quite low. Nonetheless, we have demonstrated that the hydrothermal method can be an inexpensive technique to produce multiferroic thin films with low electronic leakage for photovoltaic applications.

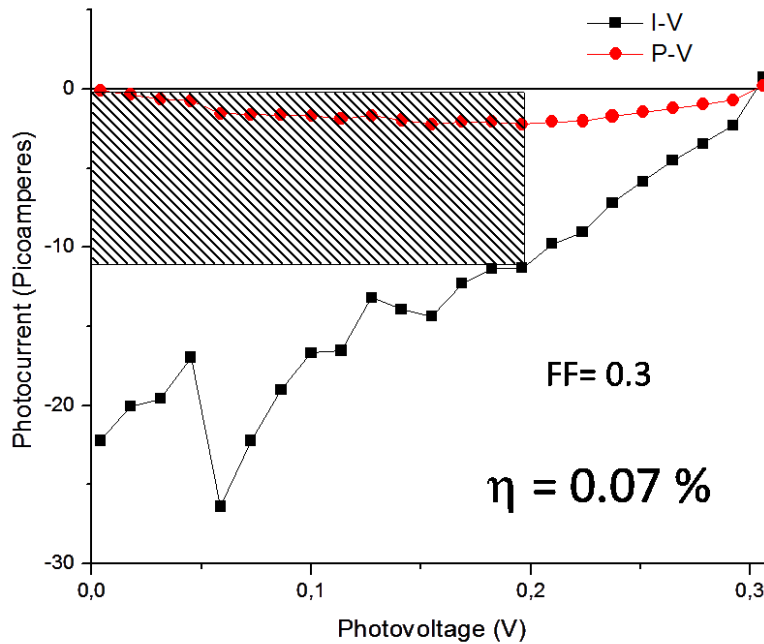


Figure 4.19: Photocurrent as function of the photovoltage recorded at a light intensity of  $1 \text{ MWcm}^2$   $FF = 0.3$  and  $\eta = 0.07 \%$ .

### 4.3 Conclusion

Phase pure epitaxial and polycrystalline  $\text{BaTiO}_3$  thin films were successfully prepared by a microwave assisted hydrothermal method on  $\text{Nb:SrTiO}_3$  and  $\text{Pt/Al}_2\text{O}_3/\text{SiO}_2/\text{Si}$  substrates, respectively. Microwave heating helped to reach the hydrothermal condition for thin film formation much faster compared to conventional heating, and that significantly reduced the processing time. At present, plastic containers for microwave assisted hydrothermal growth do not sustain sufficiently high pressure to grow dense  $\text{BaTiO}_3$  films in a single step. Raman scattering studies revealed the necessity of ‘three cycles’ with 10 min of microwave radiation at a power of 120 W for the single phase formation of  $\text{BaTiO}_3$  film. No traces of any impurity phases were present according to the x-ray diffraction and Raman scattering results. The cycled microwave radiation and sufficient cooling time for the reactor before the next radiation is ideal for the epitaxial deposition of c-axis oriented  $\text{BaTiO}_3$  on  $\text{Nb:SrTiO}_3(100)$  substrate with few grain

boundaries. Local Phase hysteresis of BaTiO<sub>3</sub> thin film on Nb:SrTiO<sub>3</sub> substrate confirms ferroelectricity and 180° switching. This process can be made even faster by reducing the cooling time of the reactor (immersing it in cold water) and by reducing the microwave exposure time (increasing the power).

Highly ordered BiFeO<sub>3</sub> thin films were successfully produced by hydrothermal synthesis on SrTiO<sub>3</sub>:Nb (100) substrates. Surfactants were avoided and we significantly reduced the concentration of potassium hydroxide (KOH) by a factor of 10 compared to reports in literature to reduce the leakage current. Due to this reduction of mineralizer, leading to less solubility of the precursors and decreasing the reaction rate, deposition time ~18 h were required to grow a 40 nm thin film. As-grown BiFeO<sub>3</sub> films were also annealed at 500 °C under nitrogen flow for better crystallization and to remove hydrogen. For the first time, polarization reversal is demonstrated by successful reduction of electronic leakage. A first demonstration of the bulk photovoltaic effect in hydrothermally grown BiFeO<sub>3</sub> shows that this technique can be used to produce multiferroics for photovoltaic applications.

## 5. Summary and Outlook

*Oxide materials* are strong contenders for silicon because they possess multifunctional properties that can be utilized in various novel electronic devices. The ability to terminate oxide substrates at well-defined planes and the realization of sharp interfaces for epitaxial heterostructures with atomic layer precision makes “oxide electronics” a field of its own and is rival to semiconductors multilayers now. The work discussed in this dissertation includes surface termination of SrTiO<sub>3</sub> substrate and epitaxial thin film deposition of multifunctional perovskite oxides by microwave and conventional hydrothermal processes.

- *Substrate surface termination:* A novel microwave-assisted hydrothermal etching was successfully applied to the surface preparation of pure and Nb-doped SrTiO<sub>3</sub> (100), (110) and (111) single crystals (Table 5-1). Without the possibility of fluorine contaminations by avoiding widely used etching chemistry involved with HF, the surface structure appears perfect within the limitations of the miscut angle with this technique. The technique developed is inexpensive, fast, safe, environmentally benign, compatible with batch processes, and showed remarkable reproducibility. Further, this method does not need an ultra-high vacuum environment and long annealing time at high temperatures. The possibility to reduce the etching time significantly avoids the formation of etch pits and holes on the substrate surface.

*Table 5-1 Shows the different crystallographic orientations and its corresponding theoretical chemical terminations and step heights.*

SrTiO <sub>3</sub> pure and Nb doped			
Crystallographic orientation	(100)	(110)	(111)
Chemical termination	SrO TiO <sub>2</sub>	(SrTiO) <sup>4+</sup> (O <sub>2</sub> ) <sup>4-</sup>	(SrO <sub>3</sub> ) <sup>4-</sup> (Ti) <sup>4+</sup>
Step height (Interplanar distance) d (nm)	0.3905	0.2761	0.254

In the case of microwave hydrothermal etching process, the etching medium does not play a significant difference in the realization of single chemically terminated surfaces in the case of (100) crystallographic orientation as both, water and alkaline solution, resulted in identical surfaces with  $d_{100}$  ( $a=0.3905$  nm). In the case of (110) oriented single crystal substrates, pure and Nb doped SrTiO<sub>3</sub> showed a step height  $\sim 0.276$  nm suggesting identical chemical termination on the terraces. Interestingly, in the case of Nb doped SrTiO<sub>3</sub> (110) substrate step-terrace surface could not be realized with water based etching route at all, even at temperature as high as 1100°C. Finally, the case of pure and Nb doped SrTiO<sub>3</sub> (111) surface, the process with deionized water and ammonia solution resulted in step heights close to the theoretical interplanar distance (0.254 nm) in pure and Nb doped SrTiO<sub>3</sub> single crystal substrates.

▪ *Microwave hydrothermal synthesis of BaTiO<sub>3</sub> thin films:* A hydrothermal processing which involves mixing of precursors at the molecular level under high pressure and moderate temperatures was applied to the synthesis of BaTiO<sub>3</sub> on Nb:SrTiO<sub>3</sub> (100) surface with TiO<sub>2</sub> termination. This processing route essentially resulted in the epitaxial BaTiO<sub>3</sub> crystallization at low temperatures. However, conventional hydrothermal method which requires exceptionally long reaction/processing time to realize a few ten nm of BaTiO<sub>3</sub> thin film make the process time problematic due to the slow buildup of pressure/temperature inside the autoclave. The novel microwave assisted hydrothermal method employed here significantly reduced the processing time of BaTiO<sub>3</sub> thin film formation on Nb:SrTiO<sub>3</sub>(100). Other drawback of hydrothermal synthesis is the incorporation of hydroxyl group onto the grown thin films and the high leakage current due to it is detrimental for any electronic application. However, a 10% H<sub>2</sub>O<sub>2</sub> addition resulted in uniform nucleation of BaTiO<sub>3</sub> over the entire Nb:SrTiO<sub>3</sub> substrate surface and growth continued at the film-solution interface as well. This oxidant action of H<sub>2</sub>O<sub>2</sub> is encouraging for realizing epitaxial ferroelectric BaTiO<sub>3</sub> thin film and additionally reduced the OH incorporation due to scavenging action of H<sub>2</sub>O<sub>2</sub> by capturing the H in the solution producing water as consequence.

▪ *Conventional hydrothermal synthesis of BiFeO<sub>3</sub> thin films:* In the present work, highly ordered BiFeO<sub>3</sub> thin films were successfully produced by conventional hydrothermal synthesis on Nb:SrTiO<sub>3</sub> (100) substrates. For the first time, polarization reversal was demonstrated by successful reduction of electronic leakage. A first demonstration of the bulk photovoltaic effect in

hydrothermally grown BiFeO<sub>3</sub> shows that this technique can be used to produce multiferroics for photovoltaic applications

*Outlook:* Ferroelectric tunnel junctions of 1 to 3 nm are free from Fe-RAM limitations of destructive readout and scalability. The read operation in this type of memory is performed by sensing a current *across* the ferroelectric layer, induced by a sub-coercive voltage which does not change the orientation of the existing polarization state and hence allows for non-destructive readout. In conventional FTJ with an ultrathin FE sandwiched between two metallic electrodes, the barrier height is modulated by the polarization reversal (to a very small extent, thickness is also modulated due to the piezoelectric effect) and hence the TER has two stable states. Typical ON/OFF resistance ratios are around 10<sup>2</sup>. However, with one of the electrode replaced by a semiconducting material, the barrier width also experiences modulation (to a greater extent by realizing a depletion region in the semiconductor near the ferroelectric/semiconductor interface) along with the barrier height. This depletion layer thickness ( $t_d$ ) adds up to the thickness of the ferroelectric thin film ( $t_f$ ) and hence the overall tunneling distance ( $t_{total}=t_f+t_d$ ) increases substantially. As the tunneling current exponentially depends on the thickness, the ON/OFF resistance ratio improves further which significantly improves the error margin for highly down-scaled cell-sizes. Also the readout current densities are very large compared to conventional Fe-RAM, making FTJ highly suitable for high density application by reducing the cell size to the nanometer regime (scalability). Due to these reasons it will be interesting to deposit ultra-thin BaTiO<sub>3</sub> and BiFeO<sub>3</sub> films on semiconducting Nb doped SrTiO<sub>3</sub> by the microwave hydrothermal method.

Due to the low concentration of the mineralizer KOH, up to 18 h were required to grow 40 nm BiFeO<sub>3</sub> thin films. This clearly represents a roadblock for industrial batch processing but recent experiments from our group with microwave-assisted hydrothermal synthesis of BiFeO<sub>3</sub> nanoplates have shown the potential to decrease the reaction time to a few minutes. Experiments to apply this technique to thin films are worth considering. Also, the understanding of BiFeO<sub>3</sub> thin films has not converged to a satisfying conclusion, in terms of its structure, dielectric constant, polarization and coercive field. Whether this deficiency depends on the methods of preparation leading to compositional differences or to stress is not clear and hence suggests further optimization of BiFeO<sub>3</sub> film properties. However, the largest switchable polarization of BiFeO<sub>3</sub>

and its environmental benevolence will find its way to the memory application by reducing the conductivity towards some industrially tolerable limits.

## 6. References

- 1 Eerenstein, W., Mathur, N. D. & Scott, J. F. Multiferroic and magnetoelectric materials. *Nature* **442**, 759-765, (2006).
- 2 Waser, R. *Nanoelectronics and Information Technology*. Wiley (2005).
- 3 von Hippel, A., Breckenridge, R. G., Chesley, F. G. & Tisza, L. High dielectric constant ceramics. *Industrial & Engineering Chemistry* **38**, 1097-1109, (1946).
- 4 Hulm, J. K. Dielectric Properties of Single Crystals of Barium Titanate. *Nature* **160**, 127-128 (1947).
- 5 Gruverman, A. & Kholkin, A. Nanoscale ferroelectrics: processing, characterization and future trends. *Reports on Progress in Physics* **69**, 2443-2474, (2006).
- 6 Ambriz-Vargas, F., Velasco-Davalos, I., Thomas, R. & Ruediger, A. Nucleation and growth of ultrathin BaTiO<sub>3</sub> films on single terminated Nb:SrTiO<sub>3</sub> (100) substrates for ferroelectric tunnel junctions. *Journal of Vacuum Science & Technology B* **34**, , (2016).
- 7 Schlom, D. G. *et al.* Strain tuning of ferroelectric thin films. *Annual Review of Materials Research* **37**, 589-626, (2007).
- 8 Garcia, V. & Bibes, M. Ferroelectric tunnel junctions for information storage and processing. *Nat Commun* **5**, (2014).
- 9 Wen, Z., Li, C., Wu, D., Li, A. & Ming, N. Ferroelectric-field-effect-enhanced electroresistance in metal/ferroelectric/semiconductor tunnel junctions. *Nat Mater* **12**, 617-621, (2013).
- 10 Schmid, H. Multi-ferroic magnetoelectrics. *Ferroelectrics* **162**, 317-338, doi:10.1080/00150199408245120 (1994).
- 11 Thomas, R., Scott, J. F., Bose, D. N. & Katiyar, R. S. Multiferroic thin-film integration onto semiconductor devices. *Journal of Physics-Condensed Matter* **22**, (2010).
- 12 Nechache, R. *et al.* Photovoltaic properties of Bi<sub>2</sub>FeCrO<sub>6</sub> epitaxial thin films. *Applied Physics Letters* **98**, 202902 (2011).
- 13 Haertling, G. H. Ferroelectric Ceramics: History and Technology. *Journal of the American Ceramic Society* **82**, 797-818, (1999).
- 14 Peter, F. *Piezoresponse Force Microscopy and Surface Effects of Perovskite Ferroelectric Nanostructures*, Jülich research center, (2006).
- 15 Scott, J. F. Ferroelectrics go bananas. *Journal of Physics: Condensed Matter* **20**, 2 (2008).
- 16 Kinase, W. & Harada, K. Ferroelectricity of Perovskite (ABO<sub>3</sub>) Type Crystals. *Ferroelectrics* **283**, 39-47, (2003).

## References

---

- 17 Spaldin, N. A. & Fiebig, M. The Renaissance of Magnetoelectric Multiferroics. *Science* **309**, 391-392, (2005).
  - 18 Rabe, K. M., Ahn, C. H. & Triscone, J. M. Physics of Ferroelectrics: A Modern Perspective. *Springer London, Limited* (2007).
  - 19 Moulson, A. J. & Herbert, J. M. *Electroceramics*. (Wiley, 2003).
  - 20 Carter, C. & Norton, M. Ceramic Materials: Science and Engineering. *Springer* (2007).
  - 21 Byrappa, K. & Ohachi, T. *Crystal Growth Technology*. (Springer, 2003).
  - 22 Wang, J. *et al.* Epitaxial BiFeO<sub>3</sub> Multiferroic Thin Film Heterostructures. *Science* **299**, 1719 (2003).
  - 23 Basu, S. *et al.* Photoconductivity in BiFeO<sub>3</sub> thin films. *Applied Physics Letters* **92** (2008).
  - 24 Nelson, J. The physics of Solar Cells. *Imperial College Press* (2004).
  - 25 Yang, S. Y. *et al.* Above-bandgap voltages from ferroelectric photovoltaic devices. *Nature Nanotechnology* **5**, 143-147, (2010).
  - 26 Ji, W., Yao, K. & Liang, Y. Bulk Photovoltaic Effect at Visible Wavelength in Epitaxial Ferroelectric BiFeO<sub>3</sub> Thin Films. *Advanced Materials* **22**, 1763-1766 (2010).
  - 27 Yang, S. *et al.* Photovoltaic effects in BiFeO<sub>3</sub>. *Applied Physics Letters* **95**, 062909 (2009).
  - 28 Young, S. M., Zheng, F. & Rappe, A. M. First-Principles Calculation of the Bulk Photovoltaic Effect in Bismuth Ferrite. *Physical Review Letters* **109**, 236601 (2012).
  - 29 Schirmer, O. F., Imlau, M. & Merschjann, C. Bulk photovoltaic effect of LiNbO<sub>3</sub>:Fe and its small-polaron-based microscopic interpretation. *Physical Review B* **83**, 165106 (2011).
  - 30 Choi, T., Lee, S., Choi, Y. J., Kiryukhin, V. & Cheong, S.-W. Switchable Ferroelectric Diode and Photovoltaic Effect in BiFeO<sub>3</sub>. *Science* **324**, 63-66 (2009).
  - 31 Baskaran, A. & Smereka, P. Mechanisms of Stranski-Krastanov growth. *Journal of Applied Physics* **111**, 044321, (2012).
  - 32 Venables, J. A., Spiller, G. D. T. & Hanbucken, M. Nucleation and growth of thin films. *Reports on Progress in Physics* **47**, 399 (1984).
  - 33 Waser, R. & Aono, M. Nanoionics-based resistive switching memories. *Nat Mater* **6**, 833-840 (2007).
  - 34 Reji, T., Scott, J. F., Dwarka, N. B. & Ram, S. K. Multiferroic thin-film integration onto semiconductor devices. *Journal of Physics: Condensed Matter* **22**, 423201 (2010).
  - 35 Schlom, D. G. *et al.* Strain Tuning of Ferroelectric Thin Films. *Annual Review of Materials Research* **37**, 589-626 (2007).
-

## References

---

- 36 Orenstein, J. Multiferroic Orenstein Research Group <http://physics.berkeley.edu/research/orenstein/Multiferroic%20web%20content.html>. (2010).
  - 37 Mukunoki, Y., Nakagawa, N., Susaki, T. & Hwang, H. Y. Atomically flat (110) SrTiO<sub>3</sub> and heteroepitaxy. *Applied Physics Letters* **86**, 171908 (2005).
  - 38 Chang, J., Park, Y.-S. & Kim, S.-K. Atomically flat single-terminated SrTiO<sub>3</sub> (111) surface. *Applied Physics Letters* **92**, 152910, (2008).
  - 39 Biswas, A. *et al.* Universal Ti-rich termination of atomically flat SrTiO<sub>3</sub> (001), (110), and (111) surfaces. *Applied Physics Letters* **98**, 051904-051903 (2011).
  - 40 Herger, R. *et al.* Surface of Strontium Titanate. *Physical Review Letters* **98**, 076102 (2007).
  - 41 Enterkin, J. A. *et al.* A homologous series of structures on the surface of SrTiO<sub>3</sub>(110). *Nat Mater* **9**, 245-248, (2010).
  - 42 Russell, B. C. & Castell, M. R. Surface of Sputtered and Annealed Polar SrTiO<sub>3</sub>(111): TiO<sub>x</sub>-Rich (n × n) Reconstructions. *The Journal of Physical Chemistry C* **112**, 6538-6545, doi:10.1021/jp711239t (2008).
  - 43 Gabaly, F. E., Bartelt, N. C. & Schmid, A. K. Preparing arrays of large atomically flat regions on single crystal substrates. *Journal of Physics: Condensed Matter* **21**, 314019 (2009).
  - 44 Kawasaki, M. *et al.* Atomic Control of the SrTiO<sub>3</sub> Crystal Surface. *Science* **266**, 1540-1542 (1994).
  - 45 Chang, J., Park, Y. S. & Kim, S. K. Atomically flat single-terminated SrTiO<sub>3</sub> (111) surface. *Applied Physics Letters* **92**, 152910 (2008).
  - 46 Chambers, S., Droubay, T., Capan, C. & Sun, G. Y. Unintentional F doping of SrTiO<sub>3</sub> (001) etched in HF acid-structure and electronic properties. *Surface Science* **606**, 554-558 (2012).
  - 47 Guhl, H., Miller, W. & Reuter, K. Water adsorption and dissociation on SrTiO<sub>3</sub> (001) revisited: A density functional theory study. *Physical Review B* **81**, 1-8 (2010).
  - 48 Cernea, M. Methods for preparation of BaTiO<sub>3</sub> thin films. *Journal of Optoelectronics and advance materials*. **6**, 1349-1356 (2004).
  - 49 Nye, J. F. Physical Properties of Crystals. *Clarendon Press Oxford* (1985).
  - 50 Byrappa, K. & Yoshimura, M. *Handbook of Hydrothermal Technology*. (William Andrew, 2013).
  - 51 Byrappa, K. *Handbook of Hydrothermal Technology*. *Noyes Publications* (2001).
  - 52 Riman, R., Suchanek, W. & Lencka, M. Hydrothermal crystallization of Ceramics. *Annales de Chimie Science des Matériaux* **27**, 15-36 (2002).
-

- 
- 53 Yoshimura, M. & Byrappa, K. Hydrothermal processing of materials: past, present and future. *Journal of Materials Science* **43**, 2085-2103, (2008).
- 54 Tan, C. K., Goh, G. K. & Lau, G. K. Growth and dielectric properties of BaTiO<sub>3</sub> thin films prepared by the microwave-hydrothermal method. *Thin Solid Films* **516**, 5545-5550, (2008).
- 55 Li, S. *et al.* Ultrafast Microwave Hydrothermal Synthesis of BiFeO<sub>3</sub> Nanoplates. *Journal of the American Ceramic Society*, 1-8, (2013).
- 56 Alexe, M. & Hesse, D. Tip-enhanced photovoltaic effects in bismuth ferrite. *Nat Commun* **2**, 256-256, (2011).
- 57 Nelson, J. & Riley, D. An Experimental Investigation of Extrapolation Methods in the Derivation of Accurate Unit-Cell Dimensions of Crystals. *Proceedings of the Physical Society* **57**, 160-177 (1945).
- 58 Watts, J. F. & Wolstenholme, J. *An introduction to surface analysis by XPS and AES*. (2003).
- 59 Sanchez, F., Ocal, C. & Fontcuberta, J. Tailored surfaces of perovskite oxide substrates for conducted growth of thin films. *Chemical Society Reviews* **43**, 2272-2285, (2014).
- 60 Perdomo, C. Technical guide, microwave oven with inverters (2013).
- 61 Vargas, F. A. *et al.* On-axis radio frequency magnetron sputtering of stoichiometric BaTiO<sub>3</sub> target: Localized re-sputtering and substrate etching during thin film growth. *Thin Solid Films*, (2015).
- 62 Eckstein, J. N. *et al.* Atomically layered heteroepitaxial growth of single-crystal films of superconducting Bi<sub>2</sub>Sr<sub>2</sub>Ca<sub>2</sub>Cu<sub>3</sub>O<sub>x</sub>. *Applied Physics Letters* **57**, 931-933 (1990).
- 63 Prellier, W., Lecoœur, P. & Mercey, B. Colossal-magnetoresistive manganite thin films. *Journal of Physics: Condensed Matter* **13** (2001).
- 64 Daumont, C. J. M. *et al.* Tuning the atomic and domain structure of epitaxial films of multiferroic BiFeO<sub>3</sub>. *Physical Review B* **81**, 144115 (2010).
- 65 Thomas R, Scott J.F, Bose D.N & Katiyar R.S. Multiferroic thin-film integration onto semiconductor devices. *Journal of physics. Condensed matter* **22** (2010).
- 66 Ohtomo, A. & Hwang, H. Y. A high-mobility electron gas at the LaAlO<sub>3</sub>/SrTiO<sub>3</sub> heterointerface. *Nature* **427**, 423-426 (2003).
- 67 Vrejoiu, I., Alexe, M., Hesse, D. & Gösele, U. Functional Perovskites – From Epitaxial Films to Nanostructured Arrays. *Advanced Functional Materials* **18**, 3892-3906, doi:10.1002/adfm.200800560 (2008).
- 68 Lu, H. *et al.* Enhancement of Ferroelectric Polarization Stability by Interface Engineering. *Advanced Materials* **24**, 1209-1216 (2012).
- 69 D.S. Jeong *et al.* Emerging memories: resistive switching mechanisms and current status. *Reports on progress in physics* **75** (2012).
-

## References

---

- 70 Bark, C. W. *et al.* Tailoring a two-dimensional electron gas at the LaAlO<sub>3</sub>/SrTiO<sub>3</sub> (001) interface by epitaxial strain. *Proceedings of the National Academy of Sciences* (2011).
- 71 Gariglio, S., Reyren, N., Caviglia, A. D. & Triscone, J. M. Superconductivity at the LaAlO<sub>3</sub>/SrTiO<sub>3</sub> interface. *Journal of Physics: Condensed Matter* **21** (2009).
- 72 Duan, C., Jaswal, S. S. & Tsymbal, E. Y. Predicted magnetoelectric effect in Fe/BaTiO<sub>3</sub> multilayers: ferroelectric control of magnetism. *Physical Review Letters* **97**, 047201 (2006).
- 73 Mannhart, J. & Schlom, D. G. Oxide Interfaces---An Opportunity for Electronics. *Science* **327**, 1607-1611, (2010).
- 74 Ohnishi, T. *et al.* Preparation of thermally stable TiO<sub>2</sub>-terminated SrTiO<sub>3</sub> (100) substrate surfaces. *Applied Physics Letters* **85**, 272-274 (2004).
- 75 Bachelet, R., Sanchez, F., Palomares, F., Ocal, C. & Fontcuberta, J. Atomically flat SrO-terminated SrTiO<sub>3</sub> (001) substrate. *Applied Physics Letters* **95** (2009).
- 76 Rodenbucher, C., Wicklein, S., Waser, R. & Szot, K. Insulator-to-metal transition of SrTiO<sub>3</sub>:Nb single crystal surfaces induced by Ar<sup>+</sup> bombardment. *Applied Physics Letters* **102**, 101603 (2013).
- 77 Akoh, H., Camerlingo, C. & Takada, S. Anisotropic Josephson junctions of Y-Ba-Cu-O/Au/Nb film sandwiches. *Applied Physics Letters* **56**, 1487-1489 (1990).
- 78 Suzuki, Y., Hwang, H. Y., Cheong, S.-W. & Dover, R. B. v. The role of strain in magnetic anisotropy of manganite thin films. *Applied Physics Letters* **71**, 140-142 (1997).
- 79 Ogimoto, Y. *et al.* Strain-induced crossover of the metal-insulator transition in perovskite manganites. *Physical Review B* **71**, 060403 (2005).
- 80 Laibowitz, R. B. *et al.* All high T<sub>c</sub> edge junctions and SQUIDS. *Applied Physics Letters* **56**, 686-688, (1990).
- 81 Ohtomo, A. & Hwang, H. Y. A high-mobility electron gas at the LaAlO<sub>3</sub>/SrTiO<sub>3</sub> heterointerface. *Nature* **427**, 423-426 (2004).
- 82 Sone, K., Naganuma, H., Miyazaki, T., Nakajima, T. & Okamura, S. Crystal Structures and Electrical Properties of Epitaxial BiFeO<sub>3</sub> Thin Films with (001), (110), and (111) Orientations. *Japanese Journal of Applied Physics* **49**, 09MB03 (2010).
- 83 Bachelet, R., Valle, F., Infante, I. C., Sanchez, F. & Fontcuberta, J. Step formation, faceting, and bunching in atomically flat SrTiO<sub>3</sub> (110) surfaces. *Applied Physics Letters* **91**, (2007).
- 84 Mukunoki, Y., Nakagawa, N., Susaki, T. & Hwang, H. Y. Atomically flat (110) SrTiO<sub>3</sub> and heteroepitaxy. *Applied Physics Letters* **86**, (2005).
- 85 Brunen, J. & Zegenhagen, J. Investigation of the SrTiO<sub>3</sub> (110) surface by means of LEED, scanning tunneling microscopy and Auger spectroscopy. *Surface Science* **389**, 349-365, (1997).
-

## References

---

- 86 Shigetani, H. *et al.* BaTiO<sub>3</sub> thin films grown on SrTiO<sub>3</sub> substrates by a molecular-beam-epitaxy method using oxygen radicals. *Journal of Applied Physics* **81**, 693-697, (1997).
- 87 Gunhold, A. *et al.* Study of the electronic and atomic structure of thermally treated SrTiO<sub>3</sub>(110) surfaces. *Surface and Interface Analysis* **35**, 998-1003, (2003).
- 88 Velasco-Davalos, I., Thomas, R. & Ruediger, A. Realization of single-termination SrTiO<sub>3</sub> (100) surfaces by a microwave-induced hydrothermal process. *Applied Physics Letters* **103**, (2013).
- 89 Velasco Davalos, I. A., Ruediger, A., Cruz-Rivera, J. & Gomez-Yanez, C. Mechanical niobium doping in barium titanate electroceramics. *Journal of Alloys and Compounds* **581**, 56-58 (2013).
- 90 Karczewski, J., Riegel, B., Gazda, M., Jasinski, P. & Kusz, B. Electrical and structural properties of Nb-doped SrTiO<sub>3</sub> ceramics. *Journal of Electroceramics* **24**, 326-330, (2010).
- 91 Hamasaki, Y. *et al.* Epitaxial growth of metastable multiferroic AlFeO<sub>3</sub> film on SrTiO<sub>3</sub> (111) substrate. *Applied Physics Letters* **104**, 082906, (2014).
- 92 Ke, C., Yang, Z., Zhu, W., Pan, J. S. & Karamat, S. Heteroepitaxial growth of SnO<sub>2</sub> thin films on SrTiO<sub>3</sub> (111) single crystal substrate by laser molecular beam epitaxy. *Journal of Applied Physics* **107**, 013515, (2010).
- 93 Asthagiri, A. *et al.* Thin Pt films on the polar SrTiO<sub>3</sub>(111) surface: an experimental and theoretical study. *Surface Science* **537**, 134-152, (2003).
- 94 McKeown Walker, S. *et al.* Control of a Two-Dimensional Electron Gas on SrTiO<sub>3</sub> by Atomic Oxygen. *Physical Review Letters* **113**, 177601 (2014).
- 95 Lo, W. J. & Somorjai, G. A. Temperature-dependent surface structure, composition, and electronic properties of the clean SrTiO<sub>3</sub> (111) crystal face: Low-energy-electron diffraction, Auger-electron spectroscopy, electron energy loss, and ultraviolet-photoelectron spectroscopy studies. *Physical Review B* **17**, 4942-4950 (1978).
- 96 Ferrer, S. & Somorjai, G. A. UPS and XPS studies of the chemisorption of O<sub>2</sub>, H<sub>2</sub> and H<sub>2</sub>O on reduced and stoichiometric SrTiO<sub>3</sub>(111) surfaces; The effects of illumination. *Surface Science* **94**, 41-56, (1980).
- 97 Tanaka, H. & Kawai, T. Surface structure of reduced SrTiO<sub>3</sub>(111) observed by scanning tunneling microscopy. *Surface Science* **365**, 437-442, (1996).
- 98 Sigmund, W. M. *et al.* A titanium-rich (111) surface of SrTiO<sub>3</sub> single crystals by thermal annealing. *Appl Phys A* **64**, 219-220, (1997).
- 99 Sekiguchi, S. *et al.* Atomic force microscopic observation of SrTiO<sub>3</sub> polar surface. *Solid State Ionics* **108**, 73-79, (1998).
- 100 Shoichi, S. *et al.* Structure Analysis of SrTiO<sub>3</sub> (111) Polar Surfaces. *Japanese Journal of Applied Physics* **37**, 4140 (1998).
-

## References

---

- 101 Pojani, A., Finocchi, F. & Noguera, C. Polarity on the SrTiO<sub>3</sub> (111) and (110) surfaces. *Surface Science* **442**, 179-198, (1999).
- 102 Kawasaki, M. *et al.* Atomic control of the SrTiO<sub>3</sub> crystal surface. *Science* **266**, 1540-1542, (1994).
- 103 Koster, G., Kropman, B. L., Rijnders, G., Blank, D. H. A. & Rogalla, H. Quasi-ideal strontium titanate crystal surfaces through formation of strontium hydroxide. *Applied Physics Letters* **73**, 2920-2922, (1998).
- 104 Chang, J., Park, Y.-S. & Kim, S.-K. Atomically flat single-terminated SrTiO<sub>3</sub> (111) surface. *Applied Physics Letters* **92**, (2008).
- 105 Yang, Y., Wang, Z., Li, J. & Viehland, D. Pulsed Laser Deposition of BaTiO<sub>3</sub> Thin Films on Different Substrates. *Journal of Nanomaterials* **2010**, 5 (2010).
- 106 Gill, D., Conrad, C., Ford, G., Wessels, B. & Ho, S. Thin-film channel waveguide electro-optic modulator in epitaxial BaTiO<sub>3</sub>. *Applied Physics Letters* **71**, 1783-1785 (1997).
- 107 Chattopadhyay, S., Teren, A., Hwang, J., Mason, T. & Wessels, W. Diffuse phase transition in epitaxial BaTiO<sub>3</sub> thin films. *Journal of Materials Research* **17**, 669-674 (2002).
- 108 Sun, J., Tian, W. & Pan, X. Evolution of dislocation arrays in epitaxial BaTiO<sub>3</sub> thin films grown on (100) SrTiO<sub>3</sub>. *Applied Physics Letters* **84**, 3298-3300 (2004).
- 109 Gersten, B. *Influences of the A and B site cation species in the kinetics of hydrothermal synthesis of ABO<sub>3</sub> perovskite type materials* PhD thesis, Rutgers University, (1999).
- 110 Chien, A., Zhao, L., Colic, M., Speck, J. & Lange, F. Microstructural development of BaTiO<sub>3</sub> heteroepitaxial thin films by hydrothermal synthesis. *Journal of Materials Research* **13**, 649-659 (1998).
- 111 Chien, A. *et al.* Electrical characterization of BaTiO<sub>3</sub> heteroepitaxial thin films by hydrothermal synthesis. *Journal of Materials Research* **14**, 3330-3339 (1999).
- 112 McCormick, M. A. & Slamovich, E. B. Microstructure development and dielectric properties of hydrothermal BaTiO<sub>3</sub> thin films. *Journal of the European Ceramic Society* **23**, 2143-2152, (2003).
- 113 Vold, R. E. *et al.* Hydrothermal synthesis of lead doped barium titanate. *Journal of Materials Science* **36**, 2019-2026, (2001).
- 114 Freire, J. D. & Katiyar, R. S. Lattice dynamics of crystals with tetragonal BaTiO<sub>3</sub> structure. *Physical Review B* **37**, 2074-2085 (1988).
- 115 Thomas, R., Varadan, V. K., Komarneni, S. & Dube, D. C. Diffuse phase transitions, electrical conduction, and low temperature dielectric properties of sol-gel derived ferroelectric barium titanate thin films. *Journal of Applied Physics* **90**, 1480-1488, (2001).

## References

---

- 116 Thomas, R., Dube, D. C., Kamalasanan, M. N. & Chandra, S. Optical and electrical properties of BaTiO<sub>3</sub> thin films prepared by chemical solution deposition. *Thin Solid Films* **346**, 212-225, (1999).
- 117 Velasco-Davalos, I. *et al.* Polar properties of hydrothermally synthesized BiFeO<sub>3</sub> thin films. *Appl. Phys. A* **115**, 1081-1085, (2014).
- 118 Huang, A., Handoko, A., Goh, G., Pallathadka, P. & Shannigrahi, S. Hydrothermal synthesis of (001) epitaxial BiFeO<sub>3</sub> films on SrTiO<sub>3</sub> substrate. *Cryst. Eng. Comm.* **12**, 3806-3814 (2010).
- 119 Rout, D. *et al.* Low temperature hydrothermal epitaxy and Raman study of heteroepitaxial BiFeO<sub>3</sub> film. *Applied Physics Letters* **95**, 122509 (2009).
- 120 Dhahri, J., Boudard, M., Zemni, S., Roussel, H. & Oumezzine, M. Structure and magnetic properties of potassium doped bismuth ferrite. *Journal of Solid State Chemistry* **181**, 802-811, (2008).
- 121 Kulkarni, A., Rohrer, G., Narayan, S. & McMillan, L. Electrical properties of ferroelectric thin film KNO<sub>3</sub> memory devices. *Thin Solid Films* **164**, 339-343 (1988).
- 122 Kim, D., Lee, H., Biegalski, M. & Christen, H. Effect of epitaxial strain on ferroelectric polarization in multiferroic BiFeO<sub>3</sub>. *Applied Physics Letters* **92** (2008).

## 7. Abbreviations

AFM	Atomic Force Microscopy
ALD	Atomic Layer Deposition
BD	Ballistic Deposition Model
BPVE	Bulk Photovoltaic Effect
CVD	Chemical Vapor Deposition
DI	Deionized Water
F	Fluor
FM	Frank- Van del Merwe
FTJ	Ferroelectric Tunnel Junction
HF	Hydrofluoric Acid
HHCF	Height-Height Correlation Function
MBE	Molecular Beam Epitaxy
MIM	Metal – Insulator – Metal
MW	Microwave radiation
PFM	Piezoresponse Force Microscopy
PCAFM	Photoconductive Atomic Force Microscopy
PLD	Pulsed Laser Deposition
PTFE	Polytetrafluoroethylene
RMS	Root Mean Square
SEM	Scanning Electron Microscopy

## Abbreviations

---

SK	Stranski- Krastanov
SOS	Solid On Solid
TSK	Terrace Step Kink
UHV	Ultra-High Vacuum
UV	Ultraviolet
VW	Volmer- Weber
XPS	X-Ray Photoelectron Spectroscopy
XRD	X-Ray Diffraction

## 8. Publications, conference presentations and awards

### First author publications

1. Mechanical niobium doping in barium titanate electroceramics, **I. A. Velasco-Davalos**, A. Ruediger, J.J. Cruz-Rivera, C. Gomez-Yanez, *Journal of Alloys and Compounds* 581, 56-58, (2013)
2. Realization of single-termination SrTiO<sub>3</sub> (100) surfaces by a microwave-induced hydrothermal process, **I Velasco-Davalos**, R Thomas, A Ruediger, *Applied Physics Letters* 103 (20), 202905, (2013)
3. Polar properties of hydrothermally synthesized BiFeO<sub>3</sub> thin films, **I. Velasco**, M. Moretti, M. Nicklaus, C. Nauenheim, S. Li, R. Nechache, C. Gomez-Yanez, A. Ruediger, *Applied Physics A*, (2013)
4. Surface preparation of (110) oriented pure and Nb-doped SrTiO<sub>3</sub> single crystal substrates by microwave assisted hydrothermal method, **I Velasco-Davalos**, F Ambriz-Vargas, R Thomas, A Ruediger, *Surface and Coatings Technology* 283, 108-114, (2015)
5. Polarization reversal in BaTiO<sub>3</sub> nanostructures synthesized by microwave-assisted hydrothermal method, **I Velasco-Davalos**, F Ambriz-Vargas, C Gómez- Yáñez, R Thomas, A Ruediger, *Journal of Alloys and Compounds*, 667, pp. 268-274 (2016)
6. Synthesis of BiFeO<sub>3</sub> thin films on single-terminated Nb:SrTiO<sub>3</sub> (111) substrates by intermittent microwave assisted hydrothermal method, **I Velasco-Davalos**, F Ambriz-Vargas, G. Kolhatkar, R Thomas, A Ruediger, **submitted** to *Journal of Applied Physics*, (2016)

Second author publications

1. Ultrafast Microwave Hydrothermal Synthesis of BiFeO<sub>3</sub> Nanoplates, S. Li, R. Nechache, **I. Velasco**, G. Goupil, L. Nikolova, M. Nicklaus, J. Laverdiere, A. Ruediger, F. Rosei, *Journal of the American Ceramic Society*, accepted, doi: 10.1111/jace.12473, (2013)
2. Interplay between  $\alpha$ -relaxation and morphology transition of perfluorosulfonate ionomer membranes, BR Matos, EI Santiago, R Muccillo, **IA Velasco-Davalos**, A Ruediger, *Journal of Power Sources* 293, 859-867, (2015)
3.  $\alpha$ -Relaxation and Morphology Transition of Perfluorosulfonate Ionomer Membranes, BR Matos, EI Santiago, R Muccillo, **IA Velasco-Davalos**, A Ruediger, *MRS Proceedings* 1735, mrsf14-1735-s05-03, (2015)
4. Structural, surface morphology and optical properties of NiSnO<sub>3</sub> thin films prepared using spray technique, A Mhamdi, R Dridi, A Arfaoui, C Awada, M Karyaoui, **IA Velasco-Davalos**, *Optical Materials* 47, 386-390, (2015)
5. Nucleation and growth of ultrathin BaTiO<sub>3</sub> films on single terminated Nb: SrTiO<sub>3</sub> (100) substrates for ferroelectric tunnel junctions, F Ambriz-Vargas, **I Velasco-Davalos**, R Thomas, A Ruediger, *Journal of Vacuum Science & Technology B* 34 (2), 02M101, (2016)
6. B. Matos, M. Drescha, E. Santiago, L. Moraesa, D. Carastan, J. Schoenmaker, **I. A. Velasco-Davalos**, A. Ruediger, A. Tavares, F. Fonseca, *Electrochimica Acta*, (2016)

## Conferences

1. - Poster: Tuneable bandgap multiferroics for high efficiency photovoltaics, CIPI AGM Ottawa, May 2011.
- 2.- Talk: Hydrothermal synthesis of epitaxial BiFeO<sub>3</sub> for bulk photovoltaics, 36th International conference & exposition on advanced ceramics and composites, Daytona, September 2011.
3. – Poster: Synthèse hydrothermale de couches minces épitaxiales de BiFeO<sub>3</sub> pour des applications photovoltaïque de volume, Conference Nanoquebec, Montreal, March 2012.
4. - Poster: Hydrothermal Synthesis of Epitaxial BiFeO<sub>3</sub> for bulk Photovoltaics, Photonics Noth, Montreal, June 2012.
5. - Poster: Hydrothermal Synthesis of epitaxial perovskite thin films, 5<sup>e</sup> Colloque nanotechnologies & nanosystemes LN2/UMI, Orford, Canada, July 2012.
6. - Poster: Hydrothermal synthesis of epitaxial BiFeO<sub>3</sub> for functional applications, Materials Science & technology, Montreal, October 2013.
7. – Talk: Surface Preparation of SrTiO<sub>3</sub> Single Crystal by Microwave Assisted Hydrothermal Technique:  
A comparative study on the etching media and crystal orientation, 56<sup>th</sup> Electronic Materials Conference, Santa Barbara, California, 2014.
8. – Poster: Surface Preparation of SrTiO<sub>3</sub> Single Crystal by Microwave Assisted Hydrothermal Technique: A Comparative study on the etching media and crystal orientation, 7<sup>th</sup> Symposium on functional coatings and surface engineering, Montreal, July 2014.
9. – Talk: Water-based preparation of single-terminated (100), (110) and (111) SrTiO<sub>3</sub> surface for the heteroepitaxy of functional oxides, XXIII International materials research congress, Cancun, Mexico, August 2014.

## Awards

1. – *Merit doctoral research scholarship program for foreign students (PBEEE)* du Fonds de recherche du Québec Nature et technologies (FRQNT)

2. –Award winner “*Étudiants-chercheur étoile*” du Fonds de recherche du Québec Nature et technologies (FRQNT) —June 2014

## Résumé en Français

### Introduction

Des matériaux d'oxyde multifonctionnels sont en développement continu pour améliorer la conversion d'énergie et le stockage d'informations. Parmi eux, les oxydes type pérovskite avec des propriétés ferroélectriques et multiferroïques jouent un rôle important dans l'état de l'art actuel pour la réalisation de nouvelles fonctionnalités et de dispositifs électroniques de pointe. Les matériaux ferroélectriques présentent une polarisation électrique bistable qui peut être commuté par l'application d'un champ électrique externe. L'intérêt récent pour le BaTiO<sub>3</sub> ferroélectrique est dans la croissance de couches minces épitaxiales pour des mémoires ferroélectriques de haute densité et des dispositifs électro-optiques. Depuis la découverte de l'amélioration de la polarisation dans des couches minces heteroepitaxiales contraints de BiFeO<sub>3</sub> ferroélectromagnétique à température ambiante, le BiFeO<sub>3</sub> multiferroïque a suscité l'intérêt des scientifiques des matériaux à travers le monde et est devenu attractif pour son application photovoltaïque.

Une bonne compréhension du processus de développement d'une couche mince est requise pour produire des couches minces épitaxiales de haute qualité sur des substrats monocristallins. Les modes de croissance cristalline correspondent au mode de développement couche par couche, ou Frank-Van der Merwe (FM), c'est-à-dire que les atomes sont attachés plus fermement au substrat qu'entre eux. Lorsqu'il n'y a pas d'attache forte entre le substrat et les particules, trois types de développement en forme d'îles peuvent s'observer appelée le mode Volmer-Weber (VW). Enfin le mode couche par couche plus croissance d'îles, ou Stranski-Krastanov (SK), est un mode intermédiaire. Après la première ou quelques monocouches, le développement de la couche est défavorable et des îles sont formées sur le dessus de cette couche « intermédiaire ».

La morphologie de la surface du substrat est un aspect important à étudier pour déterminer et comprendre la croissance de la couche mince. Un autre aspect important est de se munir d'une interface de grande qualité en préparant des surfaces à terminaison unique. Le monocristal orienté  $\text{SrTiO}_3$  (100) est de nature non polaire et contient une séquence de couches de charge neutre de SrO et  $\text{TiO}_2$  dans la direction (100) avec une distance interplanar de  $\frac{a}{2}$ . Par contre, le  $\text{SrTiO}_3$  orienté dans la direction (110) correspond à une surface polaire qui contient une séquence de couches chargées de  $\text{SrTiO}^{4+}$  et  $\text{O}_2^{4-}$  avec une distance interplanar de  $\frac{a}{2\sqrt{2}}$ . Dans le cas du cristal orienté dans la direction (111) il existe des couches alternes de  $(\text{SrO}_3)^{4-}$  et  $\text{Ti}^{4+}$  avec une distance interplanar de  $\frac{a}{2\sqrt{3}}$ . (figure 1).

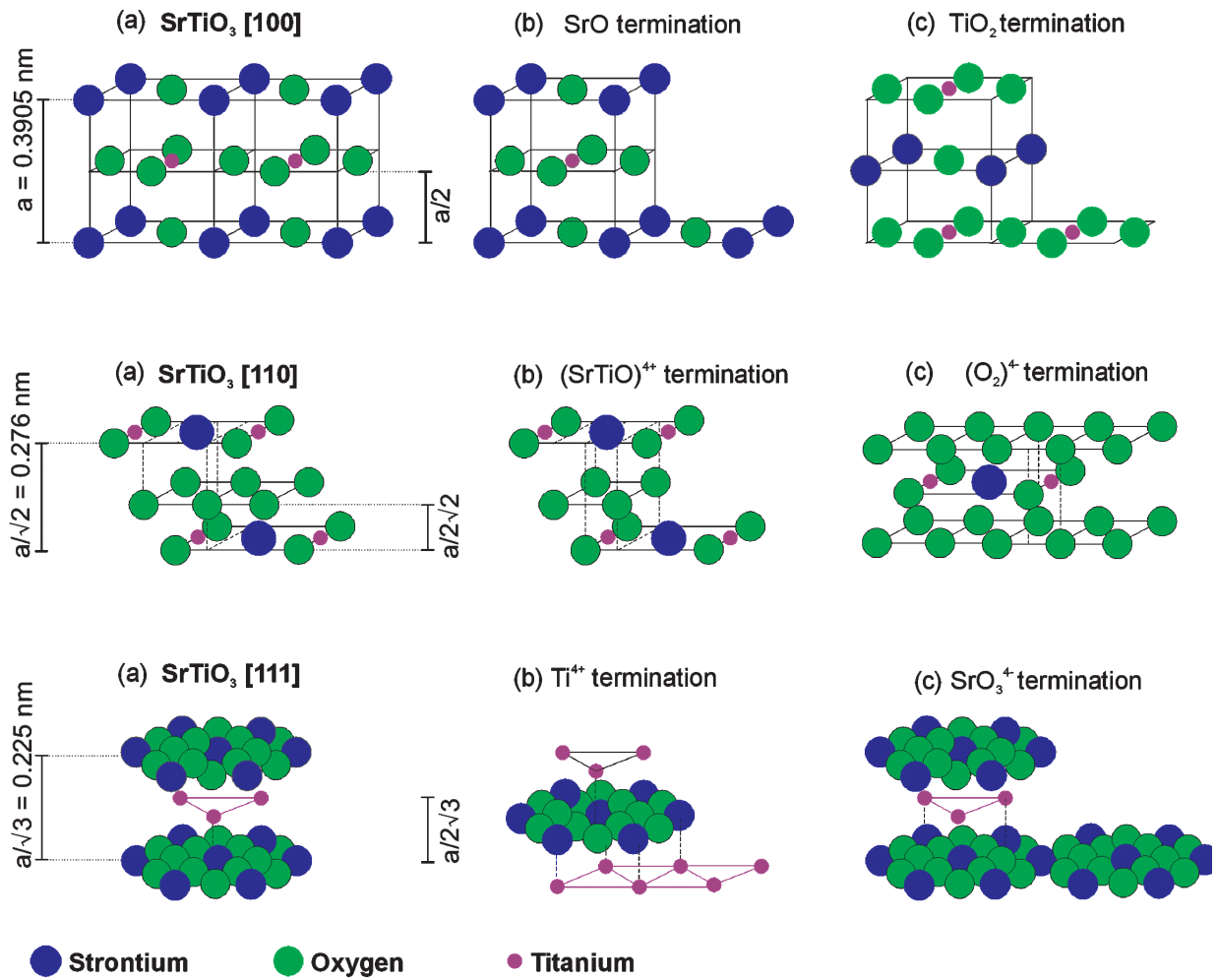


Figure 1. Représente les trois orientations cristallographiques de  $\text{SrTiO}_3$ , [100], [110] et [111] avec un espacement interplanar de  $a$ ,  $a/\sqrt{2}$ , et  $a/\sqrt{3}$ , où  $a = 0.3905 \text{ nm}$ .

Les trois orientations cristallographiques de  $\text{SrTiO}_3$  sont d'une grande importance dans la réalisation de l'hétéroépitaxie et de superréseaux multicouches de nombreux oxydes complexes ciblés pour diverses applications. Afin d'obtenir une interface substrat / couche uniforme, la surface du substrat doit être de une seule terminaison atomique, à savoir qu'il doit être soit un  $\text{SrO}$  ou  $\text{TiO}_2$  pour (100),  $(\text{SrTiO})$  ou  $(\text{O}_2)$  pour (110), et  $(\text{SrO}_3)$  ou  $\text{Ti}$  pour (111). La procédure la plus commune pour obtenir des structures atomiquement plates avec une structure d'étape-terrasse avec terminaison chimique unique se fait par immersion du substrat de  $\text{SrTiO}_3$  dans une solution fluorhydrique tamponné (HF), suivie d'un recuit à des températures élevées sous une ambiance d' $\text{O}_2$ .

La méthode hydrothermale peut être utilisée pour la préparation de surfaces monocristallines de  $\text{SrTiO}_3$  et pour le dépôt de la couche mince de  $\text{BaTiO}_3$  et  $\text{BiFeO}_3$ . Les couches minces épitaxiales  $\text{BaTiO}_3$  et  $\text{BiFeO}_3$  sont habituellement produites par des méthodes physiques comme pulvérisation cathodique, ablation laser, épitaxie par jets moléculaires; et des techniques chimiques comme dépôt chimique en phase vapeur, procédé sol-gel, atomic layer deposition ou par la méthode hydrothermale.

## Les objectifs de recherche

BaTiO<sub>3</sub> et BiFeO<sub>3</sub> sont des modèles de systèmes d'oxyde pérovskite qui présentent, respectivement, des propriétés ferroélectriques et multiferroïques. Des couches minces épitaxiales ferroélectriques de BaTiO<sub>3</sub> et de multiferroïques BiFeO<sub>3</sub> sont très intéressantes pour des mémoires non volatiles et des applications photovoltaïques respectivement. Une réalisation réussie d'une croissance épitaxiale d'une couche mince requiert un substrat monocristallin adéquat. Le monocristal SrTiO<sub>3</sub> est largement utilisé comme un matériau de substrat pour l'heteroepitaxy, de même que comme un agent actif dans différents phénomènes contrôlés d'interface. Dans le but d'avoir une interface uniforme de substrat/couche, la surface de SrTiO<sub>3</sub> devrait être à terminaison unique.

L'objectif principal de cette recherche est d'étudier la réalisation et la compréhension de la surface de substrat de SrTiO<sub>3</sub> pure et dopé avec Nb, et de relever les défis dans la fabrication de films minces de BaTiO<sub>3</sub> et BiFeO<sub>3</sub> sur des substrats avec une seule terminaison chimique de Nb: SrTiO<sub>3</sub> (100).

Les objectifs spécifiques de la recherche sont :

- Préparation de la surface du substrat SrTiO<sub>3</sub> pure et dope avec une seule terminaison par une méthode nouvelle, rapide et respectueuse de l'environnement, gravure hydrothermale.
- Faire la synthèse des couches minces BaTiO<sub>3</sub> et BiFeO<sub>3</sub> par des méthodes hydrothermales conventionnelles, et assistées d'un four à microonde.
- Caractériser la surface du substrat avec la microscopie à force atomique et spectrométrie photoélectronique X.

- Étudier la structure, microstructure et les propriétés ferroélectriques des couches épitaxiales  $\text{BaTiO}_3$  et  $\text{BiFeO}_3$  sur les substrats  $\text{Nb:SrTiO}_3$  à terminaison simple.

#### Outils de caractérisation

Le travail présenté dans cette thèse a consisté à préparer la surface à terminaison simple de substrats purs et dopés avec Nb par une méthode hydrothermale assistée d'un four à microonde. La préparation de la couche mince des oxydes multifonctionnels  $\text{BaTiO}_3$  and  $\text{BiFeO}_3$  sur  $\text{Nb:SrTiO}_3$  a également été réalisée par un four à microonde et par une technique hydrothermale conventionnelle. Les différentes orientations des surfaces  $\text{SrTiO}_3$  et les propriétés des oxydes multifonctionnels ont été caractérisés avec la microscopie à force atomique pour la topographie, microscopie à force piézoélectrique pour évaluer l'effet ferroélectrique par l'effet inverse piézoélectrique, microscopie à force atomique photoélectrique pour étudier les propriétés photovoltaïques pour le cas du  $\text{BiFeO}_3$  en illuminant l'échantillon localement avec un laser UV (355 nm) dans le but de lire les courants photo-générés par en court-circuit (lorsque le voltage est zéro); diffraction de rayon X pour les propriétés cristallines, et spectrométrie photoélectronique X pour établir l'état chimique des éléments à l'intérieur des surfaces solides.

Préparation de surface SrTiO<sub>3</sub>

Sur les trois surfaces mentionnées ci-dessus, les orientations qui permettent des gravures chimiques sélectives pour réaliser une terminaison simple sont [100] et [111] en raison du fait que chaque couche alternative contient soit Sr ou Ti. En revanche, SrTiO<sub>3</sub> (110) contient (SrTiO)<sup>4+</sup> et (O<sub>2</sub>)<sup>4-</sup> piles normales au plan (110), et par conséquent, la gravure préférentielle peut ne pas servir l'objectif par rapport aux surfaces (100) et (111). Ce traite une nouvelle voie pour la préparation de ces surfaces sur des substrats SrTiO<sub>3</sub> purs et dopés avec Nb de toutes les trois orientations par gravure hydrothermale et suivi par un recuit dans l'atmosphère O<sub>2</sub>.

La gravure hydrothermale assistée par four à micro-ondes a été adoptée pour la préparation des surfaces. Un diagramme schématique du réacteur hydrothermique compatible avec four à microondes utilisé pour la gravure du substrat de SrTiO<sub>3</sub> est représenté par la figure 2.

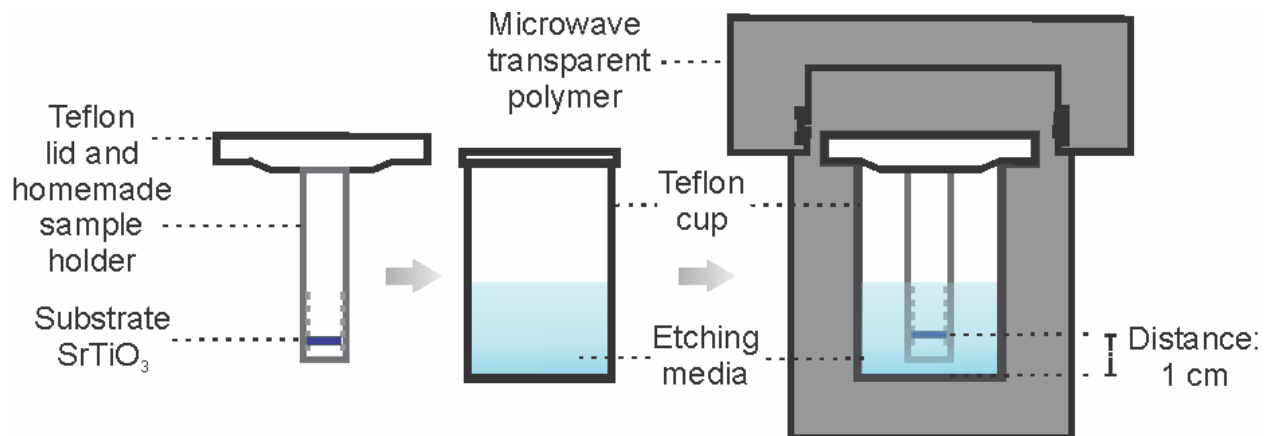


Figure 2. Schéma expérimental montrant une section transversale du réacteur hydrothermale compatible avec microondes.

Il se compose d'une coupelle de polytétrafluoroéthylène (Parr) et un support fait-maison qui peut contenir jusqu'à quatre substrats et qui est fixé sur le couvercle du récipient mentionnée ci-dessus. Cet ensemble assure un positionnement stable du substrat à une certaine distance du fond de la coupelle pendant toute la durée du traitement hydrothermal. Le côté poli des substrats monocristallins de  $\text{SrTiO}_3$  purs et dopés avec Nb (0.5 wt. %) de une taille de  $(5 \times 5 \times 0.5 \text{ mm})$ , angle de désorientation  $< 0.3^\circ$  de Crystec GmbH) ont été utilisés. Le traitement neutre a été réalisé avec de l'eau désionisée, pH 7) et le basique avec 10% d'hydroxyde d'ammonium (Sigma-Aldrich> 99,99%) à pH 10. Les substrats ont été maintenus à l'intérieur de la coupelle en PTFE à une distance de 1 cm à partir du bas avec le côté poli vers le bas pour réduire la contamination des particules et ré-adsorption sur la surface. Cet ensemble coupelle / substrat scellé a ensuite été logé dans un autoclave en polymère compatible aux microondes. La température et la pression générée à l'intérieur du réacteur dépendent uniquement du niveau de remplissage, le temps d'exposition et le niveau de puissance. Dans le cas présent, le facteur de volume de remplissage des médias de gravure a été fixé à 66% du volume total de la coupelle. Le four utilisé pour le chauffage était un four à micro-ondes commerciale (Inverter Panasonic). Le niveau de puissance a été fixé à 360 W et le temps d'exposition aux micro-ondes était de 3 minutes et 4, respectivement, pour la solution d'hydroxyde d'ammonium et de l'eau désionisée. Le réacteur a été maintenu dans le four à micro-ondes après le cycle de chauffage pendant le période mentionne pour permettre à la pression interne de chuter de manière significative et à immerger ensuite la partie inférieure du réacteur dans de l'eau pour accélérer le refroidissement jusqu'à la température ambiante.

Finalelement, les substrats gravés ont été recuits à 1000°C-1100°C pour différentes périodes dans un four à tube programmable (MTI corp) sous l'écoulement de l'oxygène de 80 sccm et le refroidissement du four permis à la température ambiante. La topographie du substrat a été ensuite analysée par microscopie à force atomique (Smart SPM1000-AIST-NT Inc.) en mode tapping. Les cantilever de silicium (Modèle PPP-NCHR-50 de NANOSENSORS™) avec un rayon de pointe typique < 10 nm, longueur 125 µm et les hauteurs 10-15 µm ont été utilisés. Sr et Ti contenus sur la surface du substrat ont été déterminées par spectroscopie photoélectronique des rayons X (VG 220i Escalab XL) en utilisant Al K $\alpha$  (1486.6 eV) rayonnement d'une source de rayons X monochromatique fonctionnant à 400 W. Les spectres ont été étalonnés en utilisant du carbone en affectant l'énergie de liaison de 284.6 eV à la position du pic C1s pour compenser un changement possible dans la position du pic dû aux effets de charge. Des substrats monocristallins de SrTiO<sub>3</sub> commercialement disponibles orientés (100, 110 et 111), purs et dopés avec Nb 0.5 % wt. de 5 x 5 x 0,5 mm (Crystec GmbH, angle de désorientation <0,3 °) ont été utilisés pour la présente étude.

La nouvelle méthode de gravure hydrothermique assistée par micro-ondes a été appliquée avec succès à la préparation de la surface des substrats monocristallins de SrTiO<sub>3</sub> purs et dopés avec Nb orientés (100), (110) et (111). Sans la possibilité de contamination du fluor à partir de la coupelle de Teflon et en évitant la chimie de gravure associé avec HF largement utilisé, la structure de surface apparaît parfait dans les limites du plan d'angle de désorientation. Ces résultats indiquent l'utilisation réussie de ce procédé, sans produits chimiques corrosifs au cours des étapes de préparation, pour obtenir une surface atomiquement plat avec terminaison chimique unique dans les substrats SrTiO<sub>3</sub> (figure 3). Cette technique est peu coûteuse, rapide, sûre, respectueuse

---

de l'environnement, compatible avec les procédés discontinus, et elle a montré une reproductibilité remarquable. En outre, ce procédé ne nécessite pas un environnement sous vide ultra-élevé et de longue durée de recuit à haute température. La possibilité de réduire le temps de gravure permet d'éviter de manière significative la formation de piqûres et de trous de gravure sur la surface du substrat.

Des substrats monocristallins de  $\text{SrTiO}_3$  purs et dopés avec Nb (100) avec une seule terminaison chimique ont été réussies avec une hauteur d'étape de  $d_{100}$  ( $a = 0.3905 \text{ nm}$ ) entre deux terrasses de  $\text{TiO}_2$  adjacentes, lors de la gravure dans l'eau et recuit à  $1000^\circ\text{C}$  pendant 10 min. Le résultat de cette surface (100) est identique à celui de surfaces traitées avec du HF au sein incertitudes expérimentales. Dans le cas de processus hydrothermal à micro-ondes, le moyen de gravure ne joue pas un rôle important dans la réalisation de surfaces simples terminées car l'utilisation de solution d'eau et solution alcaline ont donné lieu à des surfaces identiques pour (100).

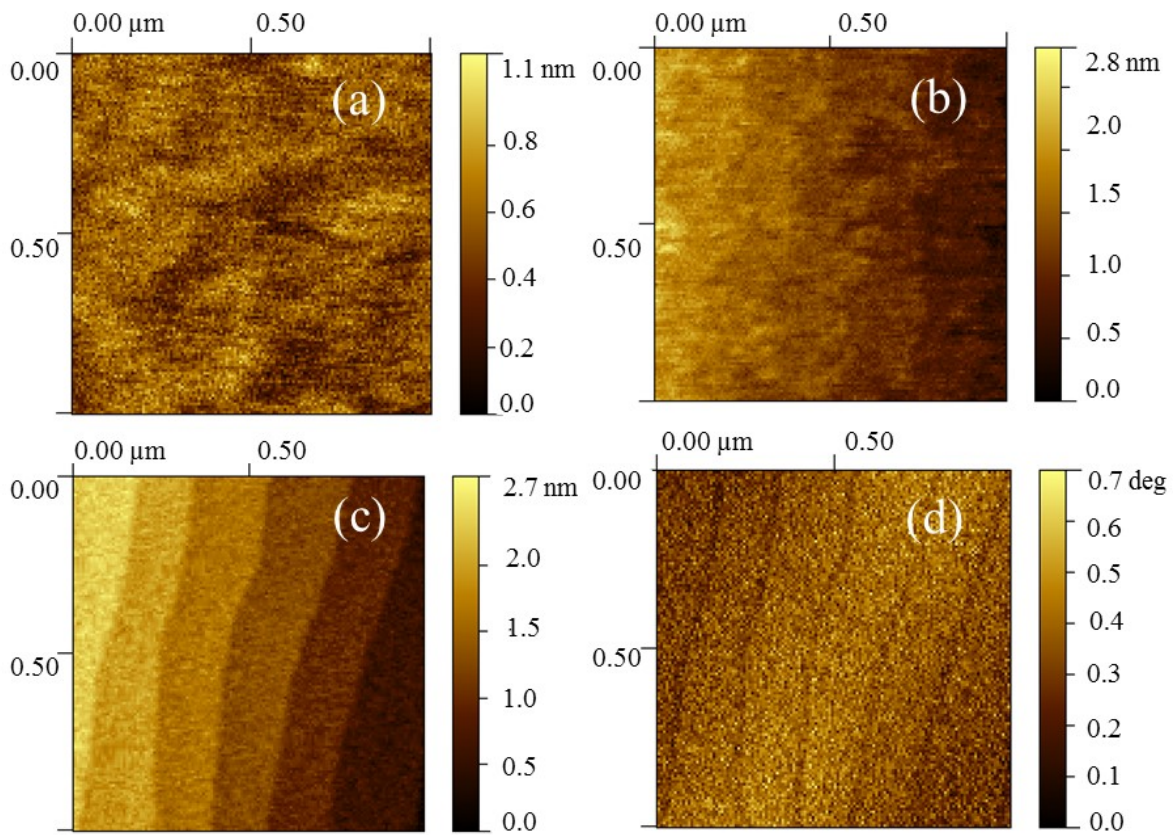


Figure 3. (a) SrTiO<sub>3</sub> (100) substrat monocristallin en tant que reçue; (b) grave par la méthode hydrothermale dans l'eau; (c) grave à l'eau suivie d'une étape de recuit, et (d) son image phase qui montre la terminaison chimique unique.

Des substrats monocristallins de SrTiO<sub>3</sub> Nb purs et dopés avec orientation (110), ont montré une hauteur de marche  $\sim 0.276\text{nm}$  entre terrasses adjacentes, une valeur adaptée très bien à la  $d_{110}$  ( $a/\sqrt{2}$ ); suggérant identiques terminaison chimique sur les terrasses. Dans le cas de SrTiO<sub>3</sub> pur (110), la gravure en milieu alcalin suivi d'un recuit à 1000 °C pendant 10 min a donné lieu à une meilleure surface par rapport à la gravure à base de l'eau. Fait intéressant, dans le cas du SrTiO<sub>3</sub>

(110) dopé avec Nb la surface type étape-terrasse n'a pas pu être réalisée avec de l'eau en même à température aussi élevée que 1100 ° C. Cependant, avec gravure en milieu alcalin et un recuit à 1100 ° C pendant 30 min, la surface du SrTiO<sub>3</sub> (110) dopé avec Nb a pu être faite avec une terminaison chimique unique.

Dans le cas de la surface de SrTiO<sub>3</sub> pure et dopé avec Nb (111), le recuit des substrats telle que reçues donne comme résultat une surface avec de terrasses alternes de (SrO<sub>3</sub>)<sup>4-</sup> ou Ti<sup>4+</sup> avec une hauteur de marche de 0.113 nm ( $d_{111}/2$ ). Un processus de gravure hydrothermique assisté par micro-ondes dans une solution d'eau désionisée et d'ammoniaque a éliminé sélectivement soit des couches (SrO<sub>3</sub>)<sup>4-</sup> ou de Ti<sup>4+</sup> de façon uniforme sur toutes les terrasses. La hauteur de marche mesurée a été de 0,225 nm ( $d_{111}$ ) et le contraste uniforme dans l'image de phase des terrasses confirme la terminaison unique pour les deux cas, purs et dopes avec Nb.

Toutefois, la surface de SrTiO<sub>3</sub> est sujette à la reconstruction pour réduire l'énergie de surface qui modifie de manière significative la coordination de surface des atomes sur une période de temps, ce qui est sévère dans le cas de surfaces chargées de (110) et (111) par rapport de celui neutre (100). Cet aspect, qui est indépendant de la façon dont la terminaison de la surface a été atteinte, influe sur la durée de conservation de la surface à terminaison unique et est soumis à examen plus approfondi. Comme il est un domaine de sa propre et est discuté assez dans la littérature pour tous les trois orientations de surfaces de SrTiO<sub>3</sub> soutenue par des modèles théoriques raisonnables, n'a pas été considéré ici. En bref, la croissance épitaxiale de couches minces d'oxydes multifonctionnels sur ces substrats simples terminé et libres de F<sup>-</sup> peut trouver de

---

nouvelles fonctionnalités et des phénomènes physiques de l'interface pour de nouvelles applications dans le domaine de d'oxydes électroniques. Cependant, afin d'avoir de dépôt de couches minces reproductible sur le substrat avec une même orientation, l'angle et l'orientation doivent être le même entre des substrats. Ceci est dû au fait que nucléation et de croissance des couches minces sur substrat monocristallins dépendent fortement de l'histoire du substrat ou à de petits défauts sur la surface du substrat. Donc, la préparation de la surface et sa caractérisation ne peut pas être contourné lorsque la couche mince épitaxiale sur  $\text{SrTiO}_3$  est considérée pour n'importe quelle application.

#### Couches minces de $\text{BaTiO}_3$ et de $\text{BiFeO}_3$

La technique hydrothermique présente un moyen pratique d'obtenir des couches minces épitaxiales d'oxyde multifonctionnel de haute qualité cristalline à basse température par rapport d'autres techniques qui nécessitent habituellement des processus à haute température. Cette méthode peut également être considérée comme une voie simple, peu coûteuse à obtenir des films minces très texturés en quantités compatibles avec le traitement par lots. Cependant, la formation de plusieurs sous-produits aqueux (principalement des composés hydrogénés) pendant le processus pourrait représenter un risque qui pourrait se déposer sur la surface du substrat, ce qui affecte gravement les propriétés structurales, diélectriques et électriques. Dans ce travail, les couches minces très texturées de  $\text{BaTiO}_3$  et de  $\text{BiFeO}_3$  ont été produites avec succès par synthèse hydrothermique qui a évité dans une grande mesure de l'incorporation de groupe hydroxyle sur la couche. L'usage des substrats de  $\text{SrTiO}_3$  (100) dopés avec 0,5% Nb a servi de l'électrode et la

gravure pour obtenir une terminaison unique sur la surface de ce substrat a été réalisé avant le dépôt.

Des couches minces d'excellente qualité épitaxiale de BaTiO<sub>3</sub> ont été produites par différentes techniques telles que le dépôt par ablation laser, le dépôt chimique en phase vapeur organométallique, etc. La température nécessaire pour synthétiser des particules de BaTiO<sub>3</sub> monophasées par procédé hydrothermale est de 90 C. En dessous de cette température, la réaction est incomplète en raison de très lentes cinétiques de réaction. Les propriétés électriques des couches minces de BaTiO<sub>3</sub> épitaxiales formes sur SrRuO<sub>3</sub>/SrTiO<sub>3</sub> par la méthode hydrothermale conventionnelle est reporté dans la littérature, mais n'as pas signal de courbes de polarisation de commutation dues à des fuites électriques élevées causées par la présence du groupe hydroxyle et le temps de déposition était exagéré.

Le dépôt de couches minces de BaTiO<sub>3</sub> par la méthode hydrothermale assistée par des micro-ondes et par la méthode conventionnelle (figure 4) a été réalisé sur des substrats polycristallins monocristallins et sur des substrats polycristallins de silicium platinés (Pt/Al<sub>2</sub>O<sub>3</sub>/SiO<sub>2</sub>/Si). Le substrat monocristallin utilisé est le SrTiO<sub>3</sub> dope avec Nb avec orientation (100) de Crystec GmbH (5 × 5 × 0,5 mm, angle de désorientation <0,5 °, 0,5% en poids de Nb.). Une surface de SrTiO<sub>3</sub> dope avec Nb (100) avec terminaison unique et atomiquement plat sont nécessaires pour la croissance épitaxiale et donc la méthode de préparation est décrit au-dessous. La mesure d'hauteur de marche est de 0,39 nm entre les terrasses adjacentes observé par microscopie à force atomique qui correspond au paramètre de maille de SrTiO<sub>3</sub> cubique. Dans le cas de la surface (100) orientée cela est égale à la distance inter-réticulaire (d<sub>100</sub>). La rugosité RMS

---

sur les terrasses étaient de l'ordre de pm. Le substrat tel que reçu de Pt/Al<sub>2</sub>O<sub>3</sub>/SiO<sub>2</sub>/Si a été nettoyé et puis recuit à 550°C pour stabiliser le Pt et pour supprimer la croissance des grains lors du dépôt hydrothermique de BaTiO<sub>3</sub>.

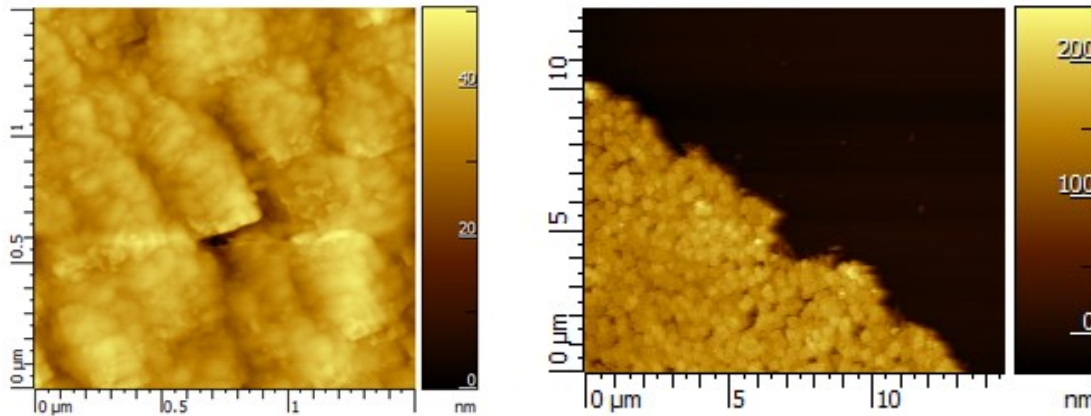


Figure 4 Topographie par microscopie à force atomique en mode tapping par la méthode conventionnel d'une couche mince de BaTiO<sub>3</sub> sintétisé pendant 24h à 90°C.

L'effet de H<sub>2</sub>O<sub>2</sub> sur la formation du film de BaTiO<sub>3</sub> sur SrTiO<sub>3</sub> dope avec Nb (100) a été étudié pour le premier processus d'optimisation. Dans cette expérience, le substrat et le précurseur ont été exposés à la radiation micro-onde pendant 10 min à un niveau de 120 W de puissance et maintenues dans le four pendant 2 h avant refroidissement à température ambiante par immersion de l'ensemble du réacteur dans de l'eau. Dans le cas du dépôt hydrothermique de BaTiO<sub>3</sub> sans l'addition de H<sub>2</sub>O<sub>2</sub> dans la solution de précurseur, dans des conditions identiques, la couverture de couche mince sur le substrat de SrTiO<sub>3</sub> était très faible par rapport au résultat ou 10% de H<sub>2</sub>O<sub>2</sub> a été utilisé. La nucléation de BaTiO<sub>3</sub> est produite à l'interface substrat-solution à des sites

spécifiques sur la surface du substrat dans le cas de la solution sans  $H_2O_2$  et il présente une croissance limitée. Autres régions du substrat manquent de dépôt et il a montré encore une surface avec une structure d'étape-terrasse caractéristiques du substrat vierge. Cependant, avec 10% de  $H_2O_2$  (remplacé par un même volume d'eau pour garder le facteur de remplissage de 66%) il présente une nucléation plus uniforme de  $BaTiO_3$  sur toute la surface du substrat de  $SrTiO_3$  dopé avec Nb survenue par la croissance continue et il a complètement masqué la morphologie type étape-terrasse de la surface.

Dans le cas du processus hydrothermal assisté par des micro-ondes, le temps de radiation d'exposition à une puissance particulière devrait être d'abord optimisé pour l'exploitation sécuritaire du réacteur. Avec méthode d'essais et erreurs nous avons optimisé le temps jusqu'à 10 min pour une puissance de sortie de 120 W. Cependant, pour la conversion complète de particules de  $TiO_2$  pour produire la couche de  $BaTiO_3$  dans des conditions hydrothermales dépend sur le temps de réaction et qui peut être beaucoup plus élevée que le temps 10 min comme il a été mentionné avant. Dans ce cas, la seule solution consiste en répétant l'expérience après refroidissement de la bombe de digestion à une température aussi basse que la température à laquelle a eu lieu la première irradiation. Dans le cas présent nous avons effectué le deuxième cycle après un intervalle de 2 h en gardant la bombe de digestion dans l'eau froide. Ce processus a été répété jusqu'à ce que nous ayons identifié comme la phase pure de  $BaTiO_3$  sur le substrat. Dans le cas de 1 cycle, un dépôt très uniforme du film a été vu sur toute la surface Pt avec un RMS 1.4 nm, comparable à la rugosité rms de la surface Pt. Dans ce cas, la croissance des grains de  $BaTiO_3$  n'était pas visible, comparativement à 2 cycles. Dans le cas de 2 cycles, une caractéristique des

---

couches granuleuses étaient claires et cette croissance du grain entraîné plus rugosité de surface (2,4 nm). Un comportement similaire a été observée de nouveau dans le cycle 3 et la réaction pour produire la couche semble presque terminée. Dans tous les cas, la morphologie de la surface de Pt était visible même après le dépôt d'un film BaTiO<sub>3</sub>.

Des couches minces multiferroïques de bismuth ferrite ont récemment attiré une attention considérable en raison de demandes liées à l'effet photovoltaïque en vrac dans lequel la direction de polarisation détermine le sens du courant photoélectrique et de la croissance épitaxiale par conséquent, est très important. Des couches minces épitaxiales BiFeO<sub>3</sub> ont été produites par différentes techniques telles que le dépôt de la solution chimique, dépôt par ablation laser, le dépôt chimique en phase vapeur organométallique etc. La technique hydrothermale a également déjà été utilisée pour synthétiser du BiFeO<sub>3</sub> et il n'a pas été pris en considération pour l'application photovoltaïque due au courant de fuite électrique élevée. Au fait que le BiFeO<sub>3</sub> étant un semi-conducteur à bande interdite large, une fuite provient de dopants qui sont introduites par le solvant (eau en hydrogène à partir d'une synthèse hydrothermique), d'autres promoteurs de réaction (catalyseurs, des tensioactifs et minéralisateurs), et la réaction de sous-produits.

Dans le présent travail, commutation ferroélectrique est montré pour la première fois dans des films minces BiFeO<sub>3</sub> hydrothermique synthétisés par une image par microscopie atomique à force piézoélectrique contraste une phase représentant un motif ferroélectrique intentionnellement écrite où certaines zones sont polarisées "vers le haut" et certains "vers le bas". En utilisant une pointe avec un revêtement conducteur et en appliquant un potentiel électrique de polarisation, nous avons polarisée trois carrés croisent situés en haut à gauche en bas à droite avec des tensions de -

8 V, 6 V et 8 V, respectivement. La superficie restante correspond à l'état vierge qui présente un haut-orientation préférentielle (figure 5). Les places se croisent montrent la capacité du matériau à passer par un cycle complet de commutation de polarisation ferroélectrique. Ceci est également confirmé par une courbe d'hystérésis ferroélectrique entre 10 V et 10 V dans laquelle un décalage de phase de  $180^\circ$  hors du plan est affiché.

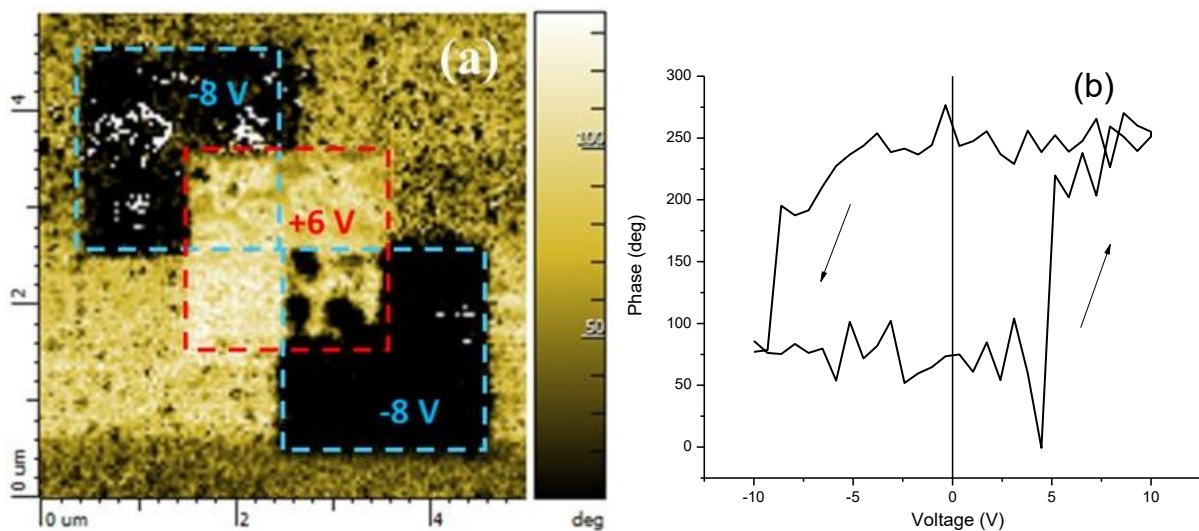


Figure 5 (a) Image de phase par microscopie a force piézoélectrique et (b) courbe d hystérésis local montre commutation de  $180^\circ$ .

L'effet photovoltaïque en vrac est représenté et la réponse de photocourant de court-circuit généré par la lumière incidente (figure 5). Il a été décrit ailleurs un mécanisme de séparation de charge et photo génération de tension qui se produit exclusivement dans des parois de domaine ferroélectriques à l'échelle nanométrique dans un ferroélectrique de modèle,  $\text{BiFeO}_3$ , sous

éclairage en lumière blanche lorsque les tensions ont été significativement plus élevée que la largeur de bande interdite électronique.

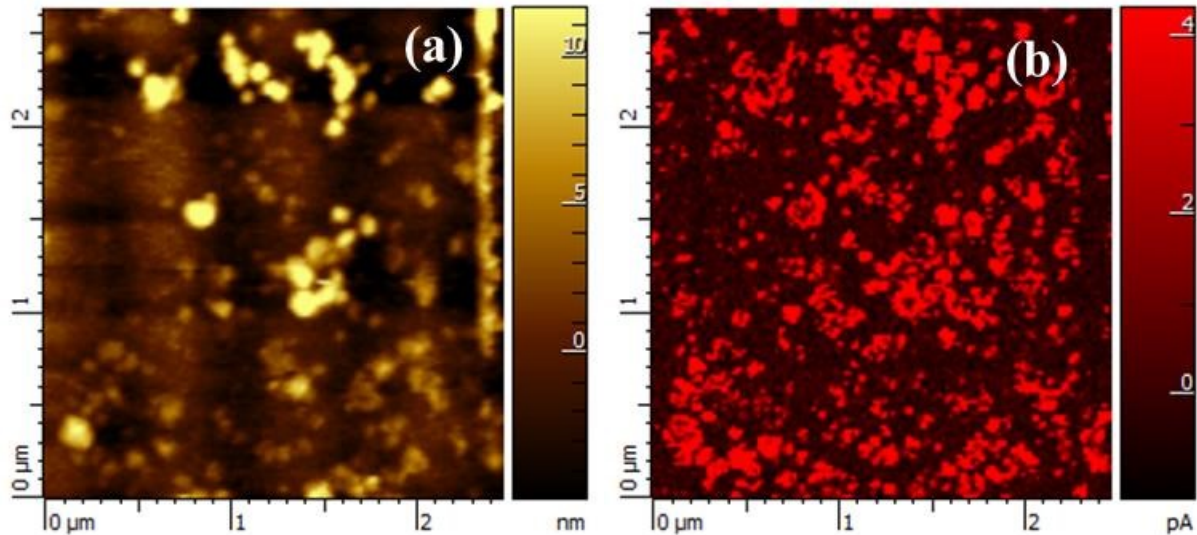


Figure 5 (a) topographie en mode contact par microscopie à force atomique et (b) mesure photoélectrique simultanée dans la configuration de court-circuit sous une excitation de 355 nm. La réponse photovoltaïque est observable que dans la présence de  $\text{BiFeO}_3$ .

En raison de la faible concentration du minéralisateur KOH, jusqu'à 18 h sont requises pour la croissance des couches minces de 40 nm. Cela représente clairement un barrage routier pour le traitement par lot industriel, mais les expériences récentes de notre groupe avec la synthèse des nanoplaques  $\text{BiFeO}_3$  hydrothermale assistée par micro-ondes ont montré le potentiel de réduire le temps de réaction à quelques minutes. Des expériences visant à appliquer cette technique à couches minces sont actuellement sur le chemin.

Des couches minces de  $\text{BiFeO}_3$  hautement ordonnés ont été produites avec succès par la synthèse hydrothermale sur  $\text{SrTiO}_3$  dopés avec du Nb (100). Les tensioactifs ont été évités et la concentration d'hydroxyde de potassium (KOH) a été réduite par un facteur de 10, en comparaison à des rapports dans la littérature, qui donne l'opportunité de réduire la fuite électronique. En raison de la réduction de la solubilité des précurseurs est affecté en diminuant la vitesse de réaction et 18 h de dépôt ont été nécessaires pour faire croître une couche mince de 40 nm. Les couches minces de  $\text{BiFeO}_3$  ont été recuites à 500 °C sous flux d'azote pour une meilleure cristallisation et pour éliminer l'hydrogène. Pour la première fois, l'inversion de la polarisation est mise en preuve par la réduction réussie de fuite électronique. Une première démonstration de l'effet photovoltaïque en vrac montre que cette technique peut être utilisée pour produire des couches minces des matériaux multiferroïques avec des applications photovoltaïques.

*Mots-clés: Oxydes fonctionnels, Pérovskites,  $\text{BaTiO}_3$ ,  $\text{BiFeO}_3$ , Couches minces, Croissance épitaxiale,  $\text{SrTiO}_3$ , Monocristallin, Préparation de surface du substrat, Gravure, Terminaison chimique unique. Synthèse hydrothermale, Microscopie à force atomique, Commutation de polarisation ferroélectrique, Procédé hydrothermique assistée par micro-ondes, Processus hydrothermal conventionnel, Topographie, Effet photovoltaïque en vrac, Photocourant.*